AD-A075 158 TETRA TECH INC JACKSONVILLE FL F/G 8/3
CONTINENTAL SHELF CIRCULATION INDUCED BY TIDAL JETS - AN ANALYT--ETC(U)
OCT 79 R B TAYLOR , P B JOSHIO N00014-78-C-0693
UNCLASSIFIED TETRAT-3249 NL

1 OF 2
AD
A075158

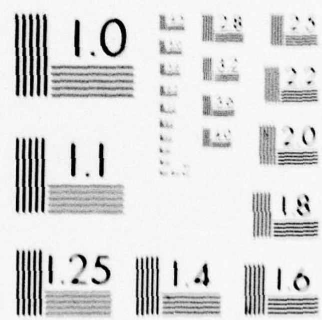

MICROCOPY RESOLUTION TEST CHART
NATIONAL BUREAU OF STANDARDS-1963-A

TC 3249

FINAL REPORT

AD A075158

LEVEL #

CONTINENTAL SHELF CIRCULATION INDUCED BY TIDAL JETS — AN ANALYTICAL STUDY

OCTOBER, 1979

Prepared For:

OFFICE OF NAVAL RESEARCH
GEOGRAPHY PROGRAMS
ARLINGTON, VIRGINIA

CONTRACT NO. N00014-78-C-0693

Prepared By:

Tetra Tech Inc.
Jacksonville, Florida

TETRA TECH

UNCLASSIFIED

SECURITY CLASSIFICATION OF THIS PAGE (When Data Entered)

REPORT DOCUMENTATION PAGE

READ INSTRUCTIONS BEFORE COMPLETING FORM

1. REPORT NUMBER: Final Report	2. GOVT ACCESSION NO.
3. RECIPIENT'S CATALOG NUMBER	
4. TITLE (and Subtitle): CONTINENTAL SHELF CIRCULATION INDUCED BY TIDAL JETS - AN ANALYTICAL STUDY.	5. TYPE OF REPORT & PERIOD COVERED: Final Report, 1 July 1978-30 Sept 1979
	6. PERFORMING ORG. REPORT NUMBER: TC 3249
7. AUTHOR(s): R. Bruce Taylor, Prakash B. Joshi	8. CONTRACT OR GRANT NUMBER(s): N00014-78-C-0693
9. PERFORMING ORGANIZATION NAME AND ADDRESS: Tetra Tech, Inc., 7825 Baymeadows Way, Suite 321-B, Jacksonville, FL 32216	10. PROGRAM ELEMENT, PROJECT, TASK AREA & WORK UNIT NUMBERS: NR 388-147
11. CONTROLLING OFFICE NAME AND ADDRESS: Office of Naval Research, Geography Programs, 800 N. Quincy St., Arlington, VA 22217	12. REPORT DATE: October 1979
	13. NUMBER OF PAGES: 108
14. MONITORING AGENCY NAME & ADDRESS (if different from Controlling Office): Office of Naval Research, Geography Programs, 800 N. Quincy St., Arlington, VA 22217	15. SECURITY CLASS. (of this report): UNCLASSIFIED
	15a. DECLASSIFICATION/DOWNGRADING SCHEDULE: N/A

16. DISTRIBUTION STATEMENT (of this Report)

Approved for public release; distribution unlimited

17. DISTRIBUTION STATEMENT (of the abstract entered in Block 20, if different from Report)

N/A

DDC RECEIVED OCT 18 1979 A

18. SUPPLEMENTARY NOTES

N/A

19. KEY WORDS (Continue on reverse side if necessary and identify by block number)

alongshore current; bottom friction; circulation; continental shelf; entrainment; jetties; multiple inlets; plumes; tidal inlets

20. ABSTRACT (Continue on reverse side if necessary and identify by block number)

Results of an analytical investigation of the shelf and nearshore circulation induced by tidal inlets are presented for steady jets issuing into coastal waters having constant depth but arbitrary bottom friction. The surrounding fluid motion is assumed to be steady and potential (i.e., inviscid and irrotational). The effects of unsteadiness, Earth's rotation, and buoyancy have been neglected; however, the important effects of lateral mixing are included. In addition, mathematical formulations are developed to describe CONT

DD FORM 1 JAN 73 1473 EDITION OF 1 NOV 65 IS OBSOLETE

S/N 0102-LF-014-6601

UNCLASSIFIED

SECURITY CLASSIFICATION OF THIS PAGE (When Data Entered)

411 408

JOB

steady potential flow with variable bathymetry; and unsteady, inviscid, rotational flow due to Coriolis forces.

To obtain the shelf circulation patterns over constant bottom topography, the tidal jet is represented by an equivalent distribution of sinks. The sinks are solutions of Laplace's equation which also governs the potential motion of the jet-induced circulation. The strength of each sink in the distribution is determined by equating the volume flow due to entrainment to the volume flow demanded by the sink, thereby establishing a complete physical and mathematical connection between the jet flow and the outer flow. Analytical expressions are derived for the stream function and velocity components. These quantities are evaluated analytically whenever possible and numerically using Gauss-Legendre quadrature. The streamline patterns obtained for a single tidal jet oriented perpendicular to the coastline bear a close resemblance to the jet-induced circulation patterns observed in a smoke tunnel. The variation of alongshore current with distance from the jet is also predicted and shown to be a strong function of bottom friction of the jet. Numerical computations are performed for various values of bottom friction. The following four tidal jet configurations of practical interest are examined: (i) a simple jet normal to the coastline, (ii) a jet with jetties of varying lengths, (iii) two parallel jets, and (iv) a jet non-perpendicular to the coastline.

Prepared by:

Tetra Tech, Inc.
Jacksonville, Florida

TABLE OF CONTENTS

LIST OF FIGURES

LIST OF FIGURES (Cont'd)

ACKNOWLEDGEMENTS

This study was supported by the Office of Naval Research, Geography Programs, under Contract No. N00014-78-C-0693. The authors wish to thank Mr. Dennis Conlon of ONR for his valuable suggestions and comments during the course of this work.

1.0 INTRODUCTION

1.1 General

The prediction and understanding of tide induced currents in coastal waters and their interaction with beaches and structures represent an intriguing and complex area of research today. These currents are especially significant in the vicinity of tidal inlets and estuary or river mouths. They affect commerce, navigation, small craft operations, water quality, bathymetric changes and shoreline stability in these densely populated coastal areas. From an engineering point of view, the primary areas of interest can be identified as the exchange between the interior and exterior waters connected by tidal inlets, the transport of coastal sediments and the circulation patterns established in the adjacent waters.

A tidal inlet is a narrow entrance region connecting an interior water body such as a bay or lagoon to the exterior ocean domain. Therefore, inlets serve as interfaces between these water bodies and contribute to their flushing and exchange mechanisms, as shown by Dean and Taylor (1). They have found that the water issuing from inlets during the ebb tide encounters a renewal of about 45% when it returns during the following flood. This efficient mechanism of flushing is due to the unique features of the flow near the narrow entrance. Since the actual hydromechanics associated with entrances have not been thoroughly understood, prior modeling efforts on the circulation and mixing in bays have often made use of assumed boundary conditions at inlets.

The mass transport near narrow entrances also has important consequences with respect to the transport of coastal sediments. It has long been recognized

that tidal inlets act as sediment sinks, trapping large amounts of littoral materials in the form of extensive shoals encircling entrance regions. There is a direct relationship between the deposition/erosion patterns near an inlet and the mass transport phenomena associated with tidal currents. Yet, the prior design of jetties, navigation channels, and sand bypass systems have often been based on considerations of the poorly understood surf zone wave dynamics, whereas the role of tidal hydromechanics has been largely ignored. The importance of the latter effects has been demonstrated by Dean and Walton (2). According to their study, the outer shoal volumes of major Florida inlets range between $10^6 m^3$ to $2 \times 10^8 m^3$, and in some areas the sand extracted from the adjacent beaches has caused 40 feet retrogressions of the shoreline each year for a period of 50 years.

The domain of influence of the above flow and mass transport phenomena extends from the confined areas of bay or estuary waters to the waters on the semi-infinite continental shelf region. In fact, due to the presence of a narrow entrance, large scale circulation patterns are generated on both the interior and the exterior regions which are extremely important from an oceanographic point of view. They affect the water mass distributions (Csanady(3)) and mean circulation of adjacent shallow seas (Rouse and Coleman (4)).

The preceding discussion is best understood when related to tidal jets observed in nature. The photograph in Fig. 1.1(a) shows a starting tidal jet at Fort Pierce inlet in Florida. The jet displays two distinct zones, a frontal region characterized by vertical flow and a region with primarily unidirectional flow. The importance of circulation patterns induced by tidal jets in adjacent waters is demonstrated in Fig. 1.1(b). This figure shows

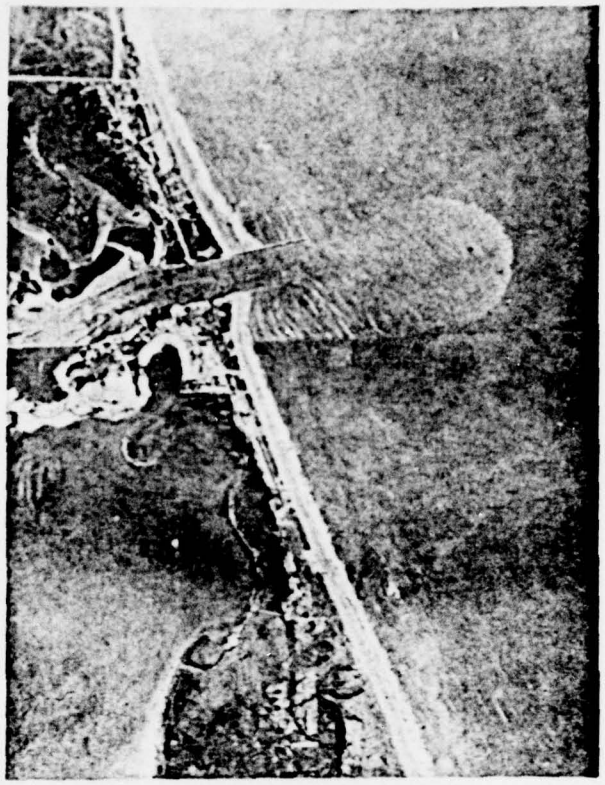

Figure 1.1a Starting Tidal Jet At Fort Pierce Inlet, Florida

Figure 1.1b Ebbing Flow At St. Mary's Entrance, Florida

ebbing flow at St. Mary's Entrance, Florida. The entrainment of effluent material released far away from the south jetty into the jet is very clearly seen. Figure 1.2 provides a striking picture of two jets issuing from two neighboring inlets at Big Hickory Pass and New Pass in Florida. The jets are attracted and eventually attached to each other due to entrainment velocities. The effects of entrainment into both jets has caused recession in the middle portion of the beach, and hence offset the geometry of the shoreline. The smaller of these two inlets has a history of closing and reopening, and has migrated toward the large inlet at a rate of 100 m. in 6 months.

The research presented herein is concerned with the study of circulation patterns induced on the continental shelf by tidal jets during ebb. Since they occur in an unconfined environment, these flows are easier to analyze than interior flows during flood which occur in a confined environment. The latter situation is more complex and will be treated in future investigations along with the mass transport phenomena associated with the flooding and ebbing flows. Before considering details of the scope of present work, which are presented in Sec. 1.3, it is useful to survey previous literature related to turbulent jets in general. This is done in the next section.

1.2 Review of Pertinent Literature

A bay or a lagoon region connected to the ocean through a tidal inlet can be idealized as in Figure 1.3. The flow patterns associated with tidal currents have rather unique features in the vicinity of a narrow entrance. As the water starts ebbing into the ocean, an unsteady flow development is observed, as schematized in Figure 1.3. Initially, a radially expanding source flow is

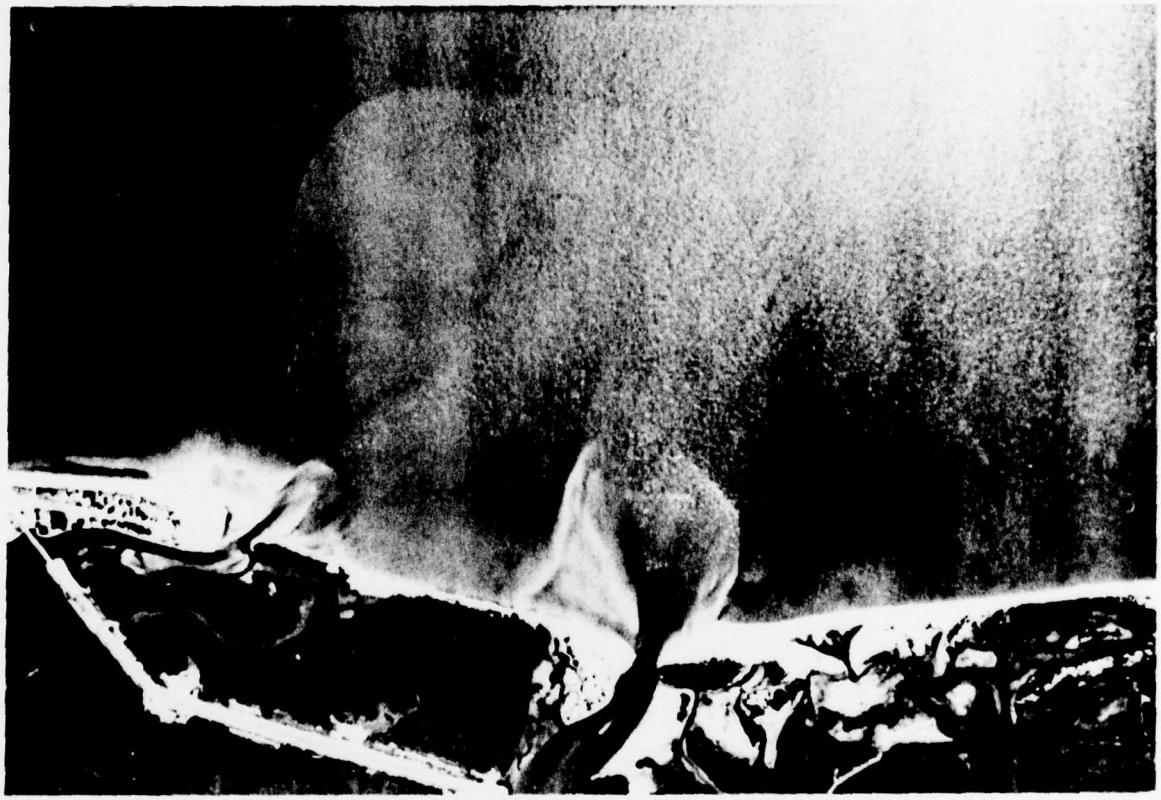

Figure 1.2 Interactions of Jets Issuing from Big Hickory Pass (left) and New Pass (right), Florida.

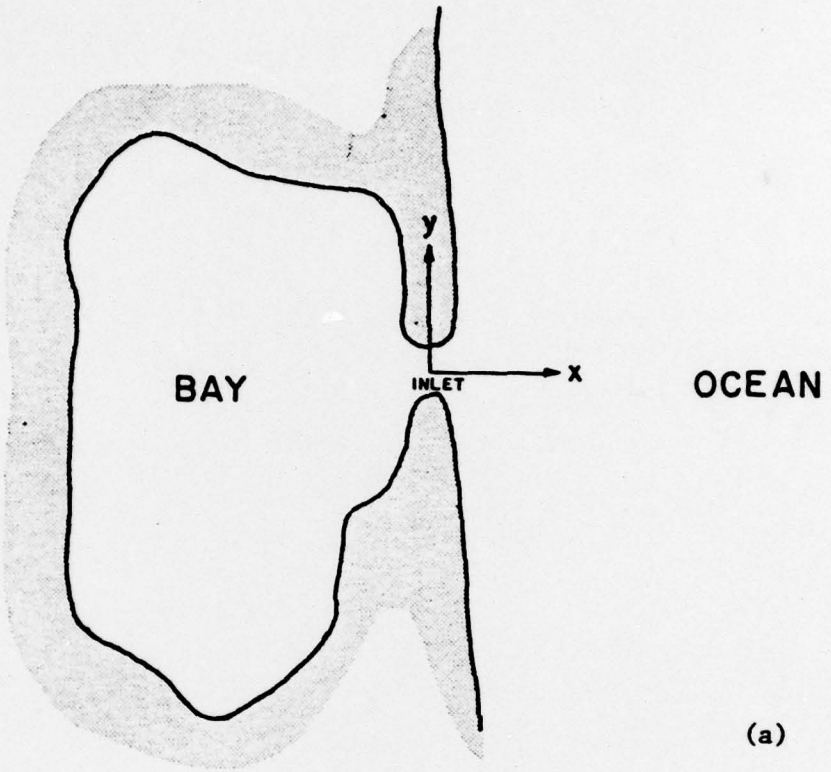

(a)

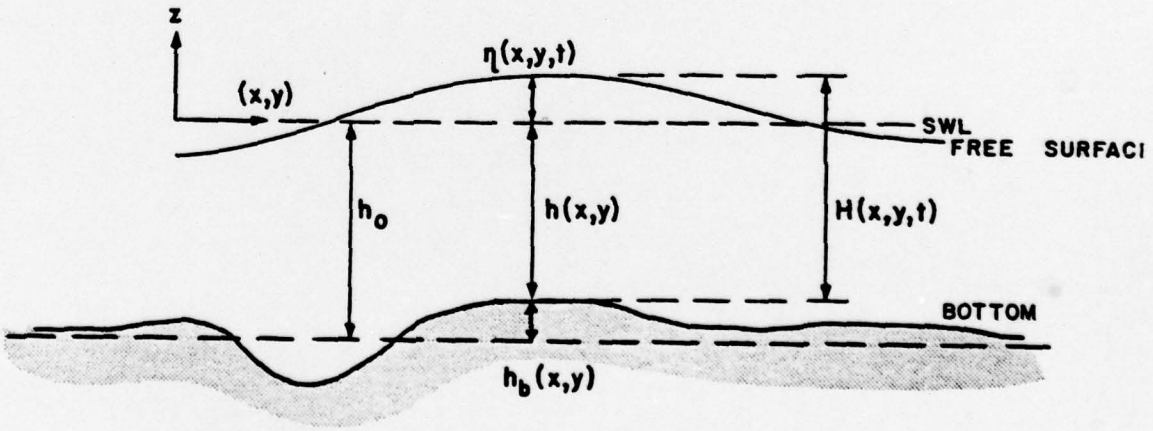

(b)

Figure 1.3 Definition Sketch (a) Bay-Inlet-Ocean System (b) Surface and Bottom Variations.

issued from the inlet (Fig. 1.4a). As the inlet velocity increases, the flow is separated from coastal boundaries (Fig. 1.4b) and becomes transformed from a source flow into a jet (Fig. 1.4c). A vortex pair, shed off during the impulsive start of the motion, moves offshore, forming the frontal portion of the jet. These features of the starting jet are shown photographically in Fig. 1.1a for Fort Pierce Inlet. The structure of the jet is determined by the Reynolds' number $Re = u_o\sqrt{h_o b_o}/\nu$ where u_o, h_o, b_o are respectively the mean velocity, the depth and the half-width of the inlet, and ν the kinematic viscosity. According to Pearce's (6) results, the flow is laminar for Re<500, becomes turbulent in the range Re=1500-2500, and remains fully turbulent for Re>3000. Thus, some time after the beginning of the ebb period, a fully developed turbulent jet is formed behind the frontal region.

The unsteady development of a starting jet can approximately be represented as a composite of a steady turbulent jet and an unsteady frontal region. This assumption has been used by Turner (7), Tsang and Wood (8), Tsang (9), and Middleton (10) in analyzing buoyant plumes, where plume solutions have been coupled with thermal solutions at the frontal region. The thermal comprises a vortex ring in axisymmetric starting plumes, or a vortex pair (such as shown in Figs. 1.4a and 1.4b) in the two dimensional case. In the case of tidal jets, an order of magnitude analysis by Özsoy (11) has shown that unsteady effects are indeed negligible in the near field of the inlet mouth. It has further been demonstrated that the front speed calculations based on steady jet solutions yield reasonable agreement with laboratory observations of starting jets. Therefore, steady analyses are sufficient to infer the quasi-steady jet properties.

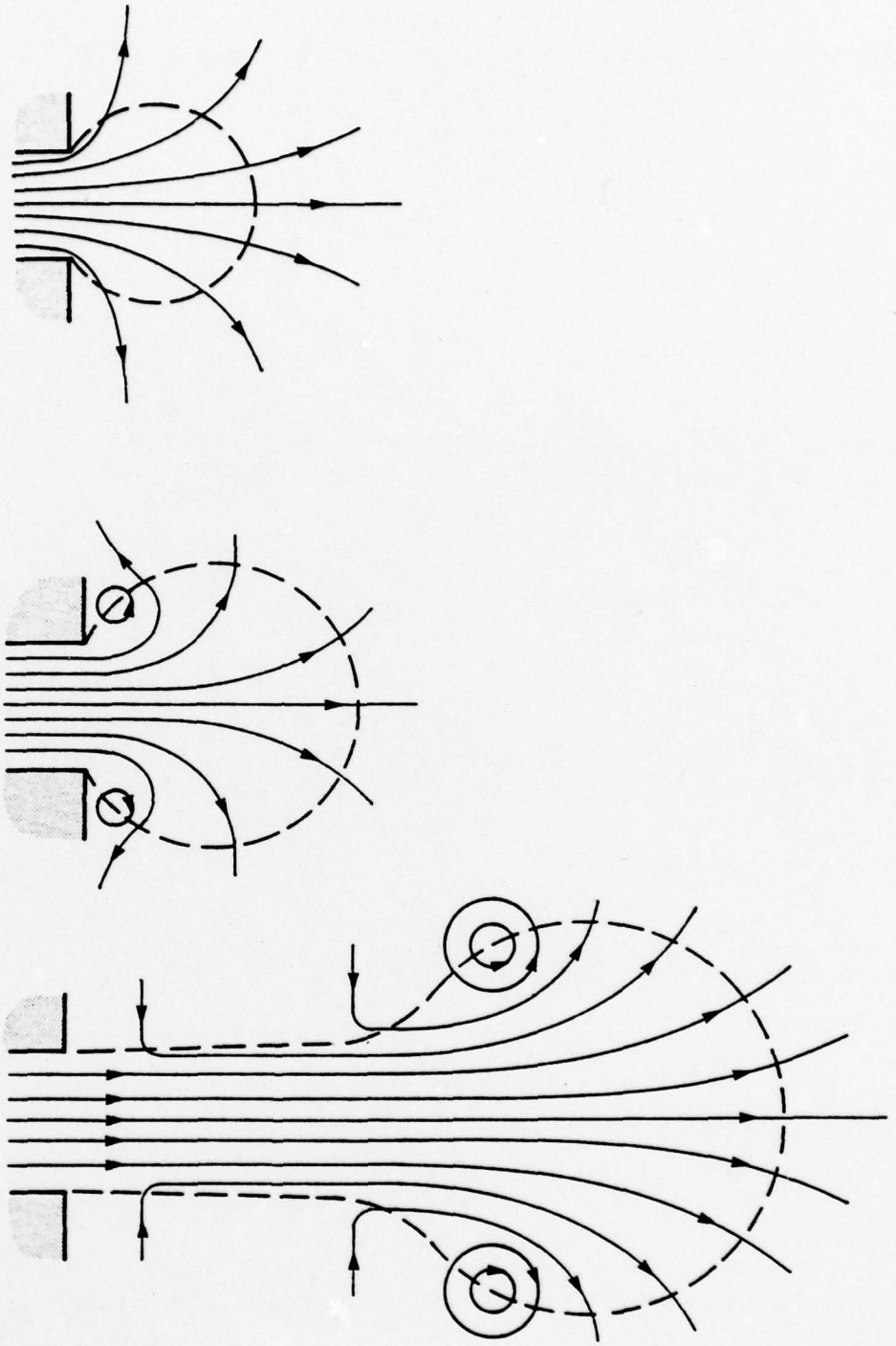

Figure 1.4 (a), (b), (c) Different Stages in the Development of a Starting Jet (Courtesy Ref. (11)).

A detailed review of turbulent jets can be found in Albertson et al (12), Abramovich (13), Schlichting (14), Stolzenbach and Harleman (15) and Rajaratnam (16).

The significance of jet flows at tidal inlets lies not only in the dynamics and mass transport within the jet itself, but also in its effects on the larger scale circulation patterns. The surrounding fluid particles near the jet boundaries are entrained and carried away by the jet, owing to the friction between the two zones (13, 14). The resulting velocity of entrainment causes induced circulation in the outer part of the fluid away from the jet region (17). Such entrainment-induced flows are possible causes for gyres generated in the vicinity of river mouths as reported by Wiseman et al (5) and circulations observed by Olsen (18) near tidal inlets.

A first attempt has been made by French (19) to study the ocean flow patterns during both portions of the tidal cycle. The flood flow is analyzed by making use of the free streamline theory, including the effects of long jetties. The ebb flow is represented by Tollmien's solution for two-dimensional turbulent jets, neglecting the effects of bottom friction and variable bathymetry. In reality, both are significant factors in the analysis of jets.

The effects of bottom friction and depth variations on a jet have been first taken into account by Borichansky and Mikhailov (20), however, their results are erroneous, since the jet momentum has been assumed to be conserved, even in the presence of bottom friction. In spite of these and other deficiencies in the analysis, these writers have shown the exponential dependence of jet expansion and velocity decay on offshore distance. Furthermore, they have demonstrated the opposing effects of a seaward slope and the bottom friction.

A similar analysis, including only the bottom frictional effects, has been performed by Taylor and Dean (21). Upon neglecting lateral mixing and entrainment, they have obtained solutions for the jet half-width b and the jet velocity u (assumed uniform across the jet) as

$$\frac{b}{b_o} = e^{\mu\xi/2} \tag{1.1a}$$

$$\frac{u}{u_o} = e^{-\mu\xi/2} \tag{1.1b}$$

where $\mu \equiv fb_o/8h_o$ is the parameter specifying bottom friction effects (f being a friction coefficient), and $\xi = x/b_o$ the normalized offshore distance from the inlet. Note that the aspect ratio b_o/h_o is also incorporated into the parameter μ, such that increasing the ratio of inlet width to depth, in effect, increases the frictional resistance.

A more detailed analysis of the jet has been performed by Ünlüata and Özsoy (22) and Özsoy (11), in which general solutions have been obtained including the effects of bottom friction, bathymetric changes, turbulent mixing and lateral entrainment. The velocity distributions are assumed to be self-similar and the boundary layer approximations are utilized in obtaining analytical solutions to the governing Navier-Stokes equations. In the near field of the inlet, it is shown that the unsteady effects, the Coriolis forces, and the surface gradients are negligible. The velocity v_e of entrainment of fluid particles into the jet is assumed to be $v_e = \alpha u_c$ after Morton et al (23), where α is the entrainment coefficient ($\alpha \simeq 0.05$), and u_c the jet centerline velocity. The analysis is, in general, similar to the one used by Stolzenbach and Harleman (15). In the absence of depth variations, and for large distance ($\xi \to \infty$), these

solutions are simplified to yield

$$\frac{b}{b_o} \rightarrow k_1 e^{\mu\xi} \tag{1.2a}$$

$$\frac{u_c}{u_o} \rightarrow k_2 e^{-\mu\xi} \tag{1.2b}$$

where k_1, k_2 are constants. The general features of these solutions are shown in Fig. 3.2 of Sec. 3.2 which contains details of Özsoy's (11) work. The exponential dependence of jet width and velocity on distance here is considerably different from that obtained by Taylor and Dean (21) in Eqs. (1.1), since the lateral mixing and entrainment have been neglected by the latter authors. Due to the additional effects of lateral entrainment, the expansion and velocity decay rates are doubled in Eqs. (1.2) as compared to the bottom frictional jet solution of Ref. (21). It is also very important that the exponential behaviour of the bottom frictional jet differs significantly from the linear expansion ($b \sim \xi$) of a classical two dimensional jet (12, 13, 14), in which the centerline velocity decays as $u_c \sim \xi^{-\frac{1}{2}}$. In the absence of bottom friction ($\mu=0$), the general solutions of Ünluata and Özsoy (22) reduce identically to the classical jet solutions. However, even the linear jet growth in the classical theory has been questioned by Kotsovinos (24) who showed that in most experiments a nonlinear growth is observed. Kotsovinos (24) attributed this nonlinear growth to ambient turbulence levels, but the frictional effects of side plates used in the experiments seem also plausible, based on the above arguments. In his further research, Kotsovinos (25) has demonstrated that the constancy of momentum flux in the axial direction of the jet is an approximation (even in the absence of bottom friction) because the jet-induced flow has a component opposite to the main jet flow and because of the pressure field generated in the ambient fluid.

Unluata and Ozsoy (22) and Ozsoy (11) have also shown the counteracting effects of a seaward slope and the bottom friction in determining the jet behaviour. In particular, when these opposing effects are in balance, a linear growth similar to the classical jet is recovered due to entrainment alone. For bottom slopes in excess of this balanced value, the growth becomes logarithmic representing a lower expansion rate. The effects of bottom slope on the jet development is shown in Fig. 1.5, where $\mu = mb_o/h_o$ is a slope parameter, m being the bottom slope. In the case of arbitrary depth variations: h=h(x), the jet is found to go through a series of expansions and contractions, depending on the local variations in the bathymetry. One such example is Jupiter Inlet, Florida shown in Fig. 1.6. Analytical solutions obtained for this case are compared with observations in Fig. 1.7. The jet expands over the shoals and contracts afterwards due to depth increases.

The effects of cross-currents in the ambient waters have also been included by Ozsoy (11). The centerline loci and the half-width for these deflected jets are shown in Fig. 1.8, where $U_A = u_a/u_o$, u_a being the cross-current velocity. Examples of deflected jets are provided by South Lake Worth and Baker's Haulover Inlets in Florida.

The offshore extent of tidal jets is often in the order of L ≈ 10 km. A simple calculation of the Rossby number yields $R_o \equiv \frac{u_o}{\beta L} = O(1)$, indicating the potential relevance of rotational effects. The effects of earth's rotation on horizontal jets have been investigated by Gadgil (26) and Savage and Sobey (27). In the case of shallow water jets (jets covering the full depth), analytical and experimental studies by Savage and Sobey (26) indicate that the jet path remains

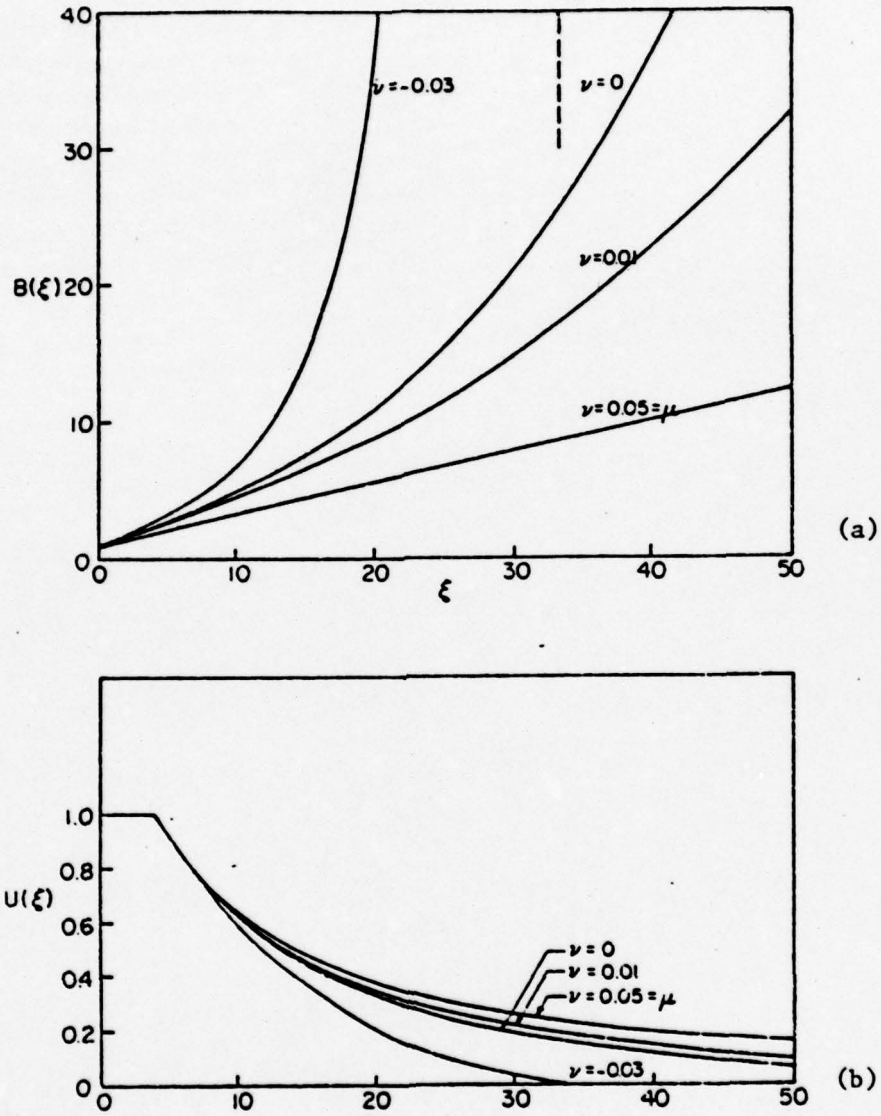

Figure 1.5 The Effect Of Bottom Slope ($\mu = 0.05$) (a) Jet Half Width (b) Centerline Velocity (Courtesy Ref. (11))

Figure 1.6 Fully Developed Tidal Jet at Jupiter Inlet, Florida

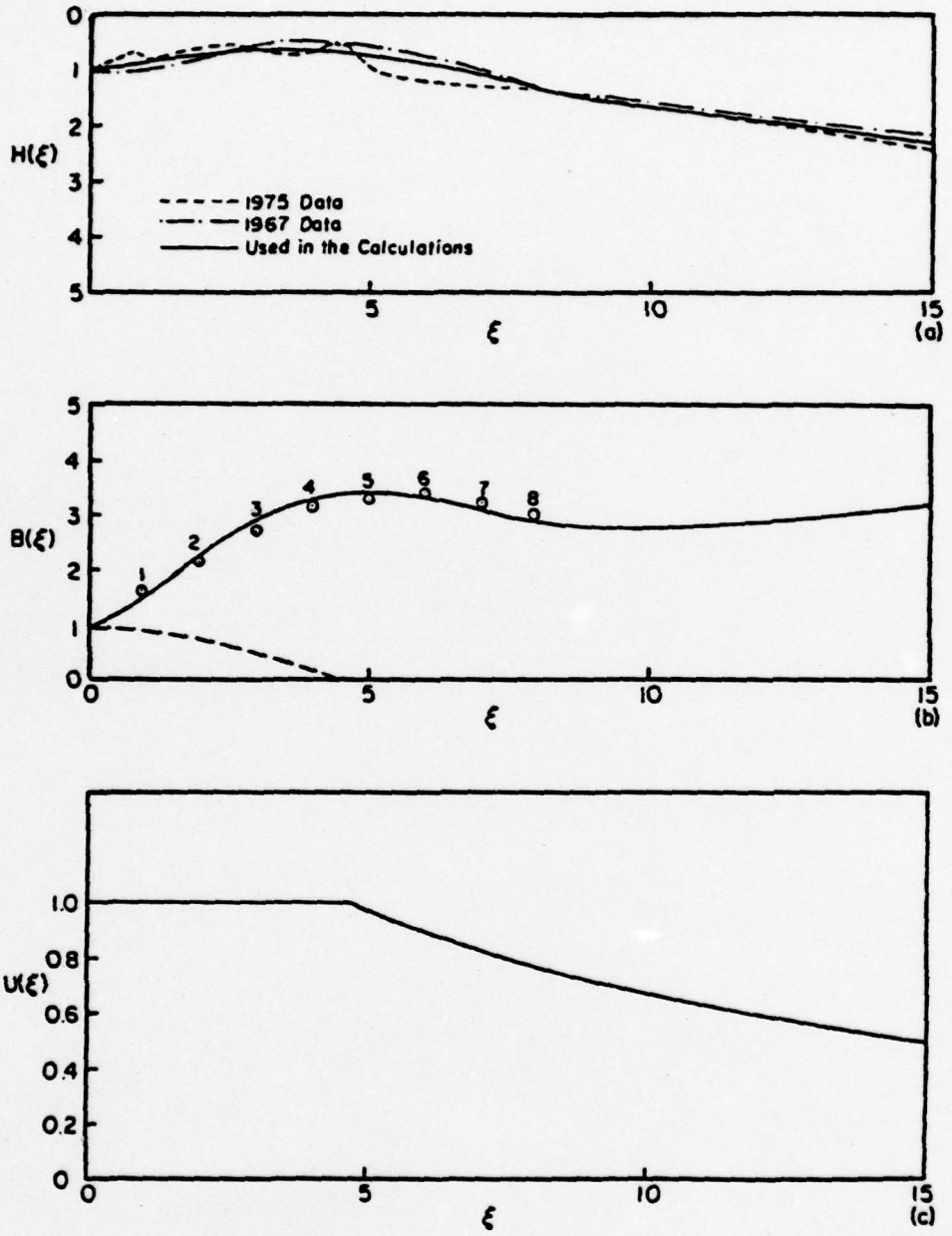

Figure 1.7 Prototype Calculations for the Jet at Jupiter Inlet, Florida (a) Depth Variations (b) Jet Half-Width (c) Centerline Velocity (Courtesy Ref. (11))

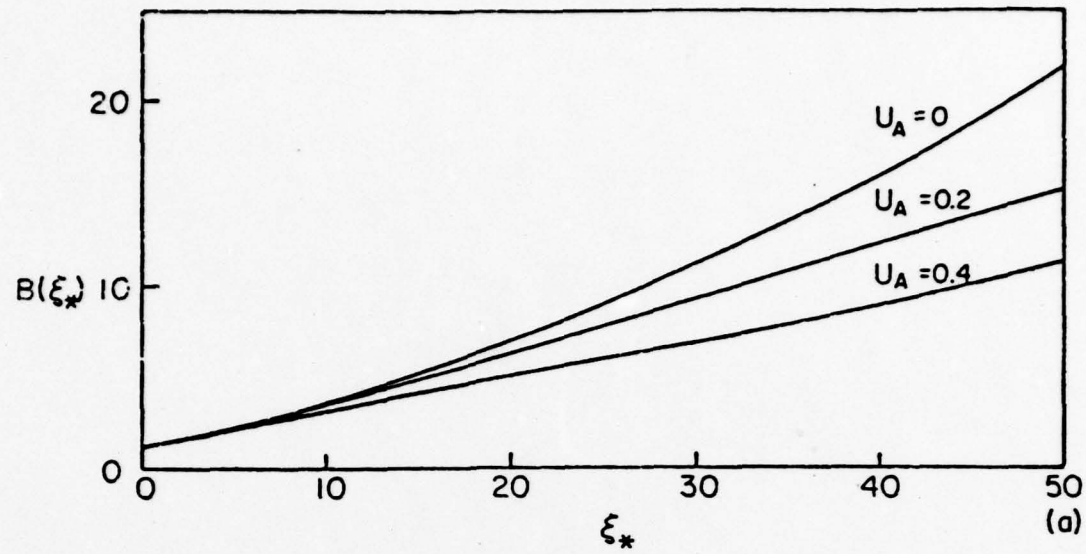

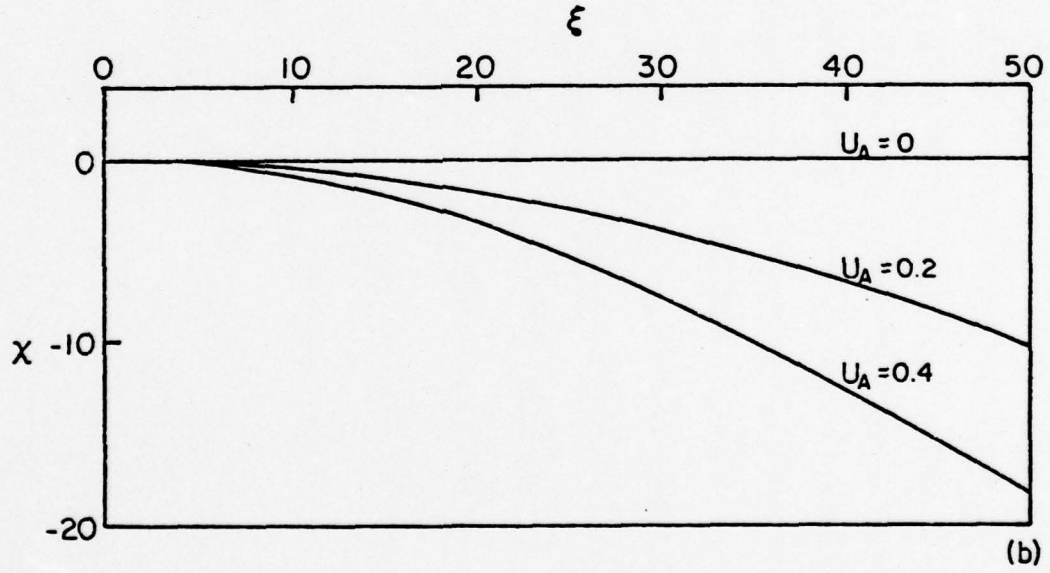

Figure 1.8 The Effects Of Cross-Currents (a) Jet Half-width (b) Centerline Trajectory (Courtesy (Ref. (11))

straight in spite of the Coriolis forces. This appears to be a confirmation of the Taylor-Proudman theorem (Greenspan (28)) in the theory of rotating fluids, since the vertical velocity distributions are not affected by rotation. However, the rotational effects are felt through the development of Ekman boundary layers, which effectively increases bottom friction. These frictional losses induced by rotation have been analyzed by Gadgil (26), for laminar, quasi-geostrophic jets. Her results indicate that there exists a finite penetration distance in which all jet momentum is lost. As opposed to shallow water (or two dimensional) horizontal jets, jets in deep water have completely different characteristics (27), since they are not able to support rotational pressure gradients and the jet path curves in a spiral shape. Such deep water jets can be formed when the orifice dimensions are much smaller than the depth or, in the case of tidal effluents, when the flow separates from the bottom due to either buoyancy or a steep slope. The combined effects of unsteady growth and rotation may also deflect the jet during its initial stages as shown by Savage and Sobey (27). In the presence of depth variations, rotational effects may also become quite significant due to the conservation of potential vorticity as shown in (28).

Due to fresh water discharges into bay or lagoon waters adjacent to tidal inlets, tidal effluents can often be buoyant. In fact, such jet flows in the presence of stratification have been studied in the field and documented by Wright et al (29) and Wright and Sonu (30) at tidal inlets and by Wright and Coleman (31, 32), and Garvine (33) at river mouths. Due to buoyancy, the plumes separate from the bottom, and therefore bottom friction and bathymetric variations lose their importance at some distance offshore from the inlet. However, in the near field of the mouth, bottom topography and friction play

significant roles, as shown in (32, 30, 34). In the presence of density contrasts, the most important mechanism in the far field is probably the buoyant spreading of the plume at the expense of a decrease in the effluent depth. By neglecting the entrainment and mixing processes, Bondar (35) has derived expressions for the plume half-width b and interfacial depth h:

$$\frac{b}{b_o} = (1+\phi\xi)^{2/3} \tag{1.3a}$$

$$\frac{h'}{h_o'} = (1+\phi\xi)^{-2/3} \tag{1.3b}$$

where $\phi = \sqrt{2g\gamma h_o'}\ (2-\gamma)/u_o$ is a measure of the ratio of the buoyant to inertial forces (proportional to the densimetric Froude number), and $\gamma = 1 - \rho_f/\rho_s$, a parameter comparing the fresh and salt water densities ρ_f and ρ_s, respectively.

The plume velocity u is constant in this model ($u = u_o$) since the turbulent mixing with the ambient waters is neglected. Observations by Wright and Coleman (32) at the mouth of South Pass, Mississippi River Delta support the predictions based on Eqs. (1.3). Calculations by Wright and Coleman (31) including vertical entrainment and mixing at the interface also indicate an approximate agreement with observations. Takano (35) has neglected the inertial effects, but has included buoyancy and shear forces as well as entrainment in his analysis, and has obtained

$$\frac{b}{b_o} = (1+\xi^2)^{\frac{1}{2}} \tag{1.4a}$$

$$\frac{\hat{h}}{\hat{h}_o} = (1+\xi^2)^{-\frac{1}{2}} \tag{1.46b}$$

where h is the interfacial depth at the plume centerline. A complete analysis including all the near field processes such as mixing, entrainment and buoyant spreading has been performed by Stolzenbach and Harleman (15). Comparison of these results with laboratory experiments show that the model is sufficiently accurate in predicting both near and far field properties of buoyant surface plumes in the absence of bottom interaction.

The effects of cross currents on buoyant plumes have been analyzed by Stolzenbach and Harleman (15). The effects of earth's rotation have been taken into account by Takano (35). Numerical modeling by Waldrop and Farmer (36) has revealed the formation of vertical secondary circulations due to buoyant spreading. Unsteady tidal effects on river plumes have been discussed by Wright and Coleman (32) and studied by Yoshida and Kashiwamura (37).

The interaction between incident waves and river plumes has been studied by Wright (34). Due to wave transformation and breaking, a rapid deceleration, vertical mixing and abrupt widening of the plume is observed, and a correlation has been obtained between the significant wave height variations and the river stage. However, the latter argument is weakened due to the presence of river flood conditions at the time of the experiments.

The unsteady development of a buoyant plume issuing from a tidal inlet has been described by Wright and Sonu (30), and Sonu and Wright (34). The latter study has also revealed a cross-current bypassing the plume under it.

The outer circulation generated by a tidal jet or a river plume has received little attention to date, even though it is one of the basic characteristics of jets or plumes. The streamlines for the entrainment induced outer flow can

be analyzed by using potential flow theory in the domain external to the jet and by replacing the jet with a line sink distribution; however, such analyses have been largely ignored in the previous literature on tidal or river plumes. The above method has been first introduced by Taylor (38) (see Turner (17)) to analyze the outer flow due to a buoyant plume. It is also conceivable in the case of unsteady tidal jets shown in Figures 1.2a and 1.2b that the propagation of the jet across the continental shelf region sets up large scale unsteady circulation patterns. Similar outer circulation patterns due to a plane starting plume have been studied by Tsang and Wood (8), by replacing the main part of the plume by a line sink and superposing a point source and a vortex doublet at the front. The general flow patterns are similar to the case of a tidal jet, but no literature exists either to document or study these effects.

1.3 Scope of Present Investigation

The objective of this investigation was to study the large scale circulations on the continental shelf region induced by tidal jets.

The results of research presented herein are concerned mainly with steady jets issuing into a shallow, vertically well-mixed body of water. The jets are assumed to be isothermal and salinity gradients are assumed to be absent so that buoyancy effects are excluded. In this initial phase of study, the considerations of unsteadiness, the Earth's rotation, wave climate, and a confined environment are ignored; however, the important effects of bottom friction in the jet have been included. Özsoy's (11) analysis has shown that in the near field of the jet Coriolis forces are negligible, and relative to the time scale of interest (30-60 mins. typically), the unsteady effects are unimportant. Furthermore, factors such as buoyancy, wave processes,

and pressure gradients (due to a jet issuing into the confined environment of a bay during a flood tide) constitute additional complexities and are not within the scope of the work presented here. Finally, during major portions of the study, the jet has been assumed to discharge over constant bathymetry, as this results in significant analytical simplifications and also because a meaningful first insight into the solution behaviour is obtained. This assumption was relaxed subsequently and some preliminary elementary solutions, which are building blocks for determining jet-induced circulation, have been derived.

The mathematical formulation of circulation generated by a jet issuing into a shallow ebbing ocean is described in Sec. 2.0. A general partial differential equation governing steady and irrotational motion of an inviscid fluid over arbitrary bottom topography has been derived first. When specialized to the case of constant bottom, this equation reduces to Laplace's equation for potential flow. Since Laplace's equation possesses well-known solutions, such as sink flows, the jet which entrains the surrounding fluid was replaced by an equivalent sink distribution alongs its axis. This approach is due to Taylor (11). The details of this procedure are contained in Sec. 3.0 and the flow field induced by a simple jet (perpendicular to the coastline) has also been solved in that section. These analyses can be readily extended to treat other flow situations related to tidal inlets which occur in nature. For example, a tidal jet discharging through a jetty, two adjacent jets as in Fig. 1.2, and a jet which is not perpendicular to the coastline. Sec. 4.0 describes the solutions for these cases. Numerical results for circulation induced by jets are given in Sec. 5.0 in terms of streamline patterns and variations of the alongshore current. Formulation of the variable bathymetry problem is presented

in Sec. 6.0. An elementary singularity solution equivalent to the sink for Laplace's equation, has been obtained for the special case of an exponentially sloping bottom. Application of this solution to the determination of jet-induced flow has been outlined. Sec. 6.0 also contains a preliminary formulation of the unsteady circulation problem which takes into account the effects of Earth's rotation, and bathymetry changes. Finally, in Sec. 7.0, conclusions derived from the present research effort have been described and some suggestions for future studies in this area have been advanced.

2.0 MATHEMATICAL FORMULATION OF JET-INDUCED CIRCULATION

2.1 Depth- and Time-averaged Governing Equations

The fluid motion in the bay/ocean system shown in Figure 1.3a is described in the most general sense by the well-known unsteady incompressible Navier-Stokes equations in three dimensions. The waters in the vicinity of tidal inlets are generally shallow and the time scale of unsteadiness equals the period (T) of tidal variations. Therefore, it is possible to simplify the Navier-Stokes equations by (i) averaging over the depth (z direction) and (ii) averaging over a time period much longer compared to the time scale of turbulent fluctuations but much shorter compared to the period of tidal variations. The details of these operations are given in Ref. (11) and the resulting two dimensional (x and y) turbulent motion is governed by the following equations.

$$\frac{\partial \eta}{\partial t} + \frac{\partial (Hu)}{\partial x} + \frac{\partial (Hv)}{\partial y} = 0 \tag{2.1}$$

$$\frac{\partial (Hu)}{\partial t} + \frac{\partial (Hu^2)}{\partial x} + \frac{\partial (Huv)}{\partial y} - \beta Hv = - gH \frac{\partial \eta}{\partial x} - \frac{f}{8} uq + \frac{1}{\rho} \frac{\partial Fxx}{\partial x} + \frac{1}{\rho} \frac{\partial Fxy}{\partial y} \tag{2.2}$$

$$\frac{\partial (Hv)}{\partial t} + \frac{\partial (Huv)}{\partial x} + \frac{\partial (Hv^2)}{\partial y} + \beta Hu = - gH \frac{\partial \eta}{\partial y} - \frac{f}{8} vq + \frac{1}{\rho} \frac{\partial Fxy}{\partial x} + \frac{1}{\rho} \frac{\partial Fyy}{\partial y} \tag{2.3}$$

where η is the free surface elevation and $H = \eta + h$ is the total depth (Figure 1.3b). The depth-averaged horizontal velocity components are denoted by u and v and the magnitude of velocity is given by $q = (u^2 + v^2)^{\frac{1}{2}}$. In Eqs. (2.2) and (2.3), β, ρ, f, and g represent the Coriolis parameter, density, bottom friction factor, and gravitational acceleration respectively. F_{xx}, $F_{xy} = F_{yx}$, and F_{yy} are the components of the depth-integrated stress tensor (including Reynolds stresses).

Eqs. (2.1), (2.2), and (2.3) present a formidable mathematical problem which cannot be solved analytically to obtain a general solution in closed form. These equations are simultaneous partial differential equations in 3 unknowns u, v, and η, and must be solved numerically on a digital computer using finite difference or finite element techniques. Such an effort, however, constitutes a major undertaking and is not justified for the fundamental research investigation reported herein. Furthermore, one can easily get involved in complications of numerics and lose sight of the physics, thereby making it difficult to ascertain the correctness of the solutions obtained. Lastly, and most importantly, the costs associated with a complete numerical approach are very high. The foregoing considerations led to the treatment of the fluid motion as a steady potential flow and is described in the next section.

2.2 Shelf Circulation As A Steady Potential Motion

Before addressing the complex problem of shelf circulation motions which include the effects of unsteadiness, bottom friction, and Earth's rotation, it is useful to introduce the assumption of steady potential flow. In other words, the motion induced by a tidal jet in the surrounding fluid is assumed to be steady, inviscid and irrotational, and in addition, the effects of Earth's rotation are ignored. It may be pointed out that the latter simplification rules out, a priori, the generation of vorticity (even in an inviscid fluid) as a result of bathymetric variations. The steady potential motion offers the following advantages:

- A simplified mathematical formulation which preserves the essential physics of the problem

- The steadiness of motion makes it possible to use the existing theory of a turbulent jet with bottom friction and bottom topography (11). Thus, although bottom friction is excluded in the analysis of the outer flow, it is included in the inner jet flow.

- Steady potential flow is governed by a single linear partial differential equation which is amenable to analytical treatment. This equation contains partial derivatives with variable coefficients for arbitrary bottom topography and reduces to Laplace's equation for constant bathymetry. A large body of knowledge is then readily available through the well-known solutions of Laplace's equation.

- Solution of the relatively simple potential flow problem yields a valuable insight which will be useful in future studies of more complex problems, taking into account the effects of unsteadiness, Earth's rotation, and bottom friction.

It should be brought to the reader's attention that the term "steadiness" in the above discussion implies time-invarient motion over a period which is large compared to the turbulence time scale but small compared to the tidal period (e.g. 30 minutes, typically). The derivation of equations governing steady potential flow with variable bathymetry is presented below.

Under steady flow conditions $\partial\eta/\partial t$ vanishes in Eq. (2.1) and it reduces to

$$\frac{\partial(Hu)}{\partial x} + \frac{\partial(Hv)}{\partial y} = 0 \qquad (2.4)$$

Assuming further that the displacement η of the free surface is small compared to the stillwater depth h (Figure 1.3) at every point in the flow field, i.e., $\eta << h$, Eq. (2.4) becomes,

$$\frac{\partial(hu)}{\partial x} + \frac{\partial(hv)}{\partial y} = 0 \tag{2.5}$$

where the function h (x,y) represents bottom variations. Eq. (2.5) now contains two unknowns, u and v, and it is independent of the free surface variations η. Therefore, it can be effectively decoupled from Eqs. (2.2) and (2.3) if an additional relation between u and v is available. Another equation in these unknowns is provided by the condition of irrotationality, under the assumption of potential motion, and it reads

$$\frac{\partial u}{\partial y} - \frac{\partial v}{\partial x} = 0 \tag{2.6}$$

for two dimensional flow. Eq. (2.6) implies the existence of a velocity potential function ϕ (x,y) such that

$$u = \frac{\partial \phi}{\partial x} \tag{2.7a}$$

$$v = \frac{\partial \phi}{\partial y} \tag{2.7b}$$

Substituting Eq. (2.7) into Eq. (2.6), and simplifying,

$$\nabla^2 \phi + \frac{h_x}{h} \phi_x + \frac{h_y}{h} \phi_y = 0 \tag{2.8}$$

This equation governs the steady potential motion of the continental shelf waters. It is a linear partial differential equation of second order with variable coefficients h_x/h and h_y/h. Eq. (2.8) brings out clearly the Laplacean operator on the left hand side; and together with the two additional terms it represents a generalized elliptic equation in the plane.

2.3 Steady Potential Motion With Constant Bathymetry

Eq. (2.8) suggests a very attractive simplification, that of constant or flat bottom, for which $h_x = h_y \equiv 0$. The result is Laplace's equation

$$\nabla^2\phi = 0 \tag{2.9}$$

For the present investigation, solutions of Eq. (2.9) which have been studied in detail, must be coupled to the characteristics of the tidal jet. The assumption of constant bathymetry allows the jet characteristics (such as centerline velocity and width) to be expressed in closed form. Clearly, important mathematical simplifications result for the case of constant bathymetry. From the physical viewpoint, a number of tidal inlets display very gradually varying bottom topography and may be treated under the above formulation as a first approximation.

The present work is mainly concerned with, but not limited to, the study of continental shelf circulation for constant bathymetry. A preliminary formulation including the effects of variable topography, unsteadiness, and Earth's rotation is given in Section 6.0.

2.4 Stream Function Formulation Of Steady Potential Motion

The problem formulation presented in the previous section was in terms of a velocity potential ϕ. An equivalent formulation in terms of a stream function ψ is also possible. It may be recalled from elementary fluid mechanics that the curves of constant ϕ are orthogonal to curves of constant ψ everywhere in the flow field. The basic kinematical equations of steady and irrotational motion are, of course, the same as before, viz. Eqs. (2.5) and (2.6). Instead of defining a velocity potential through Eqs. (2.7), a 'modified' stream function is defined as follows.

$$u = -\frac{1}{h}\frac{\partial \psi}{\partial y} \tag{2.10a}$$

$$v = \frac{1}{h}\frac{\partial \psi}{\partial x} \tag{2.10b}$$

Notice that these equations satisfy the continuity Eq. (2.5) identically. Substituting the definitions in Eqs. (2.10a) and (2.10b) into Eq. (2.6), and simplifying, the governing equation for a steady potential motion is

$$\nabla^2 \psi - \frac{h_x}{h}\psi_x - \frac{h_y}{h}\psi_y = 0 \tag{2.11}$$

The similarity between Eqs. (2.11) and (2.8) is readily observed and the comments following the latter equation are equally applicable.

For the special case of constant bathymetry, Eq. (2.11) reduces to a Laplace's equation in ψ, or,

$$\nabla^2 \psi = 0 \tag{2.12}$$

Also, in this case, h drops out of the differentiations in Eq. (2.5), and the modified stream functions in Eqs. (2.10a) and (2.10b) can be replaced by the standard definitions,

$$u = -\frac{\partial \psi}{\partial y} \tag{2.13a}$$

$$v = \frac{\partial \psi}{\partial x} \tag{2.13b}$$

There are now two alternate formulations, one in terms of a velocity potential given by Eqs. (2.9), (2.7a), and (2.7b), and the other in terms of a stream function, represented by Eqs. (2.12), (2.13a), and (2.13b). The selection of one approach

over the other is a matter of convenience of mathematical analysis and interpretation of results. In the present work, it was found useful to employ the stream function formulation to study the constant bathymetry problem. On the other hand, a velocity potential formulation appears to be more meaningful and illuminating for the variable bathymetry case (Section 6.0). The constant bottom topography solutions are discussed first in Sec. 3.0. The coupling between solutions of Eq. (2.13) and the jet characteristics is also discussed in that section.

3.0 STEADY POTENTIAL FLOW WITH CONSTANT BATHYMETRY - THE SIMPLE JET

3.1 Representation of a Tidal Jet By a Sink Distribution

It has been shown in the previous section that the steady potential flow induced by a tidal jet is governed by Laplace's equation (2.12) when the bottom topography is assumed to be constant. From potential theory, it is well-known that Laplace's equation can be solved in terms of elementary solutions which correspond to various physical flow situations (39). In the present investigation, the jet emerges into a body of water which is governed by potential motion, and therefore, only the jet need be represented in terms of elementary solutions. Thus, the treatment of jet-induced circulation reduces to relating the jet characteristics to the elementary solutions. This idea is central to the work described in this report and was originally introduced by Taylor (38) during his study of flow fields induced by steady buoyant plumes. The plume was replaced by a distribution of sink singularities which constitute elementary solutions of Eq. (2.12) and the external motion was assumed to be potential. Following this appoach, the tidal jet was represented by a distribution of sinks along its axis and as outlined before, the surrounding frictionless fluid motion over a constant bottom was treated as potential. Thus the entire flow field satisfies Laplaces equation, except for the jet axis itself.

The representation of the jet by a sink distribution also makes physical sense. It is an observed fact that a tidal jet draws in fluid adjacent to it (Fig. 1.1b), and thus, it effectively acts much like a distribution of sinks. Of course, it is necessary to establish an appropriate correspondence between the parameters that characterize a jet and those which characterize a sink distribution.

This discussion is deferred to Sec. 3.3. Before deriving the mathematical expressions for the jet-induced motion, it is important to briefly review the jet solution. The following section is devoted to that purpose.

3.2 Review Of Jet Solution For Constant Bathymetry

Özsoy (11) has obtained an analytical solution for a two dimensional turbulent jet with bottom friction and arbitrary bathymetry. Figure 3.1 shows the jet configuration considered in Ref. (11). The general expressions for the jet characteristics of interest; namely, core half-width and jet half-width in the zone of flow establishment (ZOFE), and centerline velocity and jet width in the zone of established flow (ZOEF). Whereas the solutions for arbitrary bathymetry must be obtained numerically, closed form solutions can be derived for the special case of constant depth. The solutions are given below.

ZOFE, $\xi < \xi_s$:

$$R(\xi) = \frac{I_1 e^{-\mu\xi} - I_2 (1 + \alpha\xi)}{I_1 - I_2} \tag{3.1}$$

$$B(\xi) = \frac{(1-I_2) (1+\alpha\xi) - (1-I_1) e^{-\mu\xi}}{I_1 - I_2} \tag{3.2}$$

and

ZOEF, $\xi > \xi_s$:

$$U(\xi) = \frac{e^{-\mu\xi}}{\left[e^{-2\mu\xi_s} + \frac{2\alpha I_2}{\mu I_1}\left(e^{-2\mu\xi_s} - e^{-\mu\xi}\right)\right]^{\frac{1}{2}}} \tag{3.3}$$

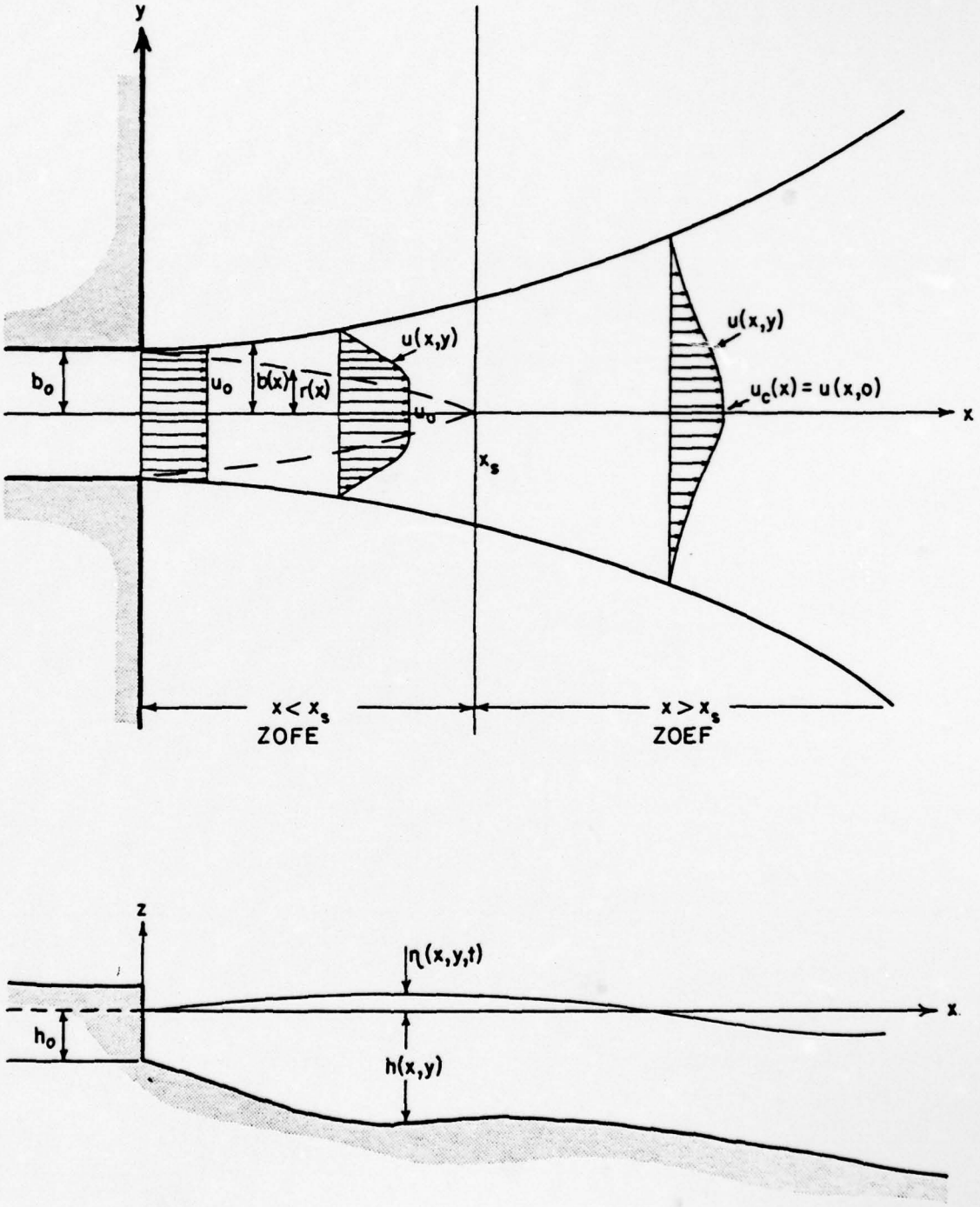

Figure 3.1 Definition Sketch For Shallow Water Jet Flows (Courtesy Ref. (11))

$$B(\xi) = \frac{e^{\mu\xi}}{I_2}\left[e^{-2\mu\xi_s} + \frac{2\alpha I_2}{I_1}\left(e^{-\mu\xi_s} - e^{-\mu\xi}\right)\right] \tag{3.4}$$

where ξ, R, B, and U are offshore distance, core half-width, jet half-width, and centerline velocity, respectively. These quantities are dimensionless and are defined as follows.

$$\xi \equiv x/b_o \tag{3.5}$$

$$R(\xi) = \frac{r}{b_o} \tag{3.6}$$

$$B(\xi) = \frac{b}{b_o} \tag{3.7}$$

$$U(\xi) = \frac{u_c}{u_o} \tag{3.8}$$

Furthermore, μ is a modified friction parameter defined by

$$\mu = \frac{fb_o}{8h_o} \tag{3.9}$$

with f = Darcy-Weisbach friction coefficient. In Eqs. (3.1) - (3.4), $I_1 = 0.450$ and $I_2 = 0.316$. The core length ξ_s is given by the condition $R(\xi) = 0$ in Eq. (3.1).

Eqs. (3.1) - (3.4) reveal that, in the presence of friction, the jet width grows and the centerline velocity decays exponentially at sufficiently large distances away from the inlet as opposed to the linear growth of the classical two-dimensional turbulent jet in which the centerline velocity decays as $\xi^{-\frac{1}{2}}$. As with the classical two dimensional jet, the linear behaviour of the jet width occurs only near the inlet and in the core region. Figure 3.2 illustrates the variations of jet half-width and centerline velocity against distance from the inlet with μ

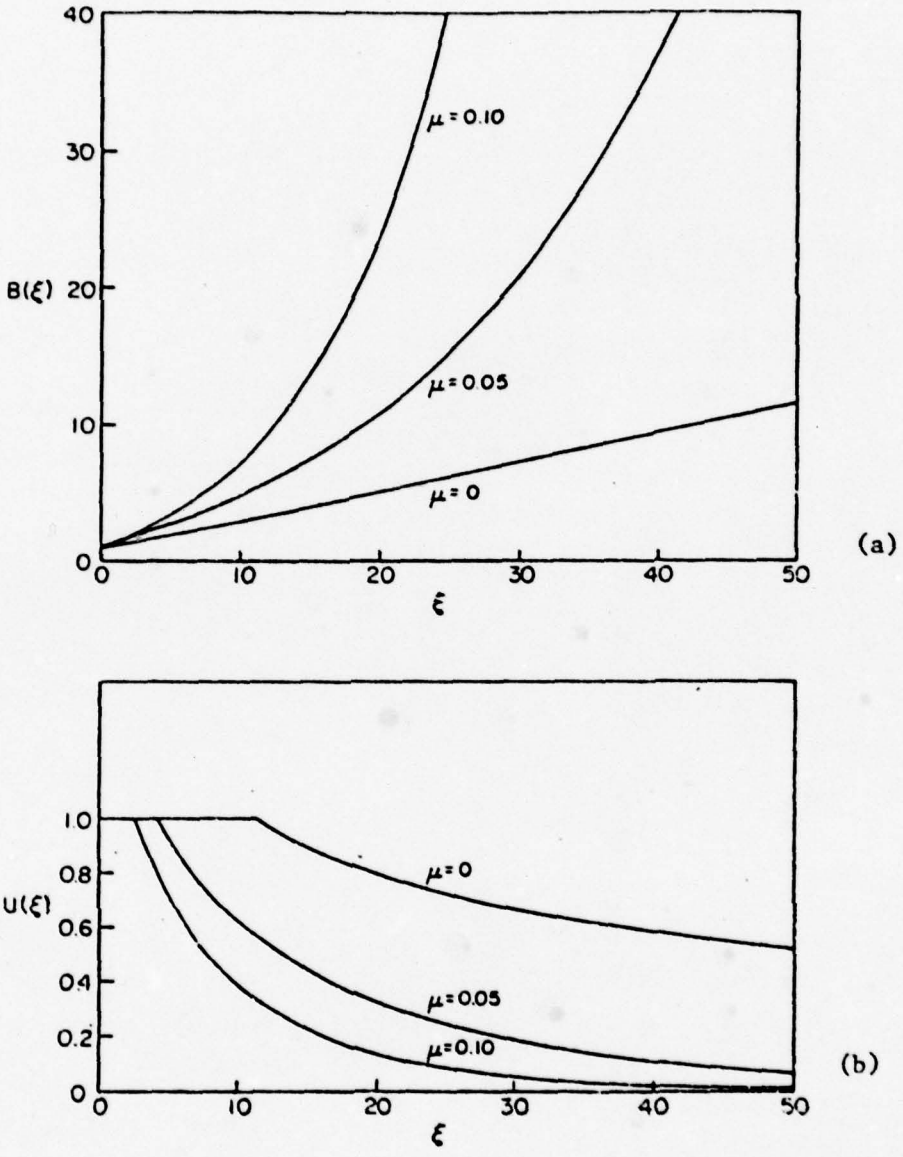

Figure 3.2 Bottom-Frictional Jet Over Constant Bottom (a) Jet Half-width (b) Centerline Velocity (Courtesy Ref. (11))

as a parameter. As seen from Eq. (3.9), μ combines the relative effects of bottom friction and inlet aspect ratio b_o/h_o. When friction is large or the inlet width is large compared to depth, the jet merely explodes as it faces the bottom resistance and loses its momentum. Thus the parameter μ strongly influences the jet characteristics. Reference (39) may be consulted for additional details regarding the jet solution.

The next step is to combine the jet solution with the sink distribution mentioned in the previous section to obtain the jet induced flow field.

3.3 Flow Field Induced By Sink Distribution

Consider a distribution of sinks representing a tidal jet along the positive x-axis in Figure 3.3. In order to make the y-axis a coastline (i.e. a solid boundary) an image distribution must also be introduced as shown.

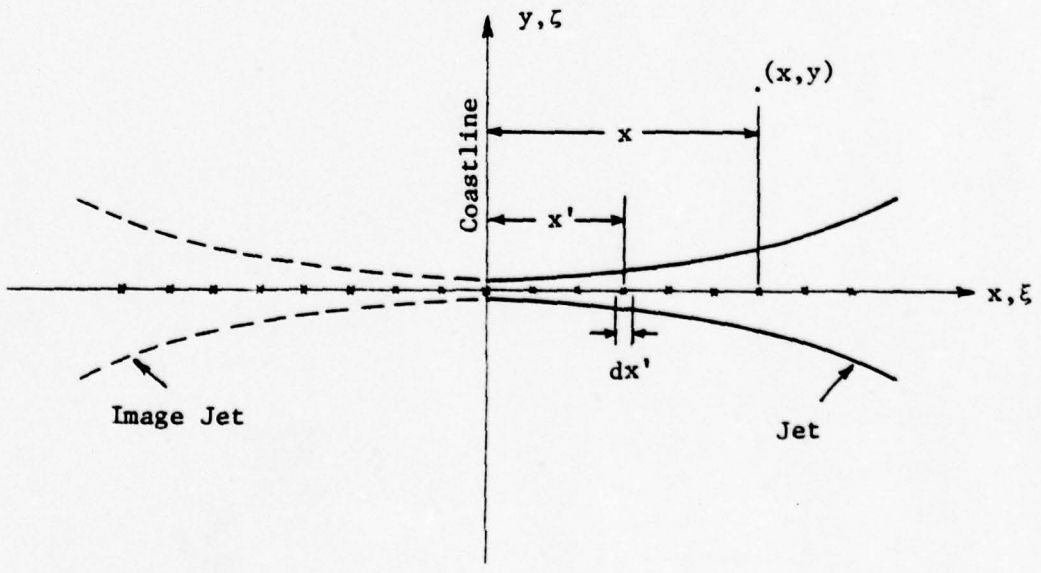

FIGURE 3.3 Sink Distribution for a Simple Jet and Its Image

(x,y) is an arbitrary point in the flow field, and the value of the stream function at (x,y) due to a sink of strength q(x') located at x = x' is given by (39).

$$\psi(x,y) = \frac{q(x')}{2\pi} \tan^{-1} \frac{y}{(x-x')} \tag{3.10}$$

ψ satisfies Laplace's equation (2.12) everywhere in the flow field except at x = x', the location of the sink itself. If the sink strength for the distribution is m(x) per unit length in x direction, then q(x') = m(x')dx' is the strength of an element dx'. Summing the stream function due to all such elements of the distribution, including the jet and its image, the effective stream function at (x,y) is

$$\psi(x,y) = \frac{1}{2\pi} \int_{-\infty}^{\infty} m(x') \tan^{-1} \frac{y}{(x-x')} \, dx' \tag{3.11}$$

The preceding superposition holds due to the linearity of Eq. (2.12). Expressing the integral in Eq. (3.11) as the sum of two integrals,

$$\psi(x,y) = \frac{1}{2\pi} \int_{-\infty}^{0} m(x') \tan^{-1} \frac{y}{(x-x')} \, dx' + \frac{1}{2\pi} \int_{0}^{\infty} m(x') \tan^{-1} \frac{y}{x-x'} \, dx' \tag{3.12}$$

Changing the variable of integration in the first integral on the RHS from x' to -x',

$$\psi(x,y) = \frac{1}{2\pi}\int_0^\infty m(-x')\,\tan^{-1}\frac{y}{x+x'}\,dx' + \frac{1}{2\pi}\int_0^\infty m(x')\,\tan^{-1}\frac{y}{x-x'}\,dx' \tag{3.13}$$

Due to symmetry of the sink distribution about the y-axis,

$$m(-x') = m(x') \tag{3.14}$$

and hence Eq. (3.13) becomes,

$$\psi(x,y) = \frac{1}{2\pi}\int_0^\infty m(x')\left[\tan^{-1}\frac{y}{x+x'} + \tan^{-1}\frac{y}{x-x'}\right]dx' \tag{3.15}$$

Summing the two arctangent functions using standard trigonometric identities, the final expression for the stream function is,

$$\psi(x,y) = \frac{1}{2\pi}\int_0^\infty m(x')\,\tan^{-1}\left[\frac{2xy}{x^2-y^2-x'^2}\right]dx' \tag{3.16}$$

In order to bring the jet characteristics (discussed in the previous section) into the flow field described by ψ, the sink strength $m(x')$ must be related to jet parameters. This is accomplished in the following manner.

Figure 3.4 shows the two-dimensional sink distribution in the horizontal (x,y) and vertical (x,z) planes. Consider an element dx of the distribution located at x.

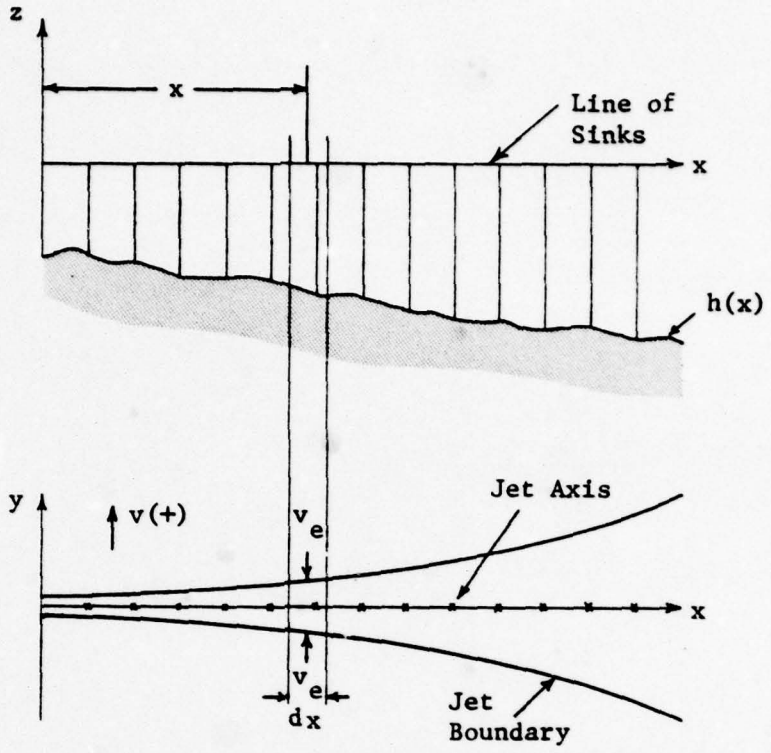

Figure 3.4 Determination of Sink Strength

Volume flow into the element demanded by the sink distribution is

$$dQ_{sink} = [m(x)dx]\ \ h(x) \tag{3.17}$$

Neglecting the second order effects of changes in jet velocity and width over a distance dx, the volume flow into dx due to jet entrainment is given by

$$dQ_{ent} = \Big[v(x,-b(x)) - v(x,b(x))\Big]\Big[h(x)\ dx\Big] \tag{3.18}$$

where v(x,-b) is the component of jet induced velocity in the y direction at y = -b and v(x,b) is similarly defined. Notice that v(x,-b) is positive when directed into the sink whereas v(x,b) is negative under the same conditions. These velocity components at the edge of the jet are referred to as entrainment velocities in the theory of jets. Due to the symmetry of the jet about the x-axis.

$$v(x,-b) = -v(x,b) \tag{3.19}$$

$$\psi(x,y) = \frac{U_\infty}{\pi}\int_0^{2\pi} u_\beta(x') \tan^{-1}\left[\frac{2xy}{x^2+y^2-x'^2}\right] dx' \tag{3.24}$$

It is useful to express Eq. (3.24) in the nondimensional form

$$\psi(\xi,\eta) = \frac{U_\infty}{\pi}\int_0^{2\pi} u(\xi') \tan^{-1}\left[\frac{2\xi\eta}{\xi^2+\eta^2-\xi'^2}\right] d\xi' \tag{3.25}$$

Since one needs to solve the flow field only for $y > 0$ (or $y < 0$), combining Eqs. (3.18) and (3.19) yields

$$\begin{aligned} dQ_{ent} &= -2v(x,b)h(x)dx, \quad y > 0 \\ &= 2v(x,-b)h(x)dx, \quad y < 0 \end{aligned} \tag{3.20}$$

If $v(x,-b) = v_e$, so that $v(x,b) = -v_e$, where v_e is the magnitude of entrainment velocity,

$$dQ_{ent} = 2v_e h(x)dx \quad \text{for all } y \tag{3.21}$$

Equating the entrainment volume flow to the sink inflow in Eqs. (3.21) and (3.17),

$$m(x) = 2v_e(x) \tag{3.22}$$

Since $h(x)$ has cancelled out throughout, Eq. (3.22) is applicable for the variable bathymetry case also. Now, following the standard procedure in turbulent shear flows, the entrainment velocity is related to the centerline velocity of the jet through an entrainment coefficient, i.e.,

$$v_e(x) = \alpha u_c(x) \tag{3.23}$$

where α is the entrainment coefficient. Substituting Eqs. (3.22) and (3.23) into Eq. (3.16),

$$\psi(x,y) = \frac{\alpha}{\pi}\int_0^\infty u_c(x') \tan^{-1}\left[\frac{2xy}{x^2-y^2-x'^2}\right] dx' \tag{3.24}$$

It is useful to express Eq. (3.24) in the nondimensional form

$$\Psi(\xi,\zeta) = \frac{\alpha}{\pi}\int_0^\infty U(\xi') \tan^{-1}\left[\frac{2\xi\zeta}{\xi^2-\zeta^2-\xi'^2}\right] d\xi' \tag{3.25}$$

where

$$\xi = \frac{x}{b_o}$$

$$\xi' = \frac{x'}{b_o}$$

$$\zeta = \frac{y}{b_o} \tag{3.26}$$

$$U = \frac{u_c}{u_o}$$

$$\Psi = \frac{\psi}{u_o b_o}$$

with u_o, b_o denoting the inlet throat velocity and inlet half-width respectively.

From the stream function in Eq. (3.25), the velocity field can be obtained by the partial differentiation

$$u = -\frac{\partial \psi}{\partial y} \quad \text{or} \quad \hat{U} = -\frac{\partial \Psi}{\partial \zeta} \tag{3.27a}$$

$$v = \frac{\partial \psi}{\partial x} \quad \text{or} \quad \hat{V} = \frac{\partial \Psi}{\partial \xi} \tag{3.27b}$$

giving the following results:

$$\hat{U}(\xi,\zeta) = \frac{2}{\pi}\alpha\xi \int_0^\infty U(\xi') \frac{(\xi'^2-\zeta^2-\xi^2)}{(\xi'^2-\zeta^2-\xi^2)^2 + 4\xi'^2\zeta^2}\, d\xi' \tag{3.28}$$

$$\hat{V}(\xi,\zeta) = -\frac{2}{\pi}\alpha\zeta \int_0^\infty U(\xi') \frac{(\xi^2+\zeta^2+\xi'^2)}{(\xi^2+\zeta^2+\xi'^2)^2 - 4\xi^2\xi'^2}\, d\xi' \tag{3.29}$$

Recall from the discussions in Sec. 3.2 that the dimensionless jet centerline velocity $U(\xi)$ in Eqs. (3.25), (3.28), and (3.29) is given by

$$U(\xi) = 1, \quad \xi < \xi_s \tag{3.30a}$$

in ZOFE and by

$$U(\xi) = \frac{e^{-\mu\xi}}{\left[e^{-2\mu\xi_s} + \frac{2\alpha I_2}{\mu I_1}\left(e^{-2\mu\xi_s} - e^{-\mu\xi}\right)\right]^{\frac{1}{2}}}, \quad \xi > \xi_s \tag{3.30b}$$

in ZOEF.

The entrainment coefficient α in the above equations has been quoted by Özsoy (11) from the experimental results of Abramovich (13). The value of α is

$$\alpha = \alpha_1 = 0.036, \quad \xi < \xi_s \tag{3.31a}$$

in the ZOFE, and

$$\alpha = \alpha_2 = 0.050, \quad \xi > \xi_s \tag{3.31b}$$

in the ZOEF.

In summary, the jet-induced steady potential flow in the presence of a constant bathymetry is described by Eq. (3.25) and Eqs. (3.28) through (3.31b). The actual evaluation and computation of Ψ, $\hat{U}$, and $\hat{V}$ is discussed in the following two sections.

3.4 Analytical Treatment Of Solutions For Ψ, $\hat{U}$, and $\hat{V}$

Eqs. (3.25) and (3.28) through (3.31b) show that they involve complicated integrals which cannot be evaluated by purely analytical means. Prior to undertaking a fully numerical evaluation, however, it is useful to investigate whether the integrals in Eqs. (3.25), (3.28), and (3.29) can be treated analytically,

at least in the core region, where the centerline velocity is a constant (Eq. (3.30a)). This approach has the advantages of giving some insight into the solution behavior and also providing a check on the accuracy of numerical solutions.

Using Eqs. (3.30) and (3.31), one can express the integrals in Eqs. (3.25), (3.28), and (3.29) as follows.

$$\Psi = \Psi_o + \Psi_r \tag{3.32}$$

$$\hat{U} = \hat{U}_o + \hat{U}_r \tag{3.33}$$

$$\hat{V} = \hat{V}_o + \hat{V}_r \tag{3.34}$$

where

$$\Psi_o(\xi,\zeta) = \frac{\alpha_1}{\pi}\int_0^{\xi_s} \tan^{-1}\left[\frac{2\xi\zeta}{\xi^2-\zeta^2-\xi'^2}\right] d\xi' \tag{3.35a}$$

$$\Psi_r(\xi,\zeta) = \frac{\alpha_2}{\pi}\int_{\xi_s}^{\infty} U(\xi') \tan^{-1}\left[\frac{2\xi\zeta}{\xi^2-\zeta^2-\xi'^2}\right] d\xi' \tag{3.35b}$$

$$\hat{U}_o(\xi,\zeta) = \frac{2}{\pi}\alpha_1\xi\int_0^{\xi_s} \frac{(\xi'^2-\zeta^2-\xi^2)}{(\xi'^2-\zeta^2-\xi^2)^2 + 4\xi'^2\zeta^2}\, d\xi' \tag{3.36a}$$

$$\hat{U}_r(\xi,\zeta) = \frac{2}{\pi}\alpha_2\xi\int_{\xi_s}^{\infty} U(\xi') \frac{(\xi'^2-\zeta^2-\xi^2)}{(\xi'^2-\zeta^2-\xi^2)^2 + 4\xi'^2\zeta^2}\, d\xi' \tag{3.36b}$$

$$\hat{V}_o(\xi,\zeta) = -\frac{2}{\pi}\alpha_1\zeta\int_0^{\xi_s} \frac{(\xi^2+\zeta^2+\xi'^2)}{(\xi^2+\zeta^2+\xi'^2)^2 - 4\xi^2\xi'^2}\, d\xi' \tag{3.37a}$$

$$\hat{V}_r(\xi,\zeta) = -\frac{2}{\pi}\alpha_2\zeta\int_{\xi_s}^{\infty} U(\xi') \frac{(\xi^2+\zeta^2+\xi'^2)}{(\xi^2+\zeta^2+\xi'^2)^2 - 4\xi^2\xi'^2}\, d\xi' \tag{3.37b}$$

In Eqs. (3.35b), (3.36b), and (3.37b), $U(\xi)$ is given by Eq. (3.30b). It will now be demonstrated that the integrals in Eqs. (3.35a), (3.36a), and (3.37a) can be integrated in closed form.

First consider Eq. (3.35a). Integrating once by parts and rearranging the denominator of the resulting integrand, it may be verified that

$$\frac{\pi\Psi_o}{\alpha_1} = \xi' \tan^{-1}\left[\frac{2\xi\zeta}{\xi^2-\zeta^2-\xi'^2}\right]\Bigg|_0^{\xi_s} - 4\xi\zeta\int_0^{\xi_s} \frac{\xi'^2\, d\xi'}{a\xi'^4 + b\xi'^2 + c} \tag{3.38a}$$

with

$$a = 1,\ b = -2(\xi^2-\zeta^2),\ c = (\xi^2+\zeta^2) \tag{3.38b}$$

Note that the descriminant

$$\begin{aligned} A &= b^2-4ac \\ &= 4(\xi^2-\zeta^2)^2 - 4(\xi^2+\zeta^2)^2 \\ &= -16\xi^2\zeta^2 \end{aligned} \tag{3.39}$$

Thus, $A < 0$ for all $\xi \neq 0$ and $\zeta \neq 0$

and $A = 0$ if $\xi = 0$

Notice that the case $\zeta = 0$ is excluded from the present considerations because the solution is not expected to be valid at the sink distribution inself. Thus, there are two possible cases.

Case I: $\xi = 0$ with $\zeta \neq 0$, i.e., the coastline

In this case A = 0 as seen in Eq. (3.39), and the integral in Eq. (3.38a) can be evaluated to yield (see Ref. 40),

$$\frac{\pi\Psi_o}{\alpha_1} = \xi_s \lim_{\xi\to 0}\left[\tan^{-1}\left\{\frac{2\xi\zeta}{\xi^2-\zeta^2-\xi_s^2}\right\}\right]$$

$$-\lim_{\xi\to 0}\left[4\xi\zeta\left\{-\frac{\xi_s}{2(\zeta^2+\xi_s^2)}+\frac{1}{2\zeta}\tan^{-1}\left\{\frac{\xi_s}{\zeta}\right\}\right\}\right]$$

Carrying out the indicated limit, the second term goes to zero and the first term approaches π. Therefore,

$$\frac{\pi\Psi_o}{\alpha_1} = \pi\xi_s$$

or

$$\Psi_o = \alpha_1\xi_s \tag{3.40}$$

Eq. (3.40) shows that along the coastline Ψ_o has a constant value.

Case II: $\xi \neq 0$ and $\zeta \neq 0$, i.e., an interior point in the flow field

For A < 0 in Eq. (3.39), defining the indefinite integral in Eq. (3.39a) as I_3,

$$I_3 = \int \frac{\xi'^2 d\xi'}{a\xi'^4 + b\xi'^2 + c}$$

It can be shown (Ref. (40)) that,

$$I_3 = \frac{1}{8ak\cos\frac{\varepsilon}{2}} \log\left[\frac{\xi'^2 - 2k\xi'\cos\frac{\varepsilon}{2} + k^2}{\xi'^2 + 2k\xi'\cos\frac{\varepsilon}{2} + k^2}\right] + \frac{1}{4ak\sin\frac{\varepsilon}{2}} \arctan\left[\frac{2k\xi'\sin\frac{\varepsilon}{2}}{k^2 - \xi'^2}\right]$$

$$\text{in which } k = \left(\frac{c}{a}\right)^{1/4}, \quad \cos\varepsilon = -\frac{b}{2\sqrt{ac}}$$

Combining the above expression with Eqs. (3.38a) and (3.38b), it can be shown upon simplification that

$$\frac{\pi\Psi_o}{\alpha_1} = \xi_s \tan^{-1}\left[\frac{2\xi\zeta}{\xi^2-\zeta^2-\xi_s^2}\right]$$

$$\mp \frac{\zeta}{2} \ln\left[\frac{\xi_s^2 \mp 2\xi\xi_s + (\xi^2+\zeta^2)}{\xi_s^2 \pm 2\xi\xi_s + (\xi^2+\zeta^2)}\right]$$

$$\mp \xi \tan^{-1}\left[\frac{\pm 2\xi_s\zeta}{\xi^2 + \zeta^2 - \xi_s^2}\right] \qquad (3.41)$$

For a selected point $\xi = \xi_s$ and $\zeta = 1$ in the flow field, it may be verified that Eq. (3.41) reduces (after considering all possible combinations of signs) to

$$\frac{\pi\Psi_o}{\alpha_1} = \frac{1}{2}\ln(4\xi_s^2 + 1) + \xi_s \tan^{-1}\left[\frac{4\xi_s}{4\xi_{s_s}^2 - 1}\right] \qquad (3.42)$$

Now consider Eq. (3.36a) which may be written in the form

$$\frac{-\pi\hat{U}_o}{2\alpha_1\xi} = \int_0^{\xi_s} \frac{(\xi^2+\zeta^2) - \xi'^2}{(\xi^2+\zeta^2-\xi'^2)^2 - 4\xi^2\xi'^2}\, d\xi' \qquad (3.43)$$

[illegible]

$$[\text{illegible}] \tag{illegible}$$

[illegible]

$$[\text{illegible}] \tag{illegible}$$

[illegible]

$$[\text{illegible}] \tag{illegible}$$

[illegible]

$$\psi_0(\xi,\zeta) = -\frac{\alpha_1}{\pi}\,\coth^{-1}\left[\frac{2\xi\xi_s}{\xi^2+\zeta^2+\xi_s^2}\right] \tag{3.45}$$

Finally, consider Eq. (3.37a) which may be written as

$$\frac{\partial\psi_0}{\partial\alpha_1\zeta} = \int_0^\infty \frac{\xi^2+\zeta^2+\xi'^2}{(\xi^2+\zeta^2-\xi'^2)^2 + 4\zeta^2\xi'^2} \tag{3.46a}$$

This equation is in the same form as Eq. (3.44a) with

$$a = 2\zeta,\ b = \xi^2+\zeta^2,\ \text{and}\ c = -1 \tag{3.46b}$$

Thus, the integral in Eq. (3.46a) can be evaluated using Eqs. (3.44c) and (3.46b) to yield,

$$\hat{V}_o(\xi,\zeta) = -\frac{\alpha_1}{\pi} \tan^{-1}\left[\frac{2\zeta\xi_s}{\xi^2+\zeta^2-\xi_s^2}\right] \tag{3.47}$$

The analytical solutions in Eqs. (3.42), (3.45), and (3.47) were employed to verify the correctness and accuracy of the numerical integration scheme described in the next section.

3.5 Development of Numerical Procedure for Evaluation of Ψ, $\hat{U}$, and $\hat{V}$

A Gauss-Legendre numerical quadrature procedure (41) was used to evaluate the complete integrals in Eqs. (3.25), (3.28), and (3.29). This method has an important advantage over the straight-forward summation approach in that it is extremely efficient from the viewpoint of computation. The method consists of evaluating the integrand at selected special points (the zeros of Legendre polynomials), multiplying by appropriate weighting factors, and summing the resulting values. In the present work, sufficient accuracy was achieved by selecting only 10 zeros, whereas a straightforward summation would require a large number (at least 50) of equi-spaced base points. Therefore, the Gauss-Legendre scheme results in a significant saving of computation time.

The application of the proposed numerical scheme requires that the integrals in Eqs. (3.25), (3.28), and (3.29) be converted to limits -1 to 1. First, the upper limit of ∞ in these integrals was replaced by 51 ξ_s so that the integration extends to 50 core lengths. In view of the exponential decay of the jet center-line velocity in Eq. (3.30b), this range of upper limit was considered sufficient. Next, each integral was subdivided into 6 integrals (0 to ξ_s, ξ_s to 11 ξ_s, etc., up to 51 ξ_s) and the numerical scheme was applied to each sub-interval.

This subdivision helped to avoid any loss of resolution that may result from converting the entire domain (0 to $51\xi_s$, or a large part thereof) to (-1, 1). The preceding manipulations are discussed in detail below.

As an example consider the integral for Ψ in Eq. (3.25) which may be written as the sum

$$\Psi(\xi,\zeta) = \sum_{n=0}^{6} \Psi_n(\xi,\zeta) \tag{3.48}$$

where Ψ_o is given by Eq. (3.35a) and

$$\Psi_n(\xi,\zeta) = \frac{\alpha_2}{\pi}\int_{(10n-9)\xi_s}^{(10n+1)\xi_s} U(\xi') \tan^{-1}\left[\frac{2\xi\zeta}{\xi^2-\zeta^2-\xi'^2}\right] d\xi'$$

$$\text{for } n = 1, 2, .., 5 \tag{3.49}$$

Similar relations may be defined for Eqs. (3.28) and (3.29). The quadrature is illustrated for Eqs. (3.35a) and (3.49) in this section. First consider Eq. (3.35a) and define a new variable

$$\theta_o = 2\frac{\xi'}{\xi_s} - 1 \tag{3.50a}$$

or

$$\xi'(\theta_o) = \frac{\xi_s}{2}(1 + \theta_o) \tag{3.50b}$$

Changing the variable of integration ξ' to θ_o in Eq. (3.35a) one obtains

$$\Psi_o(\xi,\zeta) = \frac{\alpha_1\xi_s}{2\pi}\int_{-1}^{1} \tan^{-1}\left[\frac{2\xi\zeta}{\xi^2-\zeta^2-\{\xi'(\theta_o)\}^2}\right] d\theta_o \tag{3.51}$$

This form of Eq. (3.51) permits the integration to be expressed as

$$\Psi_o(\xi,\zeta) = \frac{\alpha_1 \xi_s}{2\pi} \sum_{i=1}^{N} W_i \, G_i(\theta_{o_i}) \tag{3.52a}$$

where

$$G_1(\theta_{o_i}) = \tan^{-1}\left[\frac{2\xi\zeta}{\xi^2-\zeta^2-\{\xi'(\theta_{o_i})\}^2}\right] \tag{3.52b}$$

In Eq. (3.52a) θ_{o_i} denotes a zero of the Legendre polynomial and W_i is the corresponding weighting factor. N is the total number of zeros in the interval (-1, 1) and its choice depends on the accuracy desired. Returning now to the remaining integrals in Eq. (3.49), a series of variables of integration is introduced as follows.

$$\theta_n = \frac{1}{5}\left[\frac{\xi'}{\xi_s} + (4-10n)\right], \quad n = 1, 2, .., 5 \tag{3.53a}$$

Or

$$\xi'(\theta_n) = \left[5\theta_n - (4-10n)\right]\xi_s, \; n = 1, 2, .., 5 \tag{3.53b}$$

The integrals Ψ_n then become,

$$\Psi_n(\xi,\zeta) = \frac{5\alpha_2 \xi_s}{\pi} \int_{-1}^{1} U\left[\xi'(\theta_n)\right] \tan^{-1}\left[\frac{2\xi\zeta}{\xi^2-\zeta^2-\{\xi'(\theta_n)\}^2}\right] d\theta_n \tag{3.54}$$

which can be integrated to give

$$\Psi_n(\xi,\zeta) = \frac{5\alpha_2 \xi_s}{\pi} \sum_{i=1}^{N} W_i \; U\left[\xi'(\theta_{n_i})\right] G_1(\theta_{n_i}), \; n = 1, 2, .., 5 \tag{3.55}$$

where the function G_1 is defined by Eq. (3.52b). Following the above procedures

the integrals in Eqs. (3.28) and (3.29) can also be evaluated by means of the Gauss-Legendre method. Thus

$$\hat{U}\ (\xi,\zeta) = \sum_{n=U}^{6} \hat{U}_n \tag{3.56a}$$

with

$$\hat{U}_o(\xi,\zeta) = \frac{\alpha_1 \xi \zeta_s}{\pi} \sum_{i=1}^{N} W_i\ G_2\{\xi'(\theta_{o_i})\} \tag{3.56b}$$

and

$$\hat{U}_n(\xi,\zeta) = \frac{10\alpha_2 \xi \xi_s}{\pi} \sum_{i=1}^{N} W_i U\left[\xi'(\theta_{n_i})\right]\ G_2\{\xi'(\theta_{n_i})\},$$

$$n = 1, 2, .., 5 \tag{3.56c}$$

where

$$G_2\left[\xi'(\theta_{n_i})\right] = \frac{\{\xi'(\theta_{n_i})\}^2 - \zeta^2 - \xi^2}{\left[\{\xi'(\theta_{n_i})\}^2 - \zeta^2 - \xi^2\right]^2 + 4\zeta^2\{\xi'(\theta_{n_i})\}^2} \tag{3.56d}$$

Similarly,

$$\hat{V}(\xi,\zeta) = \sum_{n=0}^{6} \hat{V}_n \tag{3.57a}$$

with

$$\hat{V}_o(\xi,\zeta) = -\frac{\alpha_1 \zeta \xi_s}{\pi} \sum_{i=1}^{N} W_i G_3\ \{\xi'(\theta_{o_i})\} \tag{3.57b}$$

and

$$\hat{V}_n(\xi,\zeta) = -\frac{10\alpha_2\zeta\xi_s}{\pi}\sum_{i=1}^{N} W_i\, U\left[\xi'(\theta n_i)\right] G_3\, \xi'(\theta_{n_i}) \,,$$

$$n = 1, 2, .., 5 \qquad (3.57c)$$

where

$$G_3\left[\xi'(\theta_{n_i})\right] = \frac{\xi^2+\zeta^2+\{\xi'(\theta_{n_i})\}^2}{\left[\xi^2+\zeta^2+\{\xi'(\theta_{n_i})\}^2\right]^2 - 4\xi^2\{\xi'(\theta_{n_i})\}^2} \qquad (3.57d)$$

To summarize, the formulas in Eqs. (3.52a), (3.55), (3.56a) through (3.56d), and (3.57a) through (3.57d) were used for numerical computation of Ψ, $\hat{U}$, $\hat{V}$ in the flow field. The actual computational procedure is described in the next section.

3.6 Computational Sequence and Procedure

An efficient computational algorithm was written to calculate Ψ, $\hat{U}$ and $\hat{V}$ at various points (ξ,ζ) of the flow field. Typically, the computations were performed in the following sequence.

(1) For a given inlet the friction parameter μ was calculated from Eq. (3.9).

(2) The core length ξ_s was computed for the above value of μ. Recall that ξ_s is given as a solution of the condition $R(\xi_s) = 0$ in Eq. (3.1), i.e.,

$$I_1\, e^{-\mu\xi_s} - I_2(1+\alpha\xi_s) = 0 \qquad (3.58a)$$

ξ_s was obtained from this transcendental equation by a Newton-Raphson interaction. For the special case of $\mu = 0$, ξ_s is given by

$$\xi_s = \frac{(I_1-I_2)}{I_2\alpha} \qquad (3.58b)$$

(3) As mentioned earlier, 10 zeros of Legendre polynomials were chosen and $\xi'(\theta_{n_i})$ were computed for n = 0, 1, ..., 5 from Eqs. (3.50b) and (3.53b). These values and their squares were stored.

(4) $U\{\xi'(\theta_{n_i})\}$, n = 1, 2, .., 5, values were calculated from Eq. (3.3) using the values of ξ' obtained in the previous step. These values were also stored.

(5) The computation of the jet-induced flow field was then begun by choosing a point (ξ,ζ). The usual practice was to start at the origin and to proceed along the coastline (ξ=0) at selected intervals of ζ up to ζ=200 (typically). Then, another value of ξ was chosen and flow field computations were performed at the same values of ζ. These calculations were carried out for offshore distances of up to $51\xi_s$. The details of this procedure are presented below.

(6) Using the values of $\xi'(\theta_{n_i})$, $U\{\xi'(\theta_{n_i})\}$, and (ξ,ζ) from steps (3), (4), and (5) respectively, the functions G_1, G_2, and G_3 were calculated from Eqs. (3.52b), (3.56d), and (3.57d) respectively, for each zero of the Legendre polynomial. In Eq. (3.52b), the numerator and denominator were computed separately for the argument of the inverse tangent. The value of $\tan^{-1}$ was established by following an appropriate convention to account for its multiplicity w.r.t π.

(7) G_1, G_2, and G_3 were then multiplied by appropriate constants appearing in Eqs. (3.52a) & (3.55); (3.56b) & (3.56c); and (3.57b) & (3.57c) respectively. These functions were summed over the 10 zeros for each of the 6 sub-integrals. Finally, summation was performed over the 6 sub-integrals to obtain the values of Ψ, $\hat{U}$, and $\hat{V}$ at point (ξ,ζ) in the flow field.

The above numerical scheme was verified by the values computed from Eqs. (3.52a), (3.56b), and (3.57b) against the analytical results of Eqs. (3.42), (3.45), and (3.47) respectively. Good agreement was found.

4.0 POTENTIAL FLOW WITH CONSTANT BATHYMETRY - OTHER CONFIGURATIONS OF INTEREST

4.1 Jet With A Jetty

As outlined in Sec. 1.3, the analysis for a simple jet presented in the previous section can be readily extended to treat other configurations of tidal jets and river mouths as well (Fig. 1.2). A few examples are given here. Figure 4.1 shows a jet flowing normal to the coastline through a jetty of length 'a'. The jet is replaced by an equivalent sink distribution starting from the point x = a. Also shown is the image sink distribution with respect to the y-axis which must be a solid boundary.

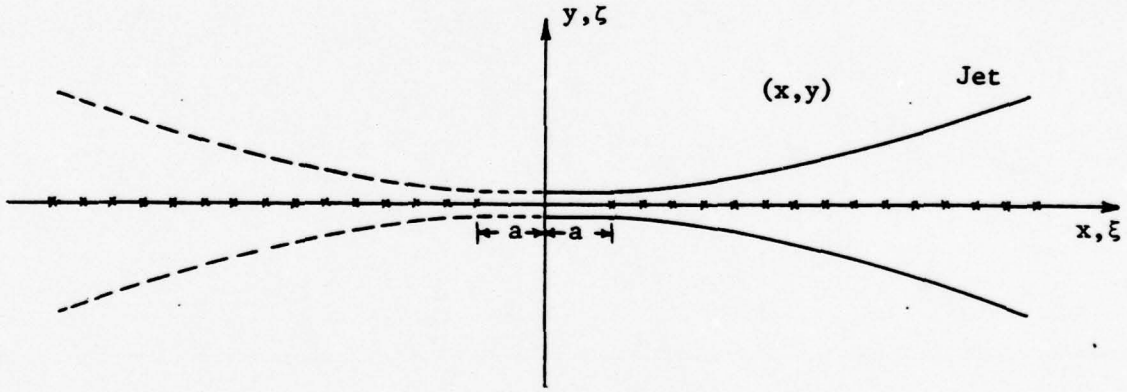

Figure 4.1 Sink Distribution for a Jet with a Jetty and Its Image

The stream function $\psi(x,y)$ at any point in the flow field due to the entire sink distribution can be obtained following the method of Sec. 3.3. The final result is Eq. (3.16) with the lower limit 'a' instead of zero. Thus,

$$\psi(x,y) = \frac{1}{2\pi} \int_a^\infty m(x') \tan^{-1}\left[\frac{2xy}{x^2-y^2-x'^2}\right] dx' \tag{4.1}$$

The sink strength m(x) is also determined on the same lines as in Sec. 3.3 (so that Eq. (3.22) holds), except that the entrainment velocity is now given by

$$v_e(x) = \alpha u_c(x-a) \tag{4.2}$$

since the jet mixes with the surrounding fluid at x=a. Combining Eqs. (4.1), (4.2), and (3.22) the expression for ψ is

$$\psi(x,y) = \frac{\alpha}{\pi} \int_a^\infty u_c(x'-a) \tan^{-1}\left[\frac{2xy}{x^2-y^2-x'^2}\right] dx' \tag{4.3}$$

Introducing dimensionless parameters defined by Eq. (3.26), the above relation transforms to

$$\Psi(\xi,\zeta) = \frac{\alpha}{\pi} \int_A^\infty U(\xi'-A) \tan^{-1}\left[\frac{2\xi\zeta}{\xi^2-\zeta^2-\xi'^2}\right] d\xi' \tag{4.4}$$

where $A = a/b_o$.

The corresponding velocity field is derived from Eqs. (3.27a) and (3.27b) to be

$$\hat{U}(\xi,\zeta) = \frac{2\alpha}{\pi} \xi \int_A^\infty U(\xi'-A) \frac{(\xi'^2-\zeta^2-\xi^2)}{(\xi'^2-\zeta^2-\xi^2)^2 + 4\xi'\zeta^2} d\xi' \tag{4.5}$$

$$\hat{V}(\xi,\zeta) = -\frac{2\alpha}{\pi} \zeta \int_A^\infty U(\xi'-A) \frac{(\xi^2+\zeta^2+\xi'^2)}{(\xi^2+\zeta^2+\xi'^2)^2 - 4\xi^2\xi'^2} d\xi' \tag{4.6}$$

Eqs. (4.4), (4.5), and (4.6) completely describe the flow field induced by a jet with a jetty.

For convenience of numerical integration, the expressions for Ψ, $\hat{U}$, and $\hat{V}$ may be written as

$$\Psi(\xi,\zeta) = \frac{\alpha}{\pi} \int_0^\infty U(\xi') \tan^{-1}\left[\frac{2\xi\zeta}{\xi^2-\zeta^2-(\xi'+A)^2}\right] d\xi' \tag{4.7}$$

$$\hat{U}(\xi,\zeta) = \frac{2\alpha}{\pi} \xi \int_0^\infty U(\xi') \frac{(\xi'+A)^2-\zeta^2-\xi^2}{\{(\xi'+A)^2-\zeta^2-\xi^2\}^2 + 4(\xi'+A)^2\zeta^2} d\xi' \tag{4.8}$$

$$\hat{V}(\xi,\zeta) = -\frac{2\alpha}{\pi} \zeta \int_0^\infty U(\xi') \frac{\xi^2+\zeta^2+(\xi'+A)^2}{\{\xi^2+\zeta^2+(\xi'+A)^2\}^2 - 4\xi^2(\xi'+A)^2} d\xi' \tag{4.9}$$

where $U(\xi')$ is defined by Eqs. (3.30a) and (3.30b) and α is given by Eqs. (3.31a) and (3.31b). Numerical evaluation of the integrals in Eqs. (4.7), (4.8), and (4.9) was performed according to the procedures in Secs. 3.5 and 3.6 with ξ' replaced by $(\xi'+A)$ in Eqs. (3.52b), (3.56d), and (3.57d). Computational results for this case are presented in Sec. 5.2.

4.2 Parallel Jets

To examine the shelf circulation patterns induced by multiple inlets, consider two jets (without jetties) perpendicular to the coastline and separated by a distance 'ℓ' (Figure 4.2). For simplicity, the jets considered are identical in that they have the same inlet dimensions, throat velocities, and inlet depth. It is assumed that the interaction between the two jets is weak, i.e., the influence of pressure gradients set up by either jet on

the other is neglected. Furthermore, the entrainment hypothesis for a simple jet must be modified to accommodate the case of two jets. Since the simple jet is symmetric about the x-axis, the magnitude of the entrainment velocity, v_e, is the same on both jet boundaries (Eq. (3.19)). With the introduction of another jet, the fluid in between the jets must be 'shared' by both jets at their inner boundaries, whereas an infinite expanse of fluid is available on the outer boundaries of the jet. Consequently, the mass entrainment is expected to be smaller at the inner boundaries than at the outer boundaries. The jet entrainment was therefore modified as follows.

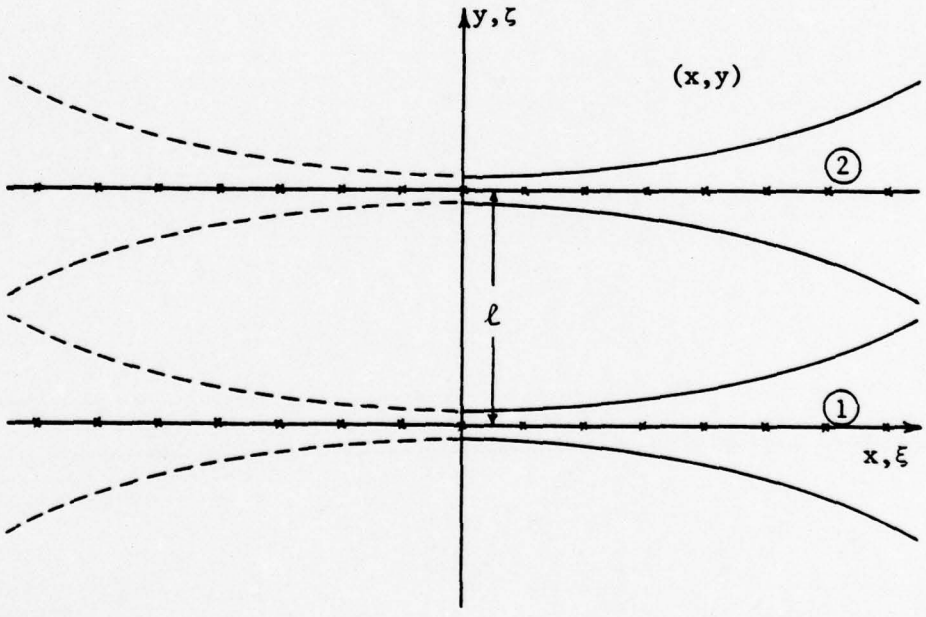

Figure 4.2 Sink Distribution for Two Parallel Jets

It is a standard procedure in the classical jet theory to integrate the depth-averaged continuity equation, Eq. (2.5), across the width of the jet to obtain (also consult Ref. 11),

$$\frac{d}{dx}\left(h\int_{-b}^{b} u\,dy\right) = -\,hv\,\Big|_{-b}^{b} \tag{4.10}$$

$$= hv(x,-b) - hv(x,b) \tag{4.11}$$

$$= 2hv_e \tag{4.12}$$

from Eq. (3.19). Eq. (4.12) is then solved simultaneously with the momentum equation, also integrated across the jet width. This equation, however, does not contain any terms in v_e and need not be considered here. If both sides of Eq. (4.12) are multiplied by the density ρ (a constant), it expresses the fact that the gradient of mass flow rate along the x-axis equals the total (i.e. both boundaries) entrainment rate per unit length across the x-axis. This is simply a statement of conservation of mass and it must hold for the individual jets in Figure 4.2 as well. Therefore, considering the lower jet as an example, Eq. (4.11) is still valid, but the entrainment velocities v(x,-b) and v(x,b) are different. At this point, due to the lack of experimental entrainment data for the two jets configuration, it is assumed that the total mass flow rate is the same as that for a simple jet. In other words, the drop in entrainment on the inner boundary equals the increase in entrainment on the other boundary. Thus, in Eq. (4.11),

$$v(x,-b) = v_e+\delta \tag{4.13a}$$

$$v(x,b) = -(v_e-\delta) \tag{4.13b}$$

where v_e is the entrainment velocity for a simple jet. Substituting Eqs. (4.13a) and (4.13b) into Eq. (4.11), Eq. (4.12) is recovered. The change in entrainment velocity δ obviously depends upon the relative strengths (such as inlet velocity, width, etc.) of the two jets. In the example of Figure 4.2, however, the jets are assumed to have equal strengths for simplicity.

Consider the two jets and their images as shown in Figure 4.2. For the lower jet, denoted by subscript 1, Eq. (3.25) gives the expression for the stream function,

$$\Psi_1(\xi,\eta) = \frac{\alpha}{\pi}\int_0^\infty U(\xi') \tan^{-1}\left[\frac{2\xi\zeta}{\xi^2-\zeta^2-\xi'^2}\right]d\xi' \tag{4.14}$$

A similar expression can be written for the upper jet (i.e., jet 2), where ζ must be replaced by $(\zeta-L)$ since the x-axis is located along the centerline of jet 1. Thus,

$$\Psi_2(\xi,\eta) = \frac{\alpha}{\pi}\int_0^\infty U(\xi') \tan^{-1}\left[\frac{2\xi(\zeta-L)}{\xi^2-(\zeta-L)^2-\xi'^2}\right]d\xi' \tag{4.15}$$

Notice that both Eqs. (4.14) and (4.15) contain the same centerline velocity $U(\xi)$ since the two jets are identical. The combined effect of two jets at any point (ξ,ζ) in the flow field is obtained by the superposition,

$$\Psi = \Psi_1 + \Psi_2 \tag{4.16}$$

or

$$\Psi(\xi,\zeta) = \frac{\alpha}{\pi}\int_0^\infty U(\xi') \tan^{-1}\left[\frac{2\xi\zeta}{\xi^2-\zeta^2-\xi'^2}\right]d\xi'$$

$$+ \frac{\alpha}{\pi}\int_0^\infty U(\xi') \tan^{-1}\left[\frac{2\xi(\zeta-L)}{\xi^2-(\zeta-L)^2-\xi'^2}\right]d\xi' \tag{4.17}$$

The jet-induced velocities, $\hat{U}$ and $\hat{V}$ may also be obtained by similar superposition or by carrying out the differentiation in Eqs. (3.27a) and (3.27b). The result is

$$\hat{U}(\xi,\zeta) = \frac{2}{\pi}\alpha\xi \int_0^\infty U(\xi') \frac{\xi'^2-\zeta^2-\xi^2}{(\xi'^2-\zeta^2-\xi^2)^2 + 4\xi'^2\zeta^2}\, d\xi'$$

$$+ \frac{2}{\pi}\alpha\xi \int_0^\infty U(\xi') \frac{\xi'^2-(\zeta-L)^2-\xi^2}{\{\xi'^2-(\zeta-L)^2-\xi^2\}^2 + 4\xi'^2(\zeta-L)^2\}}\, d\xi' \qquad (4.18)$$

$$\hat{V}(\xi,\zeta) = -\frac{2}{\pi}\alpha\zeta \int_0^\infty U(\xi') \frac{(\xi^2+\zeta^2+\xi'^2)}{(\xi^2+\zeta^2+\xi'^2)^2 - 4\xi^2\xi'^2}\, d\xi'$$

$$- \frac{2}{\pi}\alpha(\zeta-L) \int_0^\infty U(\xi') \frac{\xi^2+(\zeta-L)^2+\xi'^2}{\{\xi^2+(\zeta-L)^2+\xi'^2\}^2 - 4\xi^2\xi'^2}\, d\xi' \qquad (4.19)$$

Eqs. (4.17), (4.18), and (4.19) describe the flow field induced by two parallel jets, subject to the various assumptions outlined in the beginning of this section. It is not necessary to further simplify the above equations, since each integral can be evaluated separately using the numerical procedures in Secs. 3.5 and 3.6. The results are given in Sec. 5.3.

4.3 Jet Non-Perpendicular to Coastline

The simple jet in Fig. 4.1 shown normal to the coastline probably represents an idealization. In reality, the tidal jet is more likely to be depicted as in Fig. 4.3.

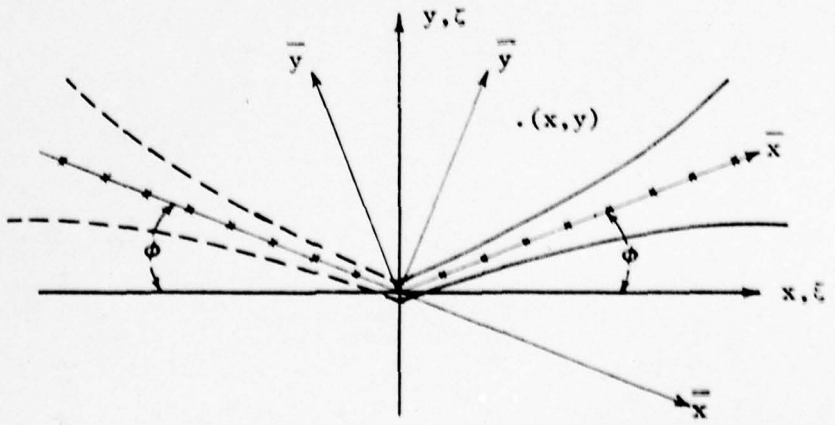

Figure 4.3 Sink Distribution for a Jet Non-Perpendicular to Coastline

As before, the jet is replaced by a sink distribution and by an image distribution in order to make the coastline a solid boundary. The coordinate systems $\bar{x}$, $\bar{y}$ (for real jet) and $\bar{\bar{x}}$, $\bar{\bar{y}}$ (for image jet) have been introduced for convenience of mathematical derivation. Once again, the entrainment velocity induced by the jet must be modified as in the previous section. In the present case, the entrainment at the jet boundary nearer to the coastline is expected to be less than the entrainment on the other boundary. The same principle, as outlined in Sec. 4.2, is extended to the configuration in Fig. 4.3, and the total mass entrainment is assumed to equal that for a simple jet. Therefore, Eq. (4.12) and the jet solution given in Sec. 3.2 are still valid. The jet induced flow field is determined as follows.

The dimensional stream function ψ due to the real jet (w.r.t. $\bar{x}$, $\bar{y}$ co-ordinates) is given by an equation similar to Eq. (3.11).

$$\psi_r(\bar{x},\bar{y}) = \frac{1}{2\pi} \int_0^\infty m(\bar{x}') \tan^{-1}\left[\frac{\bar{y}}{(\bar{x}-\bar{x}')}\right] d\bar{x}' \tag{4.20}$$

The stream function due to the image jet is

$$\psi_{im}(\bar{\bar{x}},\bar{\bar{y}}) = \frac{1}{2\pi} \int_{-\infty}^\infty m(\bar{\bar{x}}') \tan^{-1}\left[\frac{\bar{\bar{y}}}{(\bar{\bar{x}}-\bar{\bar{x}}')}\right] d\bar{\bar{x}}' \tag{4.21}$$

Eqs. (4.20) and (4.21) must be transformed to x, y coordinates using the relations

$$\bar{x} = x \cos\phi + y \sin\phi \tag{4.22a}$$

$$\bar{y} = -x \sin\phi + y \cos\phi$$

and

$$\bar{\bar{x}} = x \cos \phi - y \sin \phi \tag{4.23a}$$

$$\bar{\bar{y}} = x \sin \phi + y \cos \phi \tag{4.23b}$$

Substituting Eqs. (4.22) and (4.23) into Eqs. (4.20) and (4.21) respectively, and superposing ψ_{im} and ψ_r, the stream function in x,y coordinates is

$$\psi(x,y) = \frac{1}{2\pi} \int_{-\infty}^{\infty} m(\bar{\bar{x}}') \tan^{-1}\left[\frac{x \sin \phi + y \cos \phi}{x \cos \phi - y \sin \phi - \bar{\bar{x}}'}\right] d\bar{\bar{x}}'$$

$$+ \frac{1}{2\pi} \int_{0}^{\infty} m(\bar{x}') \tan^{-1}\left[\frac{- x \sin \phi + y \cos \phi}{x \cos \phi + y \sin \phi - \bar{x}'}\right] d\bar{x}' \tag{4.24}$$

Changing the variable of integration from $\bar{\bar{x}}'$ to $-\bar{x}'$ in the first integral of the above equation and making use of the symmetry of the sink distribution w.r.t. the y-axis, i.e., $m(\bar{x}') = - m(-\bar{x}')$, the result is,

$$\psi(x,y) = \frac{1}{2\pi} \int_{0}^{\infty} \Bigg\{ m(\bar{x}') \Bigg\{ \tan^{-1}\left[\frac{x \sin \phi + y \cos \phi}{x \cos \phi - y \sin \phi + \bar{x}'}\right] + \tan^{-1}\left[\frac{- x \sin \phi + y \cos \phi}{x \cos \phi + y \sin \phi - \bar{x}'}\right] \Bigg\} \Bigg\} d\bar{x}' \tag{4.25}$$

The arctangent functions in Eq. (4.25) are summed using standard trigonometric formulas and the sink strength m is substituted from Eqs. (3.22) and (3.23) to obtain

$$\psi(x,y) = \frac{\alpha}{\pi} \int_{0}^{\infty} u_c(\bar{x}') \tan^{-1}\left[\frac{2xy - 2x\bar{x}' \sin \phi}{x^2 - y^2 - \bar{x}'^2 + 2\bar{x}' y \sin \phi}\right] d\bar{x}' \tag{4.26}$$

Notice that Eq. (4.26) reduces to Eq. (3.24) for a simple jet when $\phi = 0$.

Replacing the dummy variable of integration $\bar{x}'$ by x' without loss of generality, and non-dimensionalizing using Eqs. (3.26), the above equation becomes,

$$\Psi(\xi,\zeta) = \frac{\alpha}{\pi} \int_0^\infty U(\xi') \tan^{-1} \left[\frac{2\xi\zeta - 2\xi\xi' \sin\phi}{\xi^2-\zeta^2-\xi'^2 + 2\xi'\zeta \sin\phi} \right] d\xi' \qquad (4.27)$$

The velocity field is obtained by differentiating Eq. (4.27) according to Eqs. (3.27) to get

$$\hat{U}(\xi,\zeta) = \frac{2}{\pi} \alpha\xi \int_0^\infty U(\xi') \frac{N_1(\xi,\zeta,\xi',\phi)}{D(\xi,\zeta,\xi',\phi)} d\xi' \qquad (4.28)$$

$$\hat{V}(\xi,\zeta) = \frac{-2}{\pi} \alpha \int_0^\infty U(\xi') \frac{N_2(\xi,\zeta,\xi',\phi)}{D(\xi,\zeta,\xi',\phi)} d\xi' \qquad (4.29)$$

where,

$$N_1(\xi,\zeta,\xi',\phi) = (\xi'^2-\zeta^2-\xi^2) + 2\xi' \sin\phi\,(\zeta-\xi' \sin\phi) \qquad (4.30a)$$

$$N_2(\xi,\zeta,\xi',\phi) = (\zeta-\xi' \sin\phi)\,(\xi^2+\zeta^2+\xi'^2-2\xi'\zeta \sin\phi) \qquad (4.30b)$$

$$D(\xi,\zeta,\xi',\phi) = 4\xi^2(\zeta-\xi' \sin\phi)^2 + (\xi^2-\zeta^2-\xi'^2 + 2\xi'\zeta \sin\phi)^2 \qquad (4.30c)$$

It may be verified that Eqs. (4.28) and (4.29) together with Eqs. (4.30), revert to Eqs. (3.28) and (3.29) when $\phi = 0$.

The flow field induced by a jet which is not perpendicular to the coastline is completely described by Eqs. (4.27), (4.28), and (4.29) supplemented by Eqs. (4.30). As in Secs. 4.1 and 4.2, numerical results were obtained by the procedures discussed in Secs. 3.5 and 3.6, and the results are presented in Sec. 5.3.

5.0 CONTINENTAL SHELF CIRCULATION RESULTS

5.1 The Simple Jet

The flow field induced by a tidal jet modeled as a simple jet is described by Eqs. (3.25) and (3.28) through (3.31). Numerical evaluation of Ψ, $\hat{U}$, and $\hat{V}$ in these equations was carried out following the procedures of Secs. 3.5 and 3.6. The computational results are presented in Figs. 5.1 through 5.5.

Figure 5.1 shows the streamline pattern for the ideal case of a jet with zero bottom friction (μ=0). Streamlines have been plotted only for $\zeta > 0$ since the flow field is symmetric about the $\xi = 0$ axis. The lines of constant Ψ were obtained by inverse linear interpolation through the values calculated by Eq. (3.25). Due to the relatively slow linear growth of the bottom-frictionless jet, as opposed to the exponential growth with bottom-friction, the jet induces circulation over a large portion of the continental shelf (up to 400 inlet half-widths offshore in Fig. 5.1). The flow direction is along the streamlines into the jet with a small onshore component which vanishes along the coastline. The case of a bottom frictional jet is shown in Fig. 5.2 for $\mu = 0.05$. This value is expected to be representative for a typical inlet (such as Redfish Pass, Florida with $b_o/h_o = 15$) with a Darcy-Weisbach friction factor $f = 0.02$ to 0.08. A comparison of Figures 5.1 and 5.2 reveals that bottom friction in the jet has a significant effect on the shelf circulation pattern. The fluid enters the jet almost radially as shown by the streamlines and the influence of the jet is confined to a small distance offshore. This is, of course, due to the rapid exponential growth of the jet near the inlet as shown in Figure 3.2.

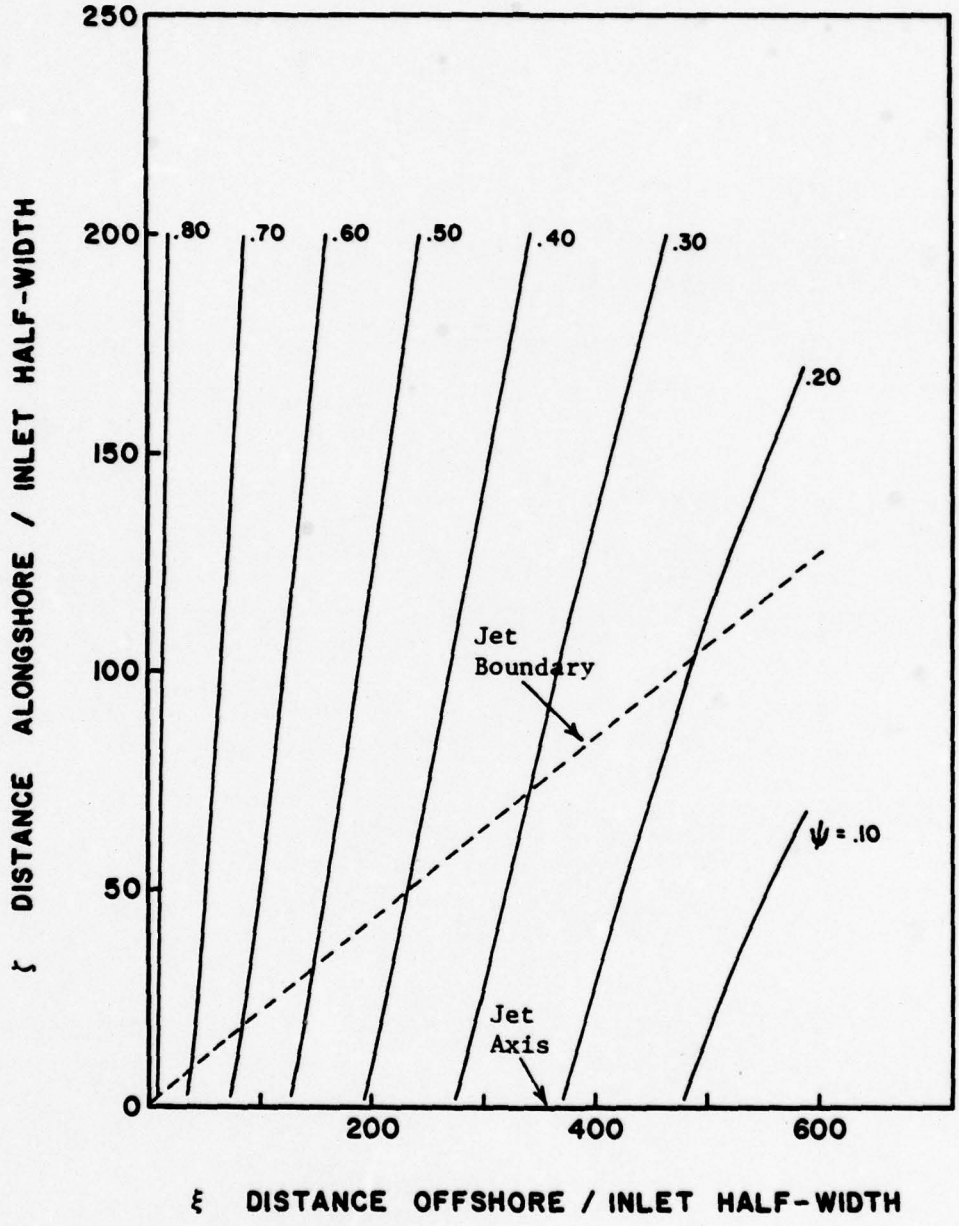

Figure 5.1 Streamlines For A Jet With Zero Bottom Friction (No Jetty)

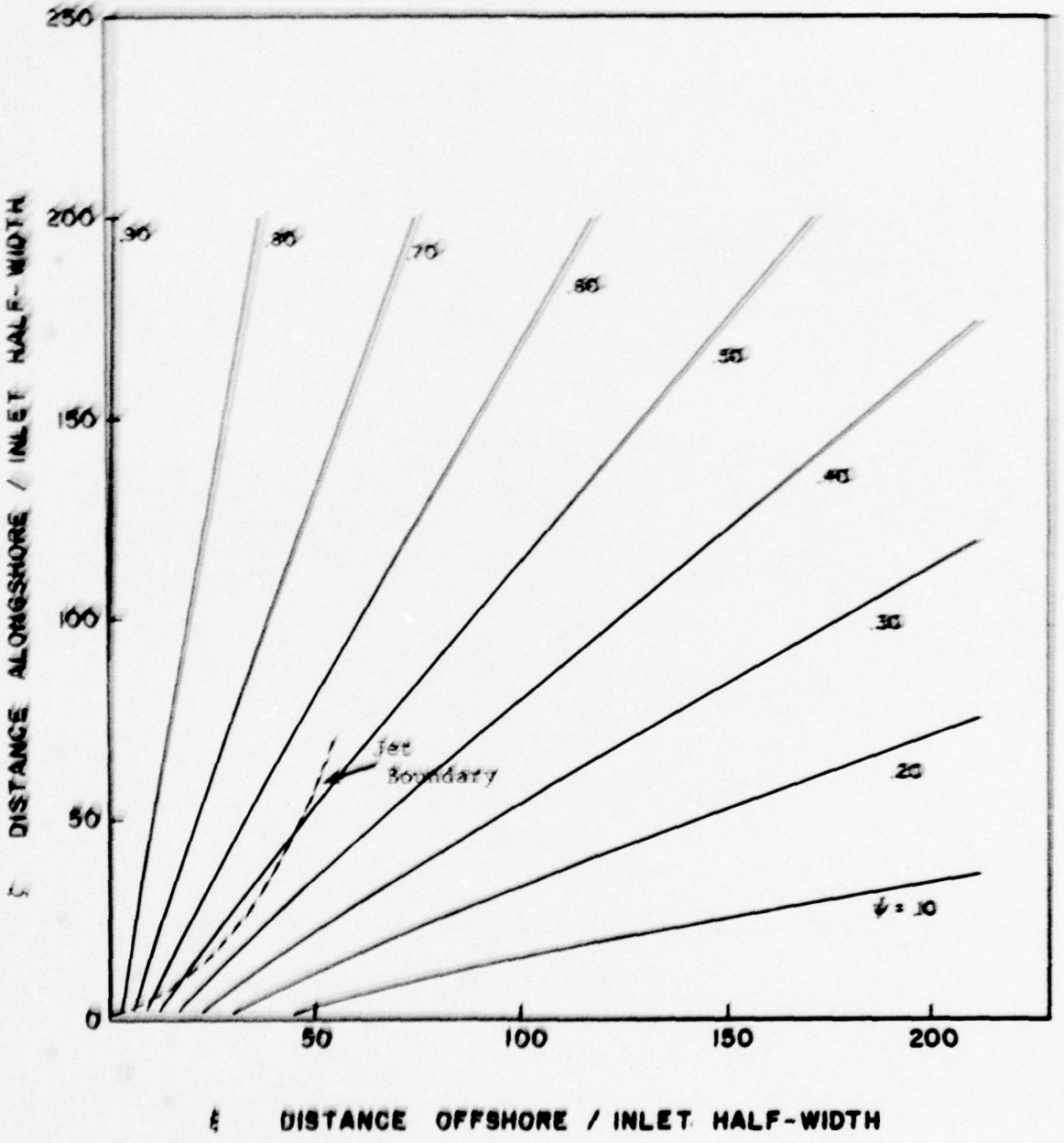

Figure 5.2 Streamlines For A Jet With Friction (μ = 0.05, No Jetty)

Figure 5.3 displays the jet induced flow pattern for a very large value of the friction parameter ($u = 0.10$). Convergence of entrainment streamlines toward the inlet is very pronounced in this case. Since all of the streamline patterns discussed were generated for jets replaced by sink distributions along their axes, the solutions shown are not applicable within the physical jet boundaries which have been superimposed in Fig. 5.1, 5.2, and 5.3.

An important aspect of the jet-induced flow fields described so far is the variation of the alongshore current. Since entrainment due to the tidal jet is a persistent phenomenon during every ebb tide, the alongshore current can be a dominant cause of sediment transport toward the inlet from the adjacent beaches. Figure 5.4 shows the variation of dimensionless alongshore velocity with distance from the inlet. The upper three curves correspond to $\mu = 0$, 0.05, and 0.1 for a simple jet (i.e., without jetty, $A = 0$) and the bottom curve corresponds to a jet with a jetty. The latter is included for the purpose of comparision and will be discussed in the next section. It is seen that near the inlet the alongshore velocity is roughly 3.6% of the inlet throat velocity for all friction parameters. This particular value is a direct result of the entrainment coefficient $\alpha_1 = 0.036$ in the core region of the jet (Eq. (3.31a)). As one moves away from the inlet, along the coastline, the alongshore velocity for the bottom-frictionless jet decreases. With the introduction of friction ($\mu = 0.05$) the reduction in velocity with distance from the inlet is quite rapid as shown by the top two curves in Figure 5.4. Further increases in friction accentuates this drop-off of the alongshore current.

It is also interesting to consider the behavior of the u-component of velocity in the flow field. Fig. 5.5 shows the variation of $\hat{U}$ with offshore distance for

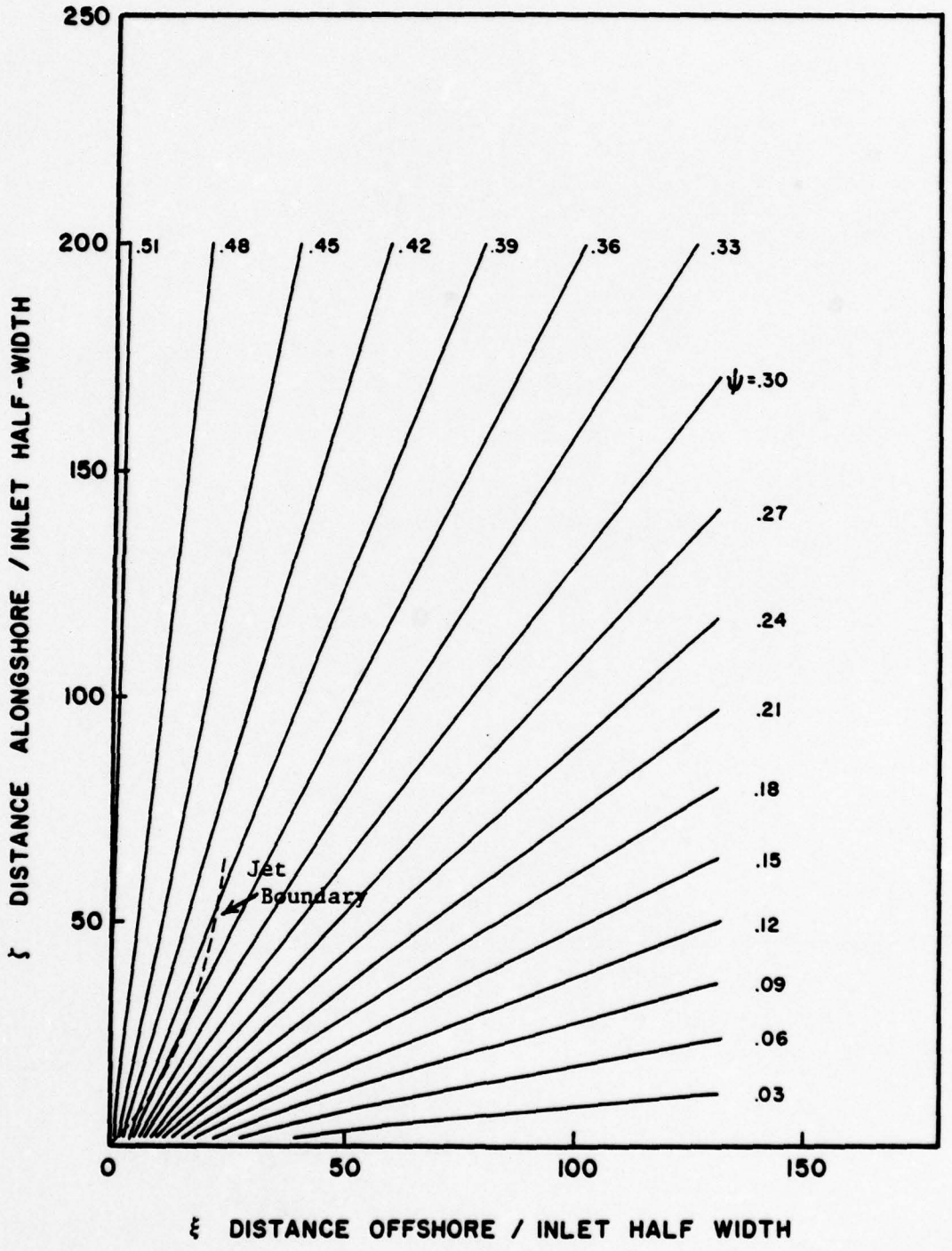

Figure 5.3 Streamlines For A Jet With Friction (μ = 0.1, No Jetty)

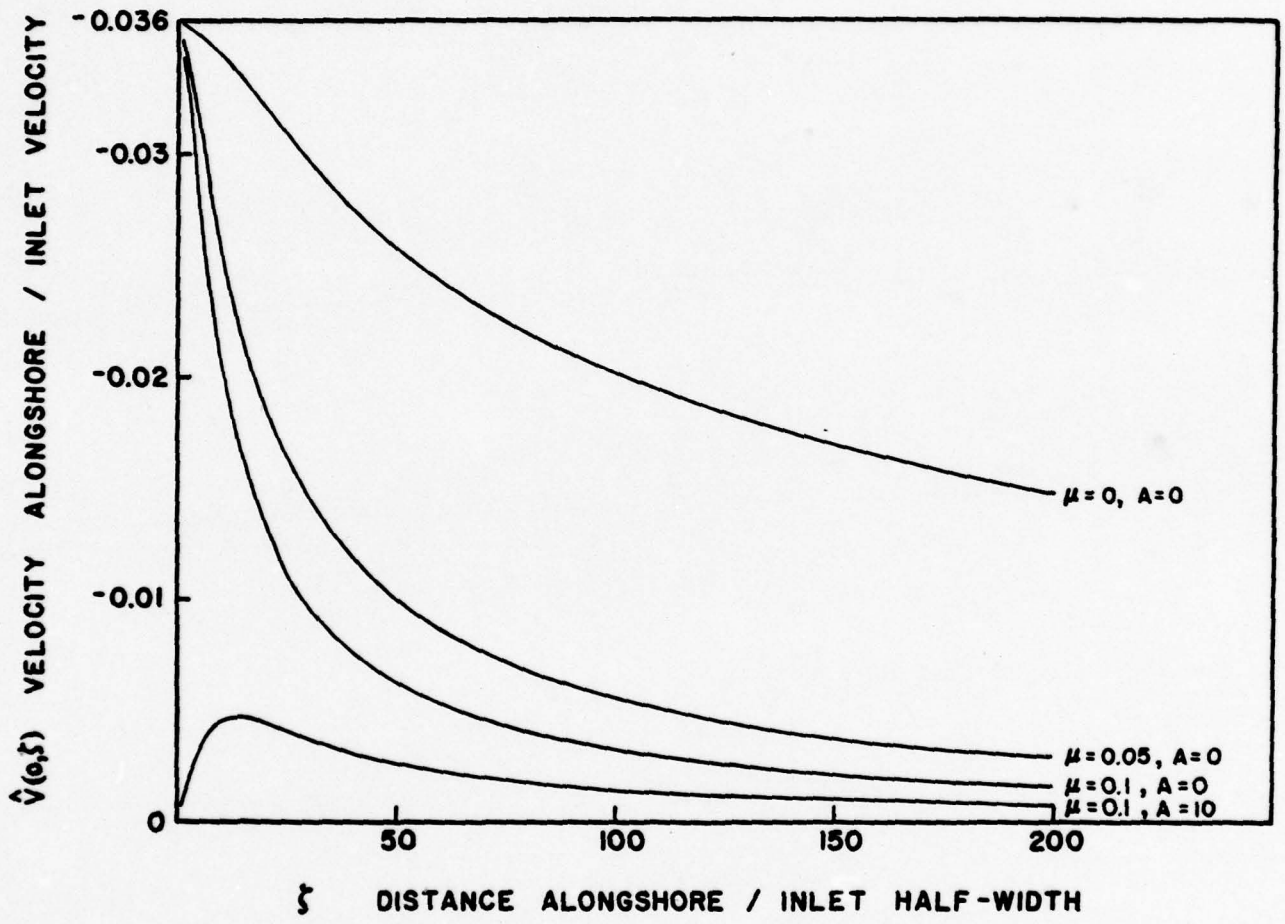

Figure 5.4 Alongshore Current For A Simple Jet And A Jet With A Jetty For Different Values of Friction Parameter

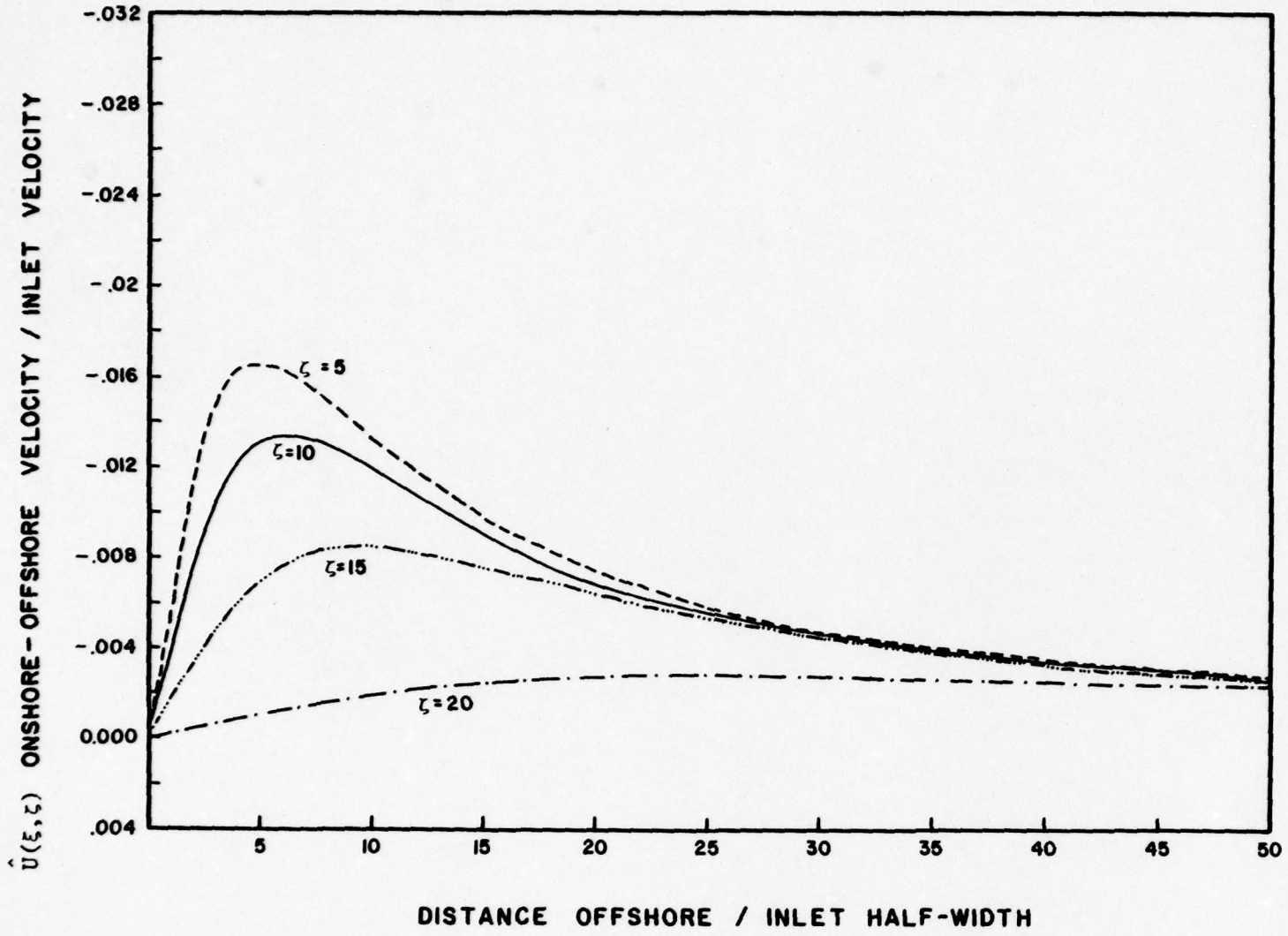

Figure 5.5 Variation Of u-velocity Component With Offshore Distance For A Simple Jet (μ = 0.05)

different locations of ζ from the inlet. Since the u- velocity is zero at $\xi = 0$ and since it must also be zero far away from the jet, the curves of $\hat{U}$ exhibit a peak as seen in the figure. The magnitude of $\hat{U}$ at the peak decreases with the increase in the distance ζ from the jet. This is expected because fluid particles closer to the jet experience a greater influence due to the jet. It is also seen that the point at which the maximum of $\hat{U}$ occurs moves further offshore as one moves away from the jet.

5.2 Jet With A Jetty

Streamlines for this case were obtained through numerical evaluation of Eqs. (4.4), (4.5), and (4.6). The results are shown in Figs. 5.6, 5.7, and 5.8 for $\mu = 0.1$ and dimensionless jetty lengths A = 2, 5, and 10 respectively. These figures should be compared with the earlier Fig. 5.3 which displays streamlines for a jet without jetty and $\mu = 0.1$. While Figs. 5.6 through 5.8 display the radially converging streamlines associated with the high value of friction parameter ($\mu = 0.1$), a significant curvature of streamlines close to the jetty is observed. In other words, fluid particles adjacent to the jetty are entrained into the jet along streamlines curving toward the discharge point of the jetty.

The variation of alongshore current is especially important in this case since accretion of material near the mouths of jetties is a common observation. Figure 5.9 contains a plot of dimensionless alongshore current against dimensionless offshore distance for different values of jetty length and $\mu = 0.01$. The curve for a jet without a jetty has been reproduced from Figure 5.4 and is included for comparison. First, as expected, the alongshore velocity $\hat{V}$ goes to zero at the jetty ($\zeta = 0$) since it is normal to a solid boundary. At some distance from the jetty, $\hat{V}$ exhibits a maximum and then decays to zero. The peak value

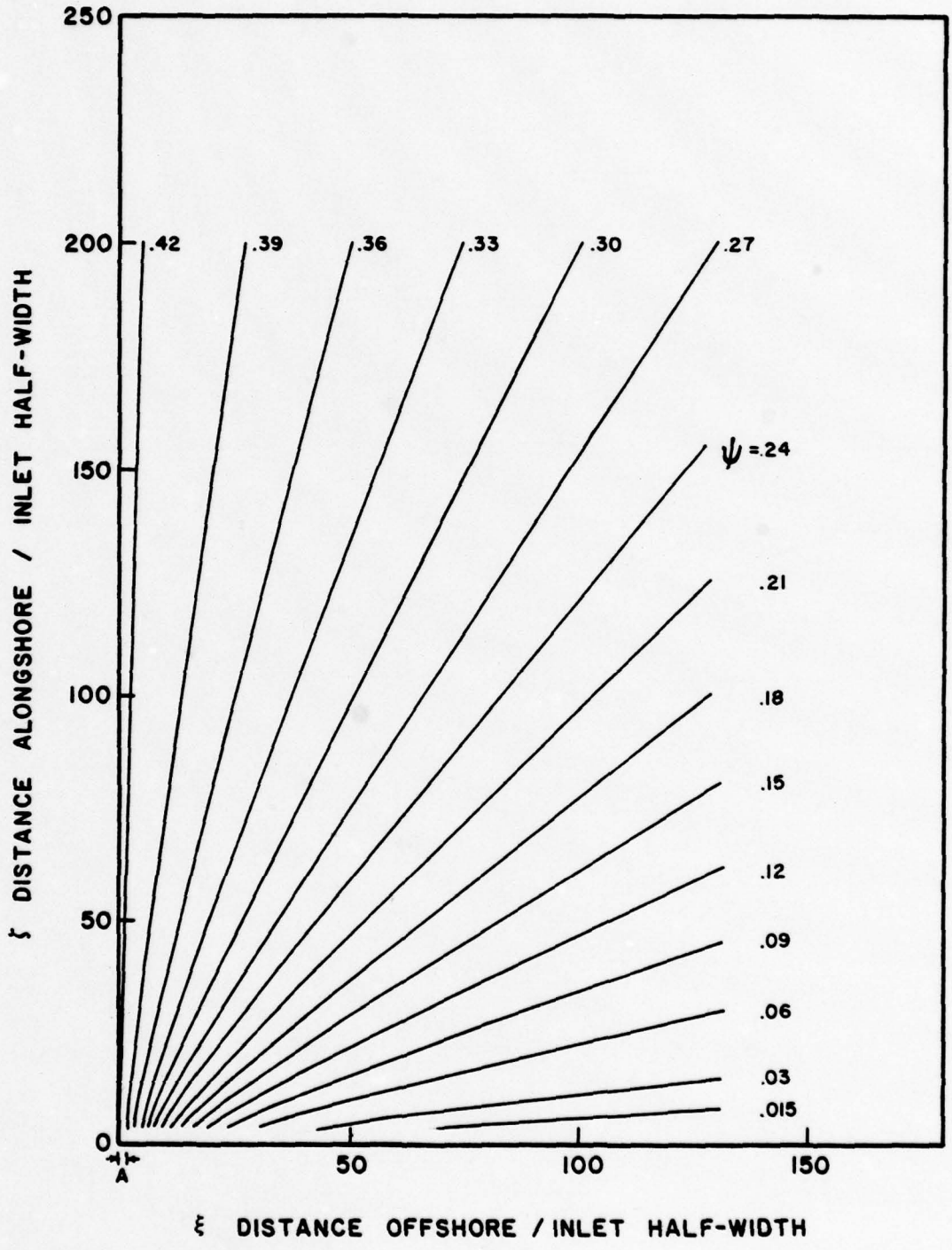

Figure 5.6 Streamlines For A Jet With Jetty (μ = 0.1, A = 2)

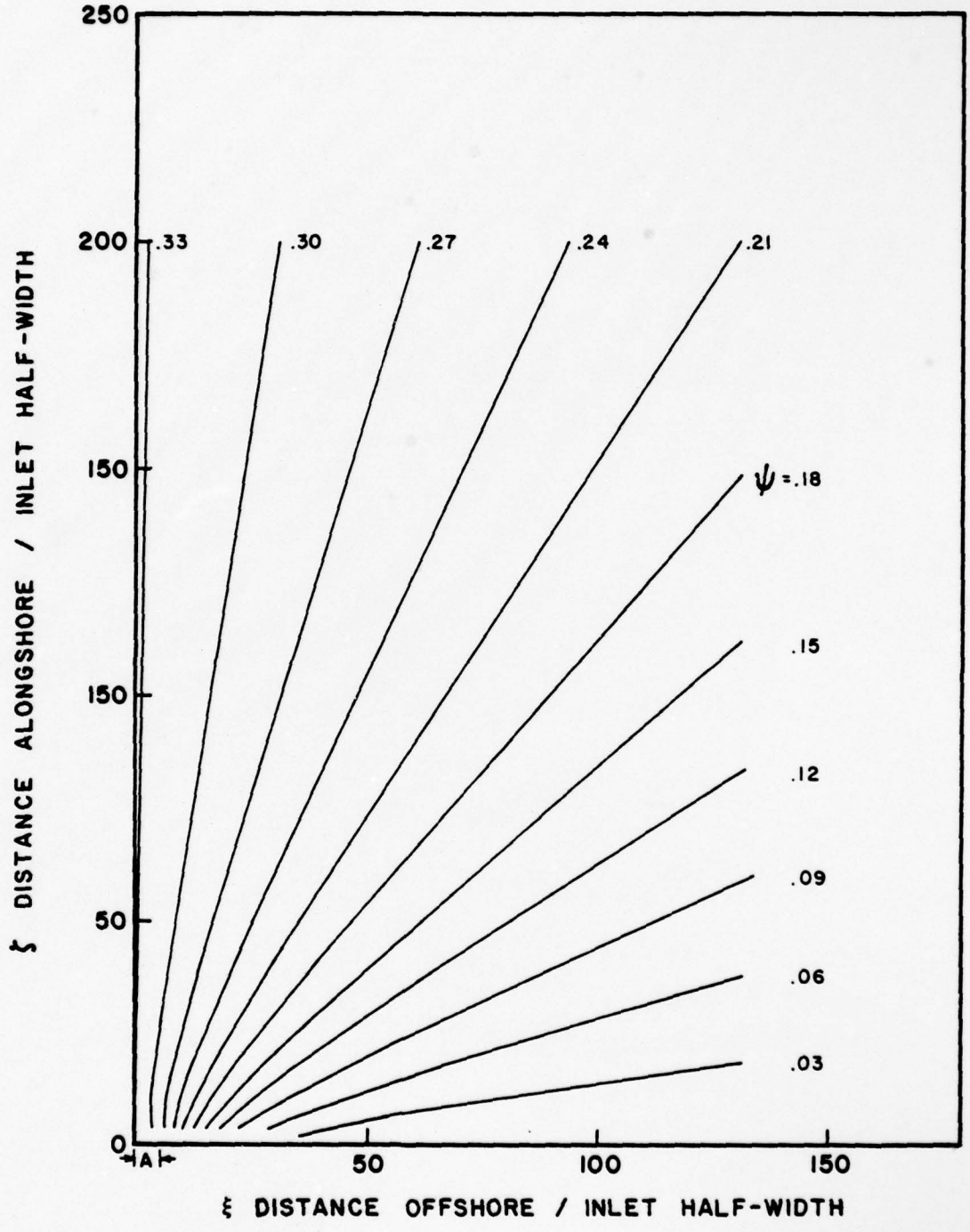

Figure 5.7 Streamlines For A Jet With Jetty (μ = 0.1, A = 5)

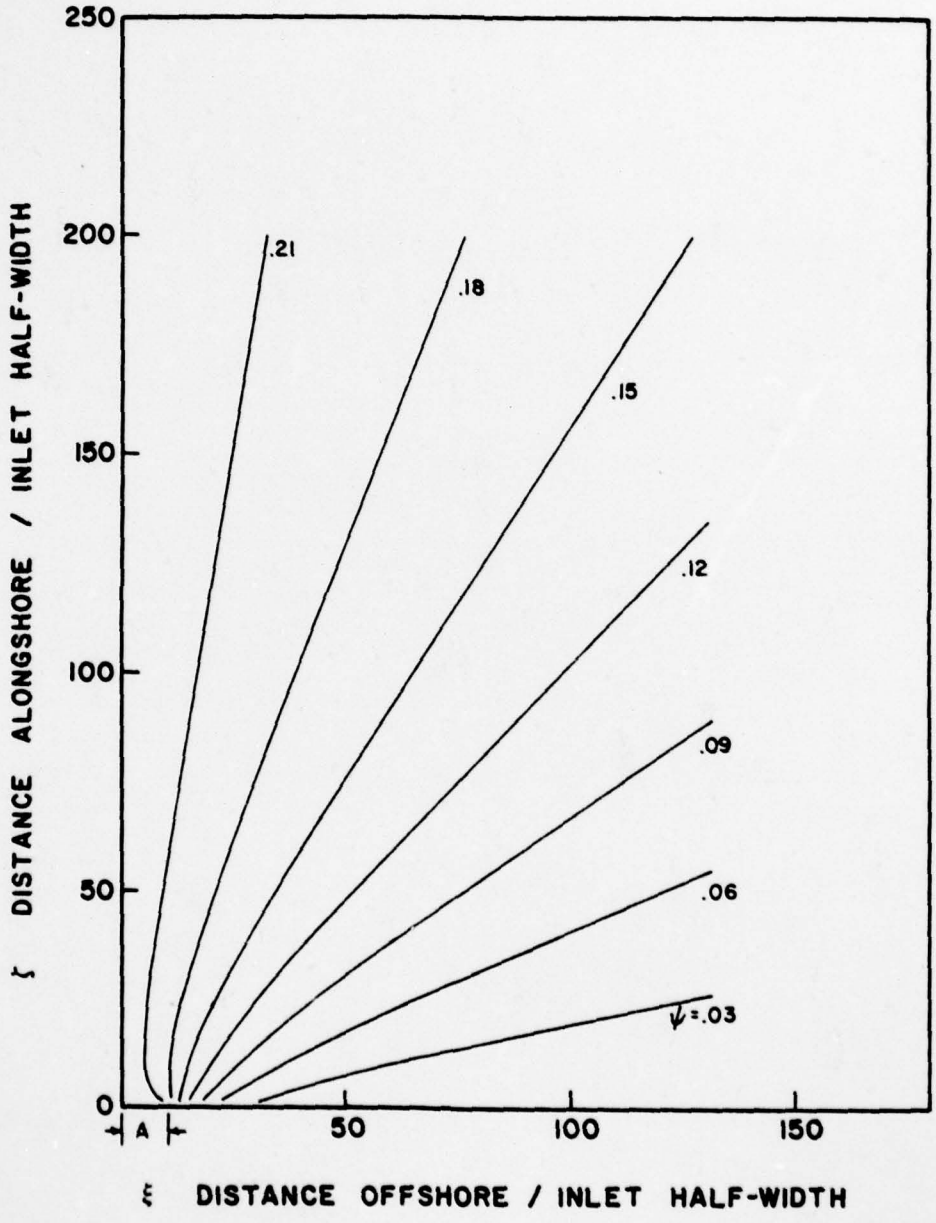

Figure 5.8 Streamlines For A Jet With Jetty (μ = 0.1, A = 10)

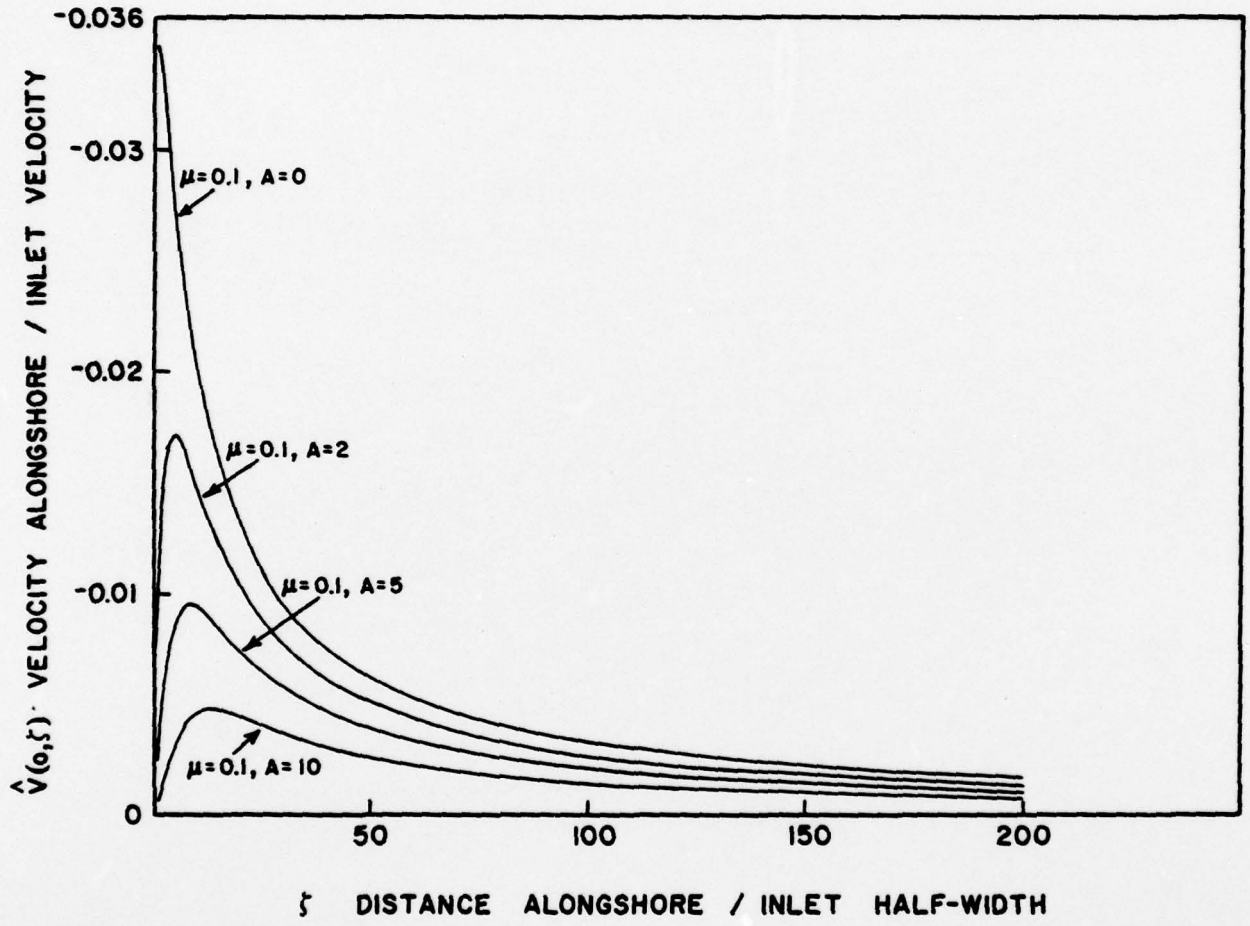

Figure 5.9 Alongshore Current For A Jet With Different Jetty Lengths

of alongshore current drops sharply with increasing jetty length. In fact, introduction of a jetty, which is only two inlet half-widths long (A=2), reduces the maximum $\hat{V}$ by a factor of 1/2. Moreover, the distance from the jetty at which the maximum velocity occurs increases with each increase in jetty length.

5.3 Parallel Jets

The streamline pattern for two parallel jets, obtained from Eq. (4.17) is shown in Figure 5.10. Both jets were considered bottom-frictionless since this allows a slow linear growth (as opposed to an exponential growth for a bottom-frictional jet) before the boundaries of the jets intersect. The jets in Figure 5.10 are separated by a distance of 50 inlet half-widths, which is typical for many adjacent inlets. The flow field is shown for $y > 0$ only since it is expected to be symmetric about the centerline between the two jets (i.e. $\zeta = 25$). The streamlines between the jets are parallel to the centerline away from the inlets and display strong curvature due to the entrainment effect on either side of the centerline. The streamlines in the outer region ($\zeta > 50$ and $\zeta < 0$ by symmetry) resemble closely the pattern for a simple jet (Fig. 5.1) It is seen that the coastline and the centerline between the jets correspond to a single streamline because the velocity component normal to these lines is zero. Thus, the centerline ($\zeta = 25$) acts as a dividing streamline. In the zone $U < \zeta < 25$, the fluid is entrained into the lower jet (labeled Jet 1) and in the zone $25 < \zeta < 50$, the fluid is entrained into the upper jet (labeled Jet 2).

The foregoing results obviously correspond to the mathematical idealization of jets acting as distributed sinks (Fig. 4.2). In reality, the physical dimensions of the jets must be considered. In Fig. 5.10, the jet boundaries are superimposed over the streamline pattern to delineate the region of applicability of the theoretical solution. For $\zeta > 50$, this region contains the flow field between the jet boundary and the coastline, and for $0 < \zeta < 50$, the region

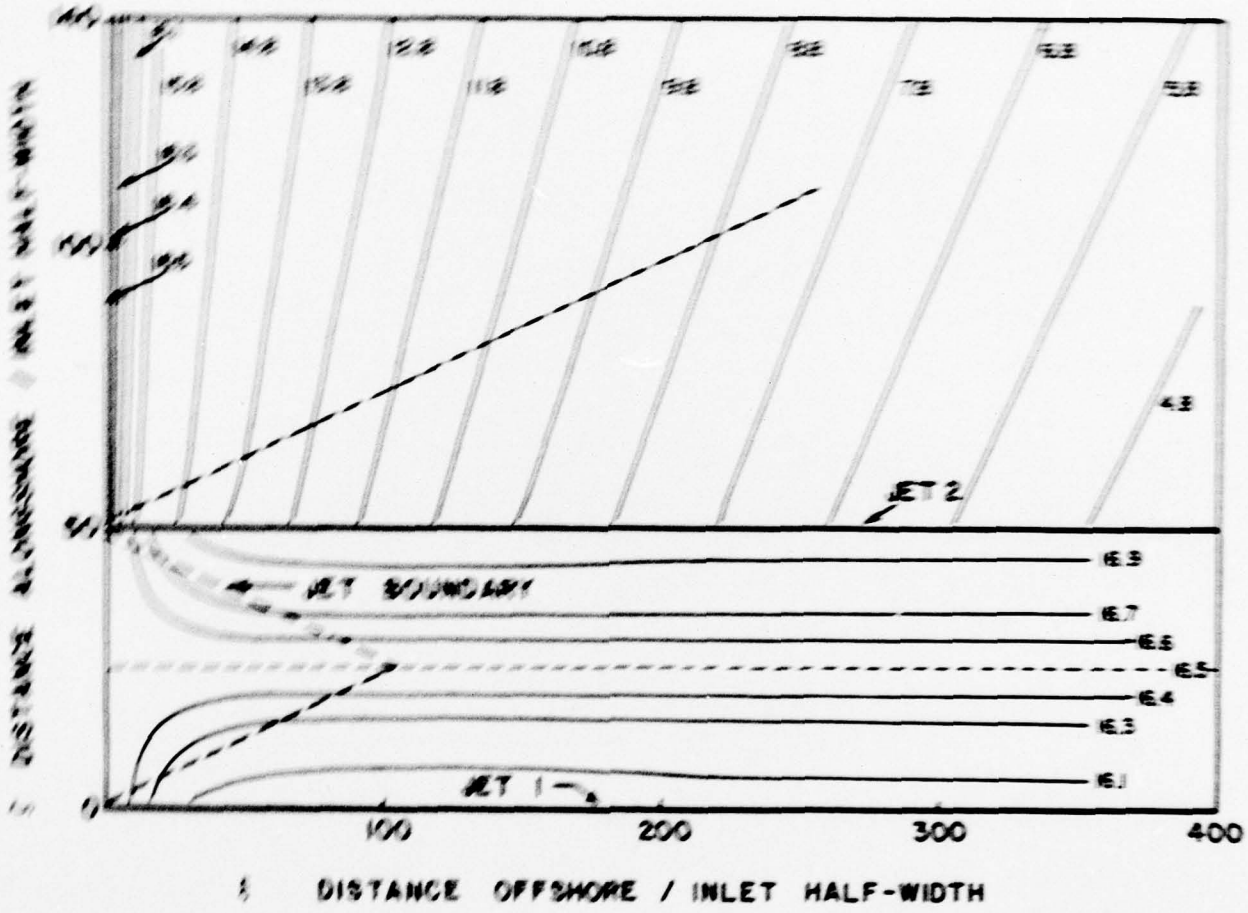

Figure 5.10 Streamlines For Two Parallel Jets (μ = 0)

includes the fluid bounded by the two jet boundaries and the coastline.

The variation of alongshore current in the present case is most interesting (Fig. 5.11). For $0 < \zeta < 25$, the vertical component velocity $\hat{V}$ is directed into the lower jet (Fig. 5.10) and hence negative. For $25 < \zeta < 50$, $\hat{V}$ is directed into the upper jet and hence positive. At the centerline between the two jets, i.e., $\zeta = 25$, $\hat{V}$ equals zero. This variation in $\hat{V}$ is antisymmetric since the two jets are identical. $\hat{V}$ changes from -0.01 near $\zeta = 0$ to +0.01 near $\zeta = 50$, passing through zero at $\zeta = 25$. Notice that the magnitude of $\hat{V}$ near the jets is much lower than that for a single jet (0.01 compared to 0.036 for the latter). This is due to the 'sharing' of fluid between the two jets as pointed out in Sec. 4.2. When one crosses the jet at $\zeta = 50$ moving along the coastline, the alongshore current jumps discontinuously to $\hat{V} = -0.062$ which is much greater than the value 0.036 for a simple jet. It may be recalled from Sec. 4.2 that, for the parallel jet situation, the entrainment on the inner boundaries decreases whereas the entrainment on the outer boundaries increases such that the total mass (or volume) entrained is the same as that for a single jet. This inequality in entrainment on the boundaries of each jet is a consequence of mass conservation. The discontinuity in $\hat{V}$ across the jet at $\zeta = 50$ (since a solution does not exist at the jet axis itself) from $|\hat{V}| = +0.01$ to 0.062 preserves the total mass entrainment of 0.072 for a simple jet.

The above results indicate that, for two adjacent jets, the alongshore current in the outer region is much stronger than the current in between the jets. Therefore, there should be an increased transport of suspended sediment toward the two inlets along the beaches external to the two jets. On the other hand, transport of material toward the inlets in between the two jets should be comparatively much smaller.

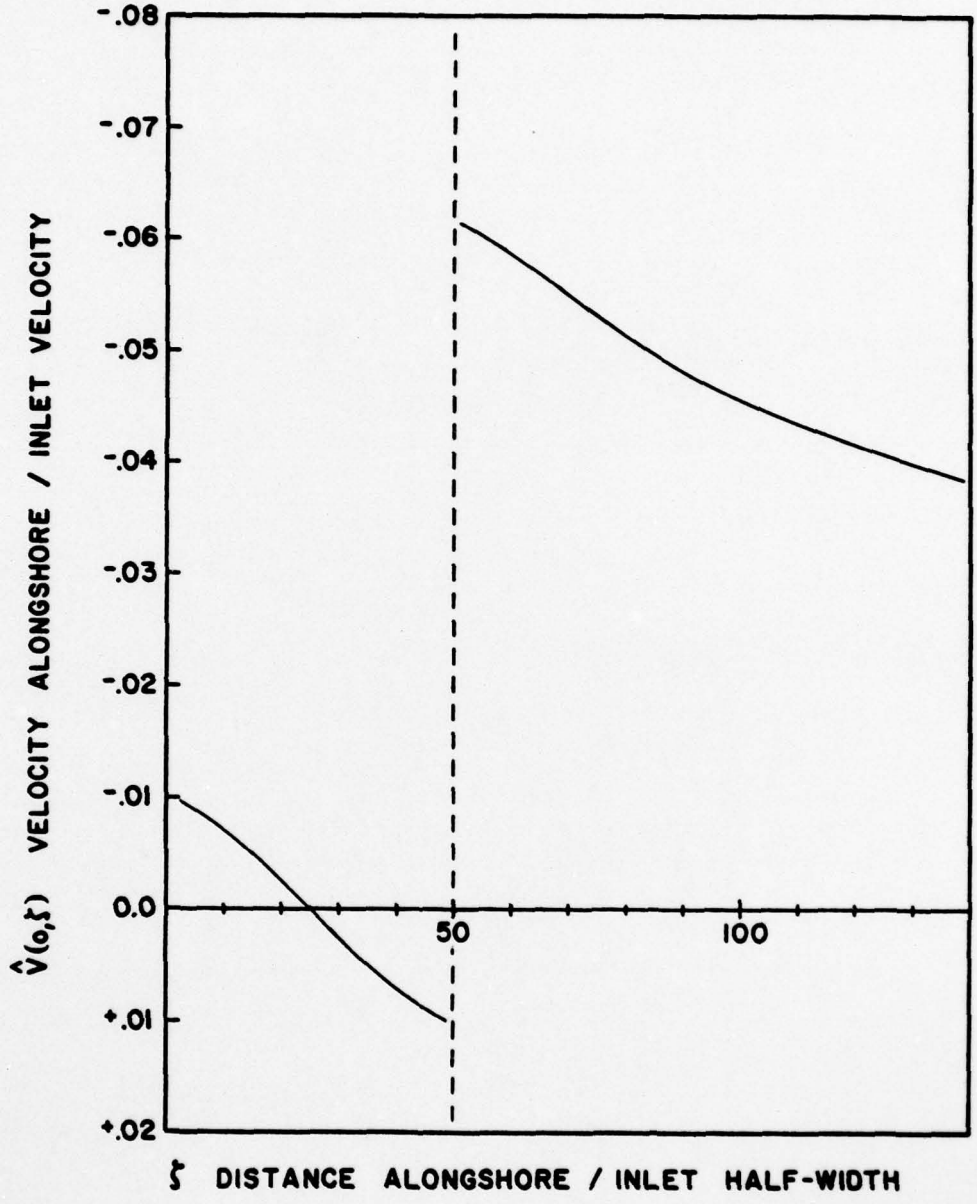

Figure 5.11 Alongshore Current For Two Parallel Jets

5.4 Jet Non-Perpendicular to Coastline

Eqs. (4.27), (4.28), and (4.29) were evaluated numerically to obtain the stream function Ψ and the velocities $\hat{U}$ and $\hat{V}$ in the flow field. Fig. 5.12 shows the streamline pattern for a simple jet (with $\mu = 0.05$) which has been rotated anticlockwise through 15^{o}. The flow field is quite similar to that in Fig. 5.2 for a simple jet perpendicular to the coastline. The asymmetrical nature of the jet induced flow is obviously due to the non-perpendicularity of the jet.

The alongshore current is plotted in Fig. 5.13. As an observer moves along the coastline, starting at $\zeta = -\infty$ (i.e. away from the jet on the negative axis in Fig. 4.3), the velocity $\hat{V}$ increases gradually from 0 to 0.05 for ζ just less than zero. When the observer crosses the $\zeta = 0$ axis on the other side of the jet (Fig. 4.3), the $\hat{V}$ changes discontinuously to -0.022. Thus, the entrainment is greater on the lower boundary of the jet and smaller on the upper boundary. This is in accordance with the mass conservation considerations discussed in Sec. 4.3. Therefore, the alongshore current on the obtuse angle side of a non-perpendicular jet is stronger than the current on the acute angle side. Consequently, there should be increased transport of sediment toward the inlet on the obtuse angle side compared to the acute angle side.

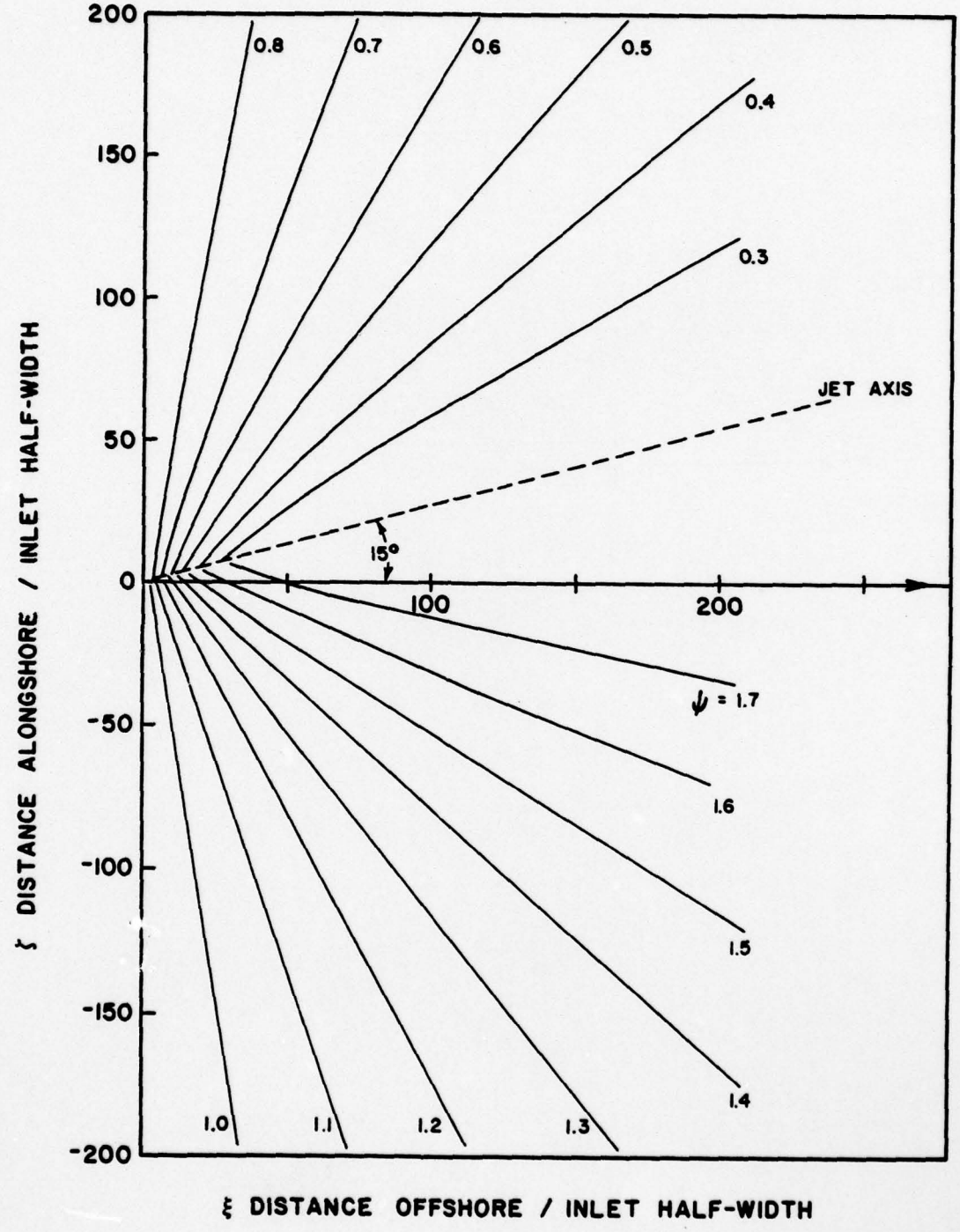

Figure 5.12 Streamlines For A Jet Non-Perpendicular to Coastline

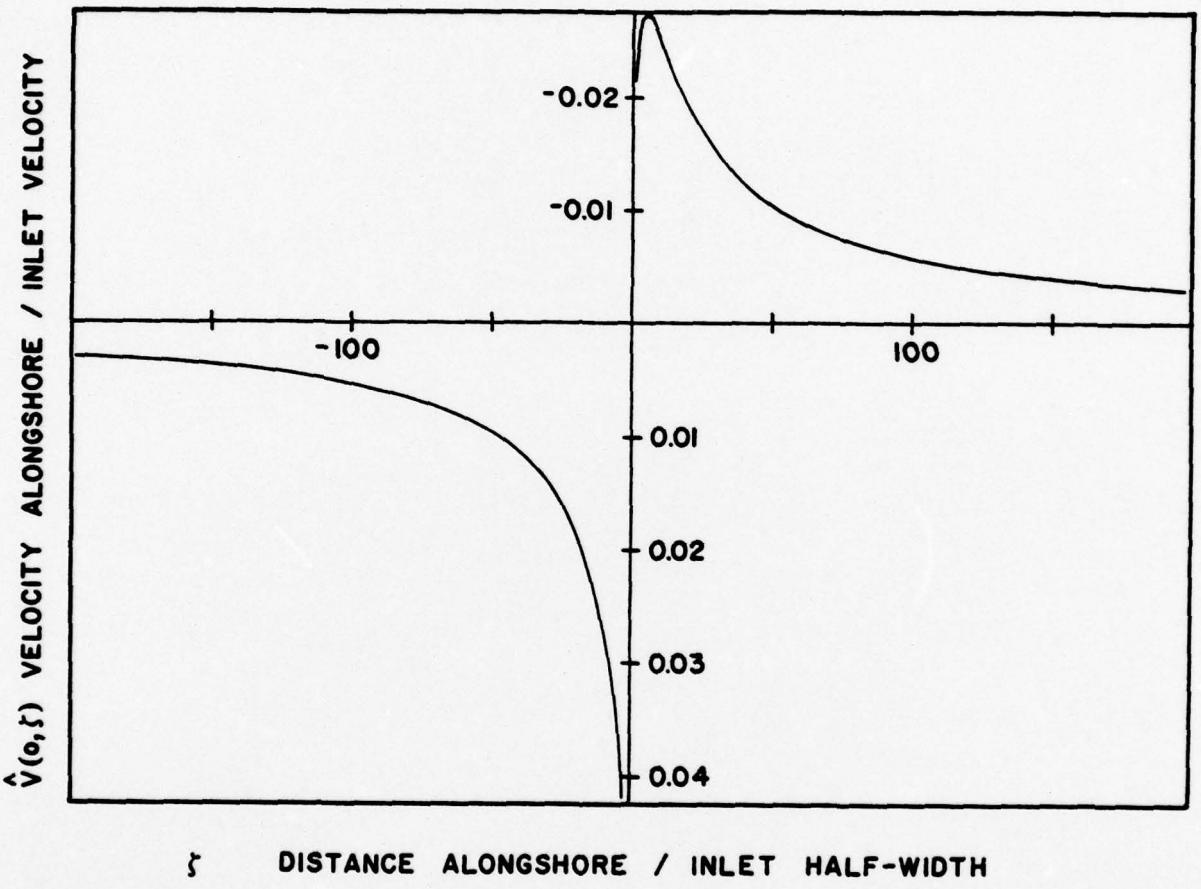

Figure 5.13 Alongshore Current For A Jet Non-Perpendicular to Coastline ($\phi = 15^{o}$, $\mu = 0.05$)

6.0 VARIABLE DEPTH AND UNSTEADY EFFECTS - PRELIMINARY CONSIDERATIONS

6.1 Potential Flow with Variable Depth

The work presented in Sections 3.0, 4.0, and 5.0 was concerned with jet-induced circulation treated as a steady, potential flow over a constant bottom. In this section, preliminary formulations are derived to include the effects of variable bathymetry, unsteadiness, and the Earth's rotation. The variable depth problem is considered first. In Sec. 2.2 it was shown that steady potential flow over arbitrary bottom topography is governed by Eq. (2.8) in terms of a velocity potential and by Eq. (2.11) in terms of a stream function. The latter formulation was employed in the constant bathymetry case which is governed by Laplace's Eq. (2.12). General solutions were obtained by replacing the tidal jet by an equivalent sink distribution and superimposing the elementary solution (Eq. (3.10)) for each sink. Had this problem been worked in terms of a velocity potential instead of the stream function, the corresponding elementary solution due to a sink located at the origin (x'=y'=0) would be

$$\phi(r) = \frac{-q}{2\pi} \ell n\ r \qquad (6.1)$$

where $r=\sqrt{x^2+y^2}$. The potential function in Eq. (6.1) has the important property that it posesses a logarithmic singularity at the origin. This is reflected in the form of an indeterminate argument and resulting multiplicity of the arctangent function at the origin in the stream function formulation (Eq. (3.10)). These behaviours of the potential and stream functions are due to the fact that Laplace's Eqs. (2.9) and (2.12) are not satisifed at the sink itself.

Consider now the governing equations for the variable depth problem, viz., Eqs. (2.8) and (2.11). As discussed in Ref. (42), it has been demonstrated by Hadamard (43) that for the general elliptic equation in the plane, such as Eq. (2.8), an elementary solution containing a singularity exists and it is unique. A method for solving Eq. (2.8) analytically is also given in Ref. (42). Therefore, the velocity potential approach was selected over the stream function approach to analyze the variable depth problem. The next three sections deal with the derivation and application of solutions of Eq. (2.8).

6.2 General Elementary Solution for Arbitrary Depth

Eq. (2.8), repeated below for convenience, is

$$\nabla^2\phi + \frac{h_x}{h}\phi_x + \frac{h_y}{h}\phi_y = 0 \tag{6.2}$$

If Eq. (6.2) is non-dimensionalized using Eqs. (3.26), the result is

$$\nabla^2\phi + \frac{H_\xi}{H}\phi_\xi + \frac{H_\zeta}{H}\phi_\zeta = 0 \tag{6.3}$$

which is identical in form to Eq. (6.2). Thus, it is sufficient to consider Eq. (6.2) and treat the quantities ϕ, h, x, and y as dimensionless. Eq. (6.2) may be written in the general form,

$$L(u) = 0 \tag{6.4a}$$

where the linear operator L is given by

$$L(u) \equiv \nabla^2 u + 2au_x + 2bu_y + cu \tag{6.4b}$$

First, an elementary solution of the generalized equation (6.4) is sought in the form

$$u = \sum_{n=0}^{\infty} U_n D^{n+\nu} \tag{6.5}$$

where

$$D = r^2 \tag{6.6a}$$

$$U_n = U_n(r,\theta) \tag{6.6b}$$

with

$$r = \sqrt{x^2+y^2} \tag{6.6c}$$

and

$$\theta = \tan^{-1} \frac{y}{x} \tag{6.6d}$$

The series in Eq. (6.5) is equivalent to the Method of Frobenius for ordinary differential equations. The constant ν is to be suitably chosen and the coefficients U_n are analytic.

The details of the substitution of Eq. (6.5) into Eq. (6.4) and determination of the solutions are given in Ref. (42). These derivations are tedious and only the final results are presented here. It can be proved that there are two linearly independent solutions of Eq. (6.4). The first solution is

$$u_1 = U_o \sum_{n=0}^{\infty} \frac{w_n}{n!} D^n \tag{6.7a}$$

where,

$$w_o = 1 \quad \text{and} \quad w_n = -\frac{1}{4r^n}\int_0^r L_1(w_{n-1})r^{n-1}\,dr \tag{6.7b}$$

and

$$L_1(w) = \frac{\partial^2 w}{\partial x^2} + \frac{\partial^2 w}{\partial y^2} + 2a_1\frac{\partial w}{\partial x} + 2b_1\frac{\partial w}{\partial y} + c_1 w \tag{6.8a}$$

with

$$a_1 = a + \frac{1}{U_o}\frac{\partial U_o}{\partial x}, \quad b_1 = b + \frac{1}{U_o}\frac{\partial U_o}{\partial y}, \quad c_1 = \frac{1}{U_o}\frac{\partial U_o}{\partial y} \tag{6.8b}$$

In Eqs. (6.7) and (6.8), U_o is given by

$$U_o = A \exp\left\{-\int_0^r \sigma\,\frac{dr}{r}\right\} \tag{6.9a}$$

where the constant A may depend on θ and

$$\sigma = ax + by \tag{6.9b}$$

A second solution of Eq. (6.4) is given by

$$u_2 = u_1 \ln D + U_o \sum_{n=0}^{\infty}\left[\frac{\partial}{\partial \nu}\left\{\frac{\Gamma(\nu+1)\,W_n}{\Gamma(\nu+n+1)}\right\}\right]_{\nu=0} D^n \tag{6.10a}$$

where

$$W_o = 1, \quad W_n = -\frac{1}{4r^{n+\nu}}\int_0^r L_1\,(W_{n-1})\,r^{n+\nu-1}\,dr \tag{6.10b}$$

In Eq. (6.10a), Γ denotes the Gamma function. It is noticed that the first solution in Eq. (6.7a) is analytic in a neighborhood of the origin. The second solution in Eq. (6.10a) has a term containing a logarithmic singularity and a

AD-A075 158 TETRA TECH INC JACKSONVILLE FL F/G 8/3
CONTINENTAL SHELF CIRCULATION INDUCED BY TIDAL JETS - AN ANALYT--ETC(U)
OCT 79 R B TAYLOR , P B JOSHIO N00014-78-C-0693
UNCLASSIFIED TETRAT-3249 NL

2 OF 2
AD A075158

END
DATE FILMED
11-79
DDC

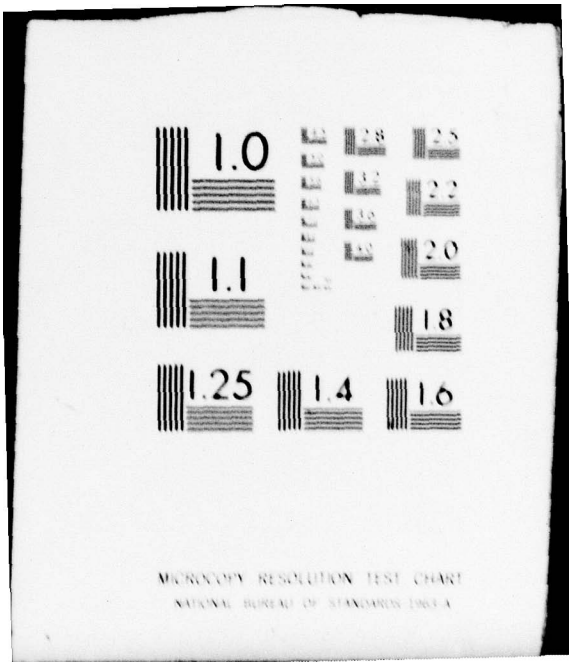
1.0
1.1
1.25
1.4
1.6
2.0
1.8
MICROCOPY RESOLUTION TEST CHART
NATIONAL BUREAU OF STANDARDS 1963-A

term which is analytic in a neighborhood of the origin. This solution is the required elementary solution for the general equation (6.4). For details regarding the convergence of the above solutions Res. (42) and (43) should be consulted.

In the next section, the general solutions discussed heretofore are applied to the special case of an exponentially sloping bottom.

6.3 Derivation of Elementary Solution for an Exponentially Sloping Bottom

Consider a special case of Fig. 1.3 in which the ocean floor slopes exponentially from the coast in the x-direction, i.e.,

$$h(x) = e^{2\beta x} \tag{6.11}$$

where h is dimensionless depth which equals unity at the inlet (x=0) and β is a non-dimensional slope parameter. In fact, 2β equals the slope at the origin, since

$$h_x = 2\beta e^{2\beta x} \tag{6.12a}$$

and

$$h_y = 0 \tag{6.13a}$$

Therefore, in Eqs. (6.4), in conjunction with Eq. (6.2),

$$2a = \frac{h_x}{h} = 2\beta$$

or

$$a = \beta = \text{constant} \tag{6.14a}$$

and

$$b = \frac{1}{2}\frac{h_y}{h} \equiv 0 \tag{6.14b}$$

Substituting Eqs. (6.14) into Eqs. (6.9) and using Eqs. (6.6), it can be shown that

$$U_o = Ae^{-\beta x} \tag{6.15}$$

Now, from Eqs. (6.7b) and (6.8), the coefficients w_n can be evaluated as

$$w_0 = 1, \quad w_1 = \frac{\beta^2}{4}, \quad w_2 = \frac{\beta^4}{32}, \quad w_3 = \frac{\beta^6}{384}, \ \ldots$$

or

$$w_n = \frac{\beta^{2n}}{2^{2n}\, n!} \tag{6.16}$$

Introducing Eq. (6.16) into Eq. (6.7a), the first solution is

$$u_1 = Ae^{-\beta x} \sum_{n=0}^{\infty} \frac{(\beta^2 r^2/4)^n}{(n!)^2} \tag{6.17}$$

In the above equation, A is a pure constant independent of θ. In fact, it can be proved that A must be a constant in order to preserve the analyticity of u_1 at the origin and to preserve symmetry of the resulting velociy field about $\theta = 0$.

To obtain the second solution in Eq. (6.10a), the coefficients W_n are evaluated from Eq. (6.10b). The result is

$$W_0 = 1, \quad W_1 = \frac{\beta^2}{4(\nu+1)}, \quad W_2 = \frac{\beta^4}{16(\nu+1)\ (\nu+2)},$$

$$\text{and } W_3 = \frac{\beta^6}{64(\nu+1)\ (\nu+2)\ (\nu+3)}, \ \ldots\ldots$$

or

$$W_n = \frac{\beta^{2n}}{2^{2n} \prod_{r=0}^{n-1} (\nu+n-r)}$$

$$= \frac{\beta^{2n}\, \Gamma(\nu+1)}{2^{2n}\, \Gamma(\nu+n+1)} \tag{6.18}$$

Substituting the series (6.18) into Eq. (6.10a), the required elementary solution is,

$$u_2 = u_1 \ln D + U_o \sum_{n=0}^{\infty} \frac{\beta^{2n}}{2^{2n}} \frac{\partial}{\partial \nu} \left\{ \frac{\Gamma(\nu+1)}{\Gamma(\nu+n+1)} \right\}^2_{\nu=0} D^n \tag{6.19}$$

When the differentiation in the above equation is carried out, and u_1 and U_0 are substituted from Eqs. (6.17) and (6.15) respectively, the result is

$$u_2 = 2Ae^{-\beta x} \left[\sum_{n=0}^{\infty} \frac{(\beta^2 r^2/4)^n}{(n!)^2} \ln r - \sum_{m=1}^{\infty} \sum_{p=1}^{m} \frac{1}{p} \frac{(\beta^2 r^2/4)^{2m}}{(m!)^2} \right] \tag{6.20}$$

u_2 is the elementary singularity solution for a sloping bottom. It can be shown that the series in Eqs. (6.17) and (6.20) are absolutely and uniformly convergent. The solutions given by Eqs. (6.17) and (6.20) appear complicated, but fortunately, the summations for u_1 and u_2 tend in the limit to the well-known Bessel functions. It may be verified from Ref. (44) that

$$u_1 = A\, e^{-\beta x}\, I_o(\beta r) \tag{6.21}$$

$$u_2 = -2Ae^{-\beta x} \left[K_o(\beta r) + I_o(\beta r) \ln (\beta e^E/2) \right] \tag{6.22}$$

where I_o and K_o are zeroth order modified Bessel functions of the first kind

and second kind respectively. E is Euler's constant equal to 0.577215664... . It can be demonstrated by direct substitution that Eqs. (6.21) and (6.22) satisfy the governing Eq. (6.2).

In Eq. (6.22), $K_o(\beta r)$ behaves like $\ell n\ r$ as $r \to 0$, and hence u_2 is the required elementary solution for ϕ in Eq. (6.2). Thus, for an exponentially sloping bottom, the velocity potential in polar co-ordinates is

$$\phi(r,\theta) = -2Ae^{-\beta r\cos\theta}\left[K_o(\beta r) + I_o(\beta r)\ \ell n\ (\beta e^E/2)\right] \tag{6.23}$$

Corresponding velocity components are given by the derivatives.

$$u_r = \frac{\partial \phi}{\partial r} \tag{6.24a}$$

$$u_\theta = \frac{1}{r}\ \frac{\partial \phi}{\partial \theta} \tag{6.24b}$$

Differentiating Eq. (6.23) one obtains

$$u_r(r,\theta) = 2A\beta e^{-\beta r\cos\theta}\left[\{K_1(\beta r) + K_o(\beta r)\cos\theta\}\right.$$
$$\left. - \ell n\ (\beta e^E/2)\ \{I_1(\beta r) - I_o(\beta r)\cos\theta\}\right] \tag{6.25}$$

$$u_\theta(r,\theta) = -2A\beta \sin\theta\ e^{-\beta r\cos\theta}\left[K_o(\beta r) + \ell n(\beta e^E/2) I_o(\beta r)\right] \tag{6.26}$$

Note that u_r is an even function of θ, i.e., $u_r(r,\theta) = u_r(r,-\theta)$, and u_θ is an odd function, i.e., $u_\theta(r,\theta) = -u_\theta(r,-\theta)$. In Eq. (6.25), I_1 and K_1 are first order modified Bessel functions of the first and second kind respectively. It should be emphasized that Eqs. (6.23), (6.25), and (6.26) describe the potential flow field about a point singularity for exponentially varying depth. To obtain solutions for outer shelf circulation one must relate the jet solution for exponential bathymetry to a distribution of singularities represented by Eq. (6.23), (6.25), and (6.26). This precedure is outlined in Sec. 6.4

Finally, the constant A in Eqs. (6.23), (6.25), and (6.26) must be given a physical interpretation by identifying it with the strength of the singularity. By analogy with the elementary solutions for the constant bottom case (Sec. 3.1), the singularity may be referred to as a 'modified' sink. Let 'q' be the strength of the modified sink at r=0. Thus, q equals the volume of fluid vanishing per unit time at the sink per unit length (measured normal to the plane of motion). Then, q also equals the volume of fluid flowing into any curve enclosing the sink. For simplicity, let the curve be a circle of vanishingly small radius ϵ with center at r=0. Therefore,

$$q = \oint_{\substack{\text{circle} \\ \epsilon}} \vec{V} \cdot \vec{e}_r \, d\lambda \tag{6.27}$$

where $d\lambda$ is a lineal element of the circumference and equals $\epsilon d\theta$. $\vec{e}_r$ is a unit vector in the radial direction and $\vec{V}$ is the velocity vector

$$\vec{V} = -u_r \vec{e}_r + u_\theta \vec{e}_\theta \tag{6.28}$$

$\vec{e}_\theta$ being the tangential unit vector. Thus,

$$q = -\lim_{\epsilon \to 0} \int_0^{2\pi} \epsilon u_r \, d\theta \tag{6.29}$$

where u_r is evaluated at $r=\epsilon$. Substituting for u_r from Eq. (6.25) into Eq. (6.29), carrying out the indicated limit, and simplifying, it can be shown that

$$A = \frac{-q}{4\pi} \tag{6.30}$$

Introduction of above result into Eq. (6.23) yields the final expression for ϕ for a modified sink singularity,

$$\phi(r,\theta) = \frac{q}{2\pi} e^{-\beta r \cos\theta}\left[K_o(\beta r) + \ell n\ (\beta e^{E}/2)\ I_o(\beta r)\right] \qquad (6.31)$$

It is interesting to investigate Eq. (6.31) when the bottom is flat and is of unit depth, i.e., $\beta=0$ in Eqs. (6.11) and (6.31). In the limit $\beta\to 0$, it may be verified that

$$\phi(r,\theta) = \frac{-q}{2\pi} \ell n\ r \qquad (6.32)$$

Thus, Eq. (6.1) which represents velocity potential for constant bathymetry has been recovered.

In summary, the jet-induced flow field for a steady potential motion over an arbitrary bathymetry is governed by Eq. (6.2). The velocity potential ϕ in this equation can be shown to possess elementary singular solutions similar to the classical solutions of Laplace's equation. For the special case of an exponentially sloping bottom, the elementary solution is given by Eq. (6.31) where the singularity is a modified Bessel function rather than a logarithm. Next, one should consider the application of Eq. (6.31) to determine the jet induced flow field. This is the subject of the following section.

6.4 Application of Elementary Solutions to Determine Jet-induced Circulation Patterns for Variable Bathymetry

In this section, an outline of the possible use of Eq. (6.31) to determine the jet-induced flow field is given. First of all, a physical interpretation of Eq. (6.31) is necessary. It is obvious from Eq. (6.32) that the equipotential lines (i.e., lines of constant potential ϕ) for a sink are perfect circles and the streamlines (i.e., lines of constant stream function ψ) are rays emanating from the origin. The streamlines and equipotential lines are mutually orthogonal. A similar interpretation of Eq. (6.31) will be very useful in understanding physically

the flow field characterized by the elementary solution.

Future efforts will attempt to solve the circulation due to a simple jet (Fig. 3.1) with an exponential bathymetry. Following the procedure in Sec. 3.1, the jet will be represented by a distribution of elementary singularities in Eq. (6.31), where q must be related to the jet solution for an exponential bottom. Since the work in Ref. 11 does not treat this special case, jet solutions will have to be obtained using the general formulation presented therein. It is hoped that these solutions will be analytical, but they can be obtained numerically, if necessary. Further, a correspondence can be established between the volume flux due to the singularity and entrainment due to the jet which will enable expressing q in terms of the jet parameters. The flow field can then be determined by integrating Eq. (6.31) with appropriate variation of q over the entire distribution. The result will be an equation similar to Eq. (3.25). Velocity components can be obtained by differentiation in Eqs. (6.24).

6.5 Effects of Unsteadiness and Earth's Rotation - Geophysical Fluid Dynamics Approach

The formulation and solution of jet induced circulation considered thus far has ignored the effects of unsteadiness of the tidal jet and the influence of the Earth's rotation. On a time scale which is comparable to the tidal period, temporal effects definitely become important in a tidal [illegible]. Moreover, tidal jets often extend to several kilometers offshore making the effects of the Earth's rotation relevant. In this section, a preliminary formulation is presented and only major steps in the derivation are included. A few possible avenues of solution are also mentioned briefly.

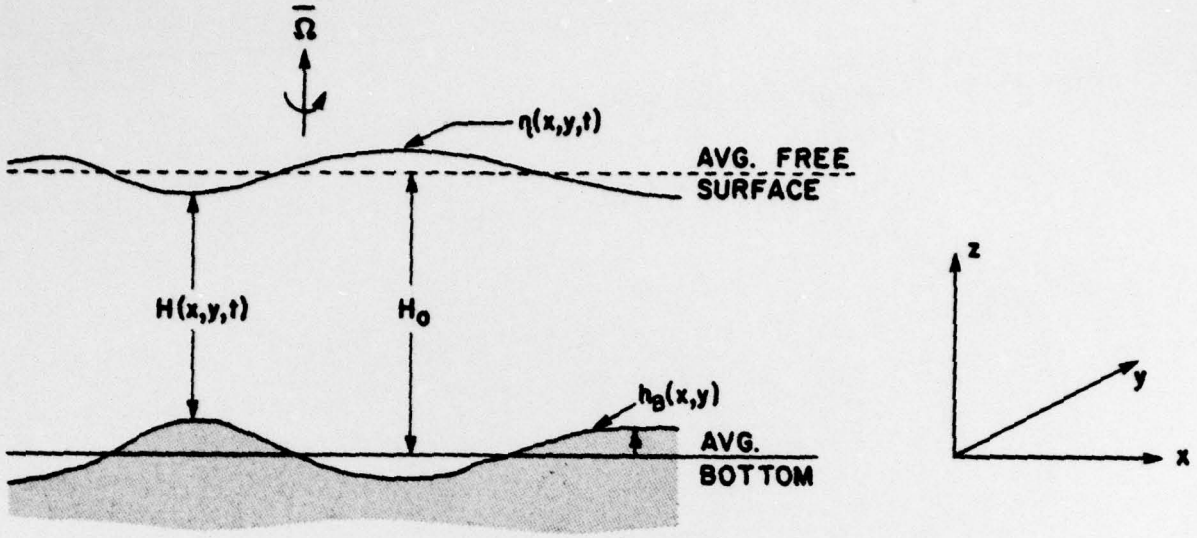

Figure 6.1 Derivation of Geophysical Fluid Dynamic Equations

Figure 6.1 shows an unsteady water suface $\eta(x,y,t)$ with arbitrary bottom variations represented by $h_B(x,y)$. $H(x,y,t)$ is the instantaneous height of water column. The fluid motion is assumed to be quasi-geostrophic or geostrophic to the lowest order. Therefore, the first order horizontal velocity components u and v are independent of z. This is equivalent to the shallow water approximation encountered earlier in Sec. 2.1. Under the assumption of quasi-geostrophy, the continuity equation can be combined with the so-called kinematic boundary condition at the free surface and the non-penetration condition at the bottom to obtain

$$\frac{D}{Dt}\left[\frac{z-h_B}{H}\right] = 0 \tag{6.33}$$

This equation has been derived in Ref. (45) for the case of a flat and steady free surface but the derivation can be easily extended to account for a time-varying free surface. Eq. (6.33) can be interpreted physically as follows. For every fluid particle located at an elevation 'z' in the coordinate system of Fig. 6.1, the ratio of its height above the bottom to the total height of liquid column at that location is a constant as the particle traverses the flow field.

Eq. (6.33) has been derived from kinematic considerations alone. Dynamic considerations are introduced through the classical Ertel's theorem of geophysical fluid dynamics. The theorem states that for an inviscid constant density (and hence trivially barotropic) fluid,

$$\frac{D}{Dt}\left[\frac{(\bar{\zeta}+2\bar{\Omega})}{\rho} \cdot \nabla\Lambda\right] = 0 \tag{6.34}$$

where $\bar{\zeta}$ = relative vorticity of fluid, $\bar{\Omega}$ = angular velocity of Earth, and Λ is a property that is conserved with fluid motion. From Eq. (6.33), $(z-h_B)/H$ is such a property and it is substituted into Eq. (6.34) in place of Λ. Upon simplifications, the result is

$$\frac{D}{Dt}\left[\frac{\bar{\zeta}+2\bar{\Omega}}{\rho H}\right] = 0 \tag{6.35}$$

Now, due to quasi-geostrophy, the first order motion is two dimensional and only that component of $\bar{\zeta}$ which is parallel to $\bar{\Omega}$ in Fig. 6.1 is significant, i.e.,

$$|\bar{\zeta}| = \zeta = \frac{\partial v}{\partial x} - \frac{\partial u}{\partial y} \tag{6.36}$$

Furthermore, in Fig. 6.1,

$$2\bar{\Omega} = 2\Omega \sin\theta = f \tag{6.37}$$

where θ = latitude.

Combining Eqs. (6.35), (6.36), and (6.37), one obtains the vorticity equation

$$\frac{D}{Dt}\left[\frac{\zeta+f}{H}\right] = 0 \tag{6.38}$$

The quantity in brackets in Eq. (6.38) is called potential vorticity

$$\Pi = \frac{\zeta+f}{H} \tag{6.39}$$

and thus

$$\frac{D\Pi}{Dt} = 0 \tag{6.40}$$

Eq. (6.40) expresses the conservation of potential vorticity. It shows that vorticity associated with a fluid particle must increase when it encounters an increase in the instantaneous depth H. Moreover, even if the particle possesses zero vorticity at some instant of time, it will acquire vorticity due to depth changes solely because of the presence of planetary vorticity f. Note that these observations hold for an inviscid fluid and the vorticity is not derived from fluid viscosity.

Eq. (6.38) can be converted to a more useful form in terms of the stream function. Since the lowest order motion is geostrophic, which represents a balance of pressure forces and Coriolis forces, the stream function is related to the pressure as follows

$$u = -\frac{1}{\rho f}\frac{\partial p}{\partial y} = -\frac{\partial(p/\rho f)}{\partial y} \tag{6.41a}$$

$$v = \frac{1}{\rho f}\frac{\partial p}{\partial x} = \frac{\partial(p/\rho f)}{\partial x} \tag{6.41b}$$

Therefore, a stream function may be defined as

$$\psi \equiv \frac{p}{\rho f} \tag{6.42}$$

Then, the vorticity in Eq. (6.36) becomes

$$\zeta = \frac{1}{\rho f} \nabla^2 p = \nabla^2 \psi \tag{6.43}$$

Combining Eqs. (6.39), (6.40), (6.41), and expanding the material derivative, it can be shown that

$$\nabla^2 \psi_t + \frac{\partial(\psi, \nabla^2\psi)}{\partial(x,y)} - \frac{(\nabla^2\psi+f)}{H} \frac{\partial(\psi,H)}{\partial(x,y)} - \frac{H_t}{H} (\nabla^2\psi+f) = 0 \tag{6.44}$$

This is the most general governing equation which allows free surface variations. Eq. (6.44) is quite complex in its present form. Introducing the following simplifying assumptions

(1) variations in H are small, and therefore, $H \simeq H_o$ in Eq. (6.44)

(2) the relative vorticity ζ (or equivalently $\nabla^2\psi$ in Eq. (6.43)) is much smaller compared to the planetary vorticity, f, i.e., $\nabla^2\psi << f$ in Eq. (6.44)

it may be verified that

$$\nabla^2 \psi_t + \frac{\partial(\psi, \nabla^2\psi)}{\partial(x,y)} - \frac{f}{H_o} \frac{\partial(\psi,H)}{\partial(x,y)} - \frac{H_t f}{H_o} = 0 \tag{6.45}$$

In Eq. (6.45), the Jacobian in the third term and the unsteady depth term H_t can be expressed in terms of ψ using Eq. (6.42) and the relations

$$\eta(x,y,t) = H(x,y,t) + h_B(x,y) \tag{6.46}$$

and

$$p(z) = p_{atm} + \rho g(\eta - z) \tag{6.47}$$

The resulting equation in ψ is

$$\nabla^2\psi_t + \frac{\partial(\psi,\nabla^2\psi)}{\partial(x,y)} + \frac{f}{H_o}\frac{\partial(\psi,h_B)}{\partial(x,y)} - \frac{f^2\psi_t}{gH_o} = 0 \qquad (6.48)$$

which can be written more compactly as

$$\left(\nabla^2 - \frac{f^2}{gH_o}\right)\psi_t + \frac{\partial(\psi,\nabla^2\psi+fh_B/H_o)}{\partial(x,y)} = 0 \qquad (6.49)$$

The second term in the coefficient of ψ_t in Eq. (6.49) owes its existence to the unsteady free surface variations. In fact, this term does not appear in a similar derivation contained in Ref.(45).

Finally, through some algebraic manipulations Eq. (6.48) can be put in the form

$$\frac{D}{Dt}\left[\nabla^2\psi - \frac{f^2}{gH_o}\psi + \frac{fH_B}{H_o}\right] = 0 \qquad (6.50)$$

This form is very illuminating in that it shows

$$\nabla^2\psi - \frac{f^2}{gH_o}\psi + \frac{fh_B}{H_o} = \text{constant along a path line} \qquad (6.51)$$

Perhaps, it is a logical first step to solve the steady flow problem including the effects of bathymetry and Earth's rotation. In this case,

$$\nabla^2\psi + \frac{fh_B}{H_o} = \text{constant along a streamline} \qquad (6.52)$$

Note that the term in f^2 has disappeared since it is a contribution due to unsteadiness as seen from Eq. (6.49). The constant on the RHS of Eq. (6.52) varies from one streamline to another, and therefore, it is a function of ψ only. Thus,

$$\nabla^2\psi + \frac{fh_B}{H_o} = F(\psi) \tag{6.53}$$

Ref. (46) provides a starting point for the choice of the function F. If F is known for a physically meaningful steady flow situation, Eq. (6.53) can be solved as a non-homogeneous reduced wave equation. In the particular case of $F \equiv 0$ and the absence of bathymetric variations, Eq. (6.53) reduces to Laplace's Eq. (2.12) which governs steady potential flows. Eqs. (6.53) and (6.51) indicate that in the absence of planetary rotation ($f = 0$), the bathymetric effects are also removed from the problem. This is because of assumption (1) under Eq. (6.44) that the depth variations are gentle. In other words, the effects of small bottom variations are exemplified only when significant rotation is present.

Solution of the general unsteady Eq. (6.49) is very difficult. References (46), (47), and (28) should be very useful in this regard.

7.0 SUMMARY AND CONCLUSIONS

7.1 Summary

An analytical investigation of the circulation induced by a tidal jet in an ebbing ocean was conducted. The jet was assumed to be steady and issuing into coastal waters having constant depth but arbitrary bottom friction. The surrounding fluid motion was assumed to be steady and potential (i.e., inviscid and irrotational). The effects of unsteadiness, Earth's rotation, and buoyancy have been neglected in this preliminary study; however, the important effects of lateral mixing have been included. During the final stages of the study reported herein, mathematical formulations were developed to describe steady potential flow with variable bathymetry and unsteady, inviscid, rotational flow due to Coriolis forces.

To obtain the shelf circulation patterns over constant bottom topography, the jet was replaced by an equivalent distribution of sinks which are themselves solutions of Laplace's equation. The latter, of course, governs the potential motion of the jet-induced circulation. The strength of each sink in the distribution is determined by equating the volume flow due to entrainment to the volume flow demanded by the sink. Thus, a complete physical and mathematical connection was established between the jet flow and the outer flow. This formulation of jet-induced motion has been adopted from Taylor (38). Analytical expressions were derived for the stream function and velocity components. These quantities were evaluated analytically whenever possible and numerically using Gauss-Legendre quadrature. The streamline patterns obtained for a simple jet (i.e., perpendicular to the coastline) bear a close resemblence to the circulation patterns observed by Lippisch (48) in a smoke tunnel. The variation of alongshore current with distance from the jet was also predicted and shown to be a strong function

of bottom friction of the jet. These numerical computations were performed for various values of bottom friction. The following four jet configurations of practical interest were studied:

(i) A simple jet normal to the coastline.

(ii) A jet with jetties of varying lengths.

(iii) Two parallel jets.

(iv) A jet non-perpendicular to the coastline.

7.2 Conclusions

Computational results for the above cases were generated to obtain the jet-induced circulation patterns, the alongshore current, and the onshore-offshore current. The general conclusions drawn from the numerical results are:

Continental Shelf Circulation Patterns:

(i) The jet-induced circulation patterns are very sensitive to the bottom friction, f, and the half-width/depth ratio, b_o/h_o, of the inlet. The combined effect of these two variables can be expressed in terms of a single parameter $\mu = fb_o/8h_o$. For two inlets of identical dimensions and throat velocities, the jet with less bottom friction (small f) induces circulation over a much larger area of the continental shelf than a jet with large bottom friction (large f). This is because the offshore extent of the jet is reduced significantly by the increased bottom friction. Similarly, for two jets with identical values of the friction factor f and width b_o, a jet with a smaller aspect ratio b_o/h_o induces circulation over a greater portion of the continental shelf than a jet with a large aspect ratio.

(ii) The introduction of a jetty affects the jet-induced circulation patterns very characteristically. The streamlines close to the inlet display strong curvature toward the mouth of the jetty and thus demonstrate clearly the influence of the jet-induced entrainment.

(iii) For the case of two parallel jets, the induced flow field is symmetric about the centerline between the jets which divides the flow field into two regions. The waters in between the jets are entrained by both the jets. The circulation patterns in the outer regions, however, are similar to those for a simple jet.

(iv) The outer circulation patterns associated with a jet which is not perpendicular to the coastline exhibit asymmetries (when compared to the symmetric streamline pattern for a simple jet) as one would expect.

Alongshore Current:

(i) The alongshore current toward the inlet has a maximum value (about 3.5 percent of the throat velocity) near the inlet and drops off as one moves away from the inlet along the coastline. This drop-off is a strong function of the bottom friction of the jet. An increase in bottom friction results in a significantly faster decay of the alongshore current.

(ii) The introduction of a jetty changes the character of the variation of the alongshore current from that described above. The current is zero at the inlet, increases to a maximum value at some location along the coast, and decreases to zero far away from the inlet. The maximum value attained depends upon the jetty length and reduces sharply with increased jetty length.

(iii) For two identical parallel tidal jets, it was found that the presence of a second jet reduces the alongshore current (below the value for a simple jet) between the jets, but increases it in the outer flow. This conclusion is based on the assumption that each jet entrains the same amount of fluid as a simple jet in spite of the proximity of the other jet. Consequently, the entrainment on the inner boundaries of the jets drops and increases on the outer boundaries.

(iv) Under the same assumption regarding jet entrainment as in (iii) above, for a jet non-perpendicular to the coastline, the alongshore current on the acute angle side is reduced, whereas it is increased on the obtuse angle side.

Onshore-Offshore Current:

The behavior of onshore-offshore currents was investigated for a simple jet and the conclusions are expected to be similar for other cases, except for minor modifications. For a bottom-frictional jet, the current is always directed onshore. As one proceeds from the coast in the offshore direction parallel to the jet, the magnitude of the onshore current increases from zero to a maximum value at some point and drops off to zero further offshore. The peak value of the onshore current decreases as one moves farther from the jet.

Steady Potential Flow with Variable Bathymetry:

The problem of steady potential flow with variable bathymetry was also formulated. It was shown that arbitrary bottom topography can be handled by introducing a velocity potential rather than a stream function. The sinks for Laplace's equation were replaced by special singularities whose form was obtained for an exponentially sloping bottom. It was found that a generalized

series solution can be employed to determine the nature of the singularities for arbitrary bathymetry. It is expected that the jet can be replaced by an equivalent singularity distribution and the outer flow solution obtained in a manner similar to that used for the constant bathymetry case.

Effects of Unsteadiness and Earth's Rotation:

The effects of unsteady jet-induced circulation in the presence of the Earth's rotation and variable bathymetry were formulated within the framework of geophysical fluid dynamics. It appears that the special case of steady and inviscid but rotational flow with arbitrary bottom variations represents a logical extension of the problem detailed in the previous paragraph.

Recommendations for Future Research Efforts:

The short-term goals of future research in this area should include (i) a refinement of the algorithm which generates stream function and streamlines for the constant depth case; (ii) a parametric study of the effects of jetty length, distance between two adjacent jets, jet angle with respect to the coastline, etc. on the circulation patterns and the alongshore current; (iii) a complete analytical solution of jet-induced circulation for an exponential bathymetry and an extension to other bathymetric features for which analytical solutions are possible; (iv) a study of possible analytical solutions to the steady, inviscid, and rotational jet-induced circulation with arbitrary bathymetry and Earth's rotation.

The long-term goals of research programs in this area should be to include the effects of unsteadiness in the jet as well as the induced flow, buoyancy of the jet, wave climate, and viscosity in the outer flow. In an entirely different but parallel effort, the mass transport associated with circulation induced by tidal jets should be investigated.

8.0 REFERENCES

1. Dean, R. G. and R. B. Taylor. Numerical Modeling of Constituent Transport in Bay Systems, Proc. 13th Coastal Engineering Conference ASCE, pp. 2227-2249, 1972.

2. Dean, R. G. and T. L. Walton. Sediment Transport Processes in the Vicinity of Inlets with Special Reference to Sand Trapping, Estuarine Research, v. 2, pp. 129-149, Academic Press, New York, 1974.

3. Csanady, G. T. Turbulent Diffusion in the Environment, D. Rediel Publishing Co., Boston, Massachusetts, 1973.

4. Rouse, L. J., And J. M. Coleman. Circulation Observations in the Louisiana Bight Using LANDSAT Imagery, Remote Sensing of Environment, v. 5, pp. 55-66, 1976.

5. Wiseman, W. J., S. P. Murray, J. M. Bane and M. W. Tubman. Offshore Physical Oceanography, Appendix III in Environmental Assessment of a Louisiana Offshore Oil Port and Appertinent Storage and Pipeline Facilities, v. II, unpublished manuscript, Louisiana State University, 1975.

6. Pearce, A. F. Critical Reynolds Number for Fully Developed Turbulence in Circular Submerged Water Jets: Nat. Mech. Eng. Research Inst., South Africa, CSIR, Report No. MEG475, 1966.

7. Turner, J.S. The 'Starting Plume' in Neutral Surroundings, J. Fluid Mech., v. 13, pp. 356-368, 1962.

8. Tsang, G., and I. R. Wood. Motion of Two-Dimensional Starting Plume, J. Engineering Mechanics Div., ASCE, v. 94, No. EM6, pp. 1547-1561, 1968.

9. Tsang, G. Laboratory Study of Two-Dimensional Starting Plumes, Atmospheric Environment, v. 4, pp. 519-544, 1970.

10. Middleton, J. H. The Asymptotic Behaviour of a Starting Plume, J. Fluid Mech., v. 72, pp. 753-771, 1975.

11. Özsoy, E. Flow and Mass Transport in the Vicinity of Tidal Inlets, University of Florida, Coastal and Oceanographic Engineering Laboratory, Technical Report No. TR-036, 1977.

12. Albertson, M. L., Y. B. Dai, R. A. Jensen, and H. Rouse. Diffusion of Submerged Jets, Trans., ASCE, v 115, p. 639, 1950.

13. Ambramovich, G. N. The Theory of Turbulent Jets, The M.I.T. Press, Cambridge, Massachusetts, 1963.

14. Schlichting, H. Boundary Layer Theory, 6th ed., McGraw-Hill, New York, 1968.

15. Stolzenbach, K.D., and D. R. F. Harleman. An Analytical and Experimental Investigation of Surface Discharges of Heated Water, Ralph M. Parsons Laboratory of Water Resources and Hydrodynamics, M.I.T., Report No. 135, 1971.

16. Rajaratnam, N. Turbulent Jets, Elsevier, 1976.

17. Turner, J.S. Buoyancy Effects in Fluids, Cambridge University Press, 1973.

18. Olsen, E. A Study of the Effects of Inlet Stabilization of St. Mary's Entrance Florida, ASCE, Coastal Sediments '77, pp. 311-329, 1977.

19. French, J. L. Tidal Flow in Entrances, U. S. Army Corps of Engineers, Committee on Tidal Hydraulics, Technical Bulletin No. 3, 1960.

20. Borichansky, L. S., and V. N. Mikhailov. Interaction of River and Sea Water in the Absence of Tides, Scientific Problems of the Humid Tropical Zone Deltas and Their Implications, UNESCO, pp. 175-180, 1966.

21. Taylor, R. B., and R. G. Dean. Exchange Characteristics of Tidal Inlets, Proc. 14th Coastal Engineering Conference, ASCE, pp. 2268-2289, 1974.

22. Unluata, U. A. and E. Ozsoy. Tidal Jet Flows Near Inlets, Hydraulics in the Coastal Zone, ASCE, pp. 90-98, 1977.

23. Morton, B. R., G. I. Taylor, and J. S. Turner. Turbulent Gravitational Convection from Maintained and Instantaneous Sources, Proc. Roy. Soc., v. A234, pp. 1-23, 1956.

24. Kotsovinos, N. E. A Note on the Spreading Rate and Virtual Origin of a Plane Turbulent Jet, J. Fluid Mech., v. 77, pp. 305-311, 1976.

25. Kotsovinos, N. E. A Note on the Conservation of the Axial Momentum of a Turbulent Jet, J. Fluid Mech., v. 87, part 1, pp. 55-63, 1978.

26. Gadgil, S. Structure of Jets in Rotating Systems, J. Fluid Mech., v. 47, pp. 417-436, 1971.

27. Savage, S. B., and R. J. Sobey. Horizontal Momentum Jets in Rotating Basins, J. Fluid Mech., v. 71, pp. 755-768, 1975.

28. Greenspan, H. P. The Theory of Rotating Fluids, Cambridge University Press, 1969.

29. Wright, L. B., C. J. Sonu and W. V. Kielhorn. Water-Mass Stratification and Bed Form Characteristics in East Pass, Destin, Florida, Mar. Geol. v. 12, pp. 43-58, 1972.

30. Wright, L. D. and C. J. Sonu. Processes of Sediment Transport and Tidal Delta Development in a Stratified Tidal Inlet, Estuaries, v. 2, pp. 63-76, 1974.

31. Wright, L. D. and J. M. Coleman. Effluent Expansion and Interfacial Mixing in the Presence of a Salt Wedge, Mississippi River Delta, J. Geophys. Res., v. 76, pp. 8649-8661, 1971.

32. Wright, L. D. and J. M. Coleman. Mississippi River Mouth Processes: Effluent Dynamics and Morphologic Development, Journal of Geology, v. 82, pp. 751-778, 1974.

33. Garvine, R. W. Observations of the Motion Field of the Connecticut River Plume, J. Geophys. Res., v. 82, pp. 441-454, 1977.

34. Wright, L. D. Morphodynamics of a Wave Dominated River Mouth, Proc. 15th Coastal Engineering Conference, pp. 1721-1737, 1976.

35. Takano, K. A Complementary Note on the Diffusion of the Seaward Flow Off the Mouth of a River, J. Oceanographic Soc. Japan, v. 11, pp. 1-3, 1955.

36. Waldrop, W. R. and R. C. Farmer. Three-Dimensional Flow and Sediment Transport at River Mouths, Louisiana State University, Coastal Studies Institute, Technical Report No. 150, 1973.

37. Yoshida, S. and M. Kashiwamura. Tidal Response of Two-Layer Flow at a River Mouth, Proc. 15th Coastal Engineering Conference, pp. 3189-3207, 1976.

38. Taylor, G. I. Flow Induced by Jets, J. Aero/Space Sci., v. 25, pp. 464-465, 1958.

39. Karamcheti, K. Principles of Ideal-Fluid Aerodynamics, John Wiley & Sons, Inc., 1966.

40. Bois, G. Petit. Tables of Indefinite Integrals, Dover Publication, Inc., 1961.

41. Carnaham, B., Luther, H., and Wilkes, J. Applied Numerical Methods, John Wiley & Sons, Inc., 1969.

42. Copson, E. T. Partial Differential Equations, Cambridge University Press, 1975.

43. Hadamard, J. Lectures on Cauchy's Problem in Linear Partial Differential Equations, Yale 1923, reprinted New York 1952.

44. Abramowitz, M. and Stegun, I. Handbook of Mathematical Functions, Dover Publications Inc., 1970.

45. Pedlosky, J. Geophysical Fluid Dynamics, in W. H. Reid (Editor), Mathematical Problems in Geophysical Sciences, American Mathematical Society, 1971.

46. Batchelor, G. An Introduction to Fluid Dynamics, Cambridge University Press, 1977.

47. Roberts, P. and Soward, A. Rotating Fluids in Geophysics, Academic Press, 1978.

48. Lippisch, A. M. Flow Visualization, Aernautical Engineering Review, Vol. 36, pp. 24-36, 1958.